Functional Genomics Investigation of Siroheme and Heme d_1 Biosynthesis

by

Victoria Leigh Owens

A dissertation submitted to the Graduate Faculty of
Auburn University
in partial fulfillment of the
requirements for the Degree of
Doctor of Philosophy

Auburn, Alabama
August 3, 2019

Keywords: Siorheme, Heme d_1, Biosynthetic Pathways, Enzymes,
Heme Oxygenase, Bacterioferritin

Approved by

Steven Mansoorabadi, Chair, Assistant Professor of Chemistry
Douglas Goodwin, Associate Professor of Chemistry
Eduardus Duin, Associate Professor of Chemistry
Sang-Jin Suh, Associate Professor of Biological Sciences

Abstract

Many bacteria and archaea grow under anaerobic or microaerophilic conditions. In order for these organisms to survive under these conditions, many utilize nitrate or nitrite as terminal electron acceptors for anaerobic respiration. In addition, some organisms can reduce nitrate or nitrite to ammonia in order to assimilate nitrogen for the synthesis of N-containing biomolecules. The first committed step in both denitrification and/or assimilation is carried out by a nitrite reductase (NIR). There are different types of NIRs and they can be classified by their products (NO vs. NH_4^+) or by their cofactors, two of which are heme d_1 and siroheme. The unique heme d_1 cofactor is only found in denitrifying bacteria containing a cytochrome cd_1 NIR, and is the site of nitrite reduction. Interestingly, siroheme, the cofactor of some ammonia-forming NIRs, has recently been identified as an intermediate in the biosynthesis of heme d_1.

In most organisms that produce siroheme and heme d_1, a multifunctional enzyme CysG is responsible for the conversion of uroporphyrinogen III to siroheme. However, some nitrate reducing organisms, such as *Paracoccus denitrificans* and *Methanosarcina acetivorans*, lack CysG and it is not clear how siroheme is made. In Chapter 2 of this dissertation, we investigate the activity of SirC, a precorrin 2 dehydrogenase from *M. acetivorans* that is found in the alternative heme biosynthesis (*ahb*) gene cluster. SirC is homologous to the dehydrogenase/ferrochelatase domain of CysG and it was found that this enzyme converts precorrin 2 to sirohydrochlorin. However, instead of catalyzing iron insertion into sirohydrochlorin, it was found that increasing concentrations of SirC inhibits ferrochelation. We show that multiple tetrapyrroles (uroporphyrinogen III, precorrin 2, and sirohydrochlorin) are able to spontaneously chelate different metal ions, even at physiological concentrations. We therefore propose

that SirC protects its product, sirohydrochlorin, from the spontaneous chelation of incorrect metals and passes it on to the next enzyme in the pathway via substrate channeling.

Iron is required for the synthesis of siroheme and heme d_1. Some organisms (pathogenic bacteria in particular) can acquire the necessary iron from heme using a specific transport system and a cytosolic heme oxygenase (HemO). The denitrifying bacterium *P. denitrificans* contains a gene cluster with homology to the heme uptake system; however, it lacks the *hemO* gene. Within this cluster is a gene, *pden_1323*, that is annotated as a pyridoxamine 5'-phosphate (PMP) oxidase and contains a conserved domain of unknown function (DUF2470). In Chapter 3 we show that this gene is not a PMP oxidase, but rather a non-canonical heme oxygenase. When determining the function of Pden_1323, we also explored the substrate scope of the enzyme and found that deuteroheme and Mn-protoporphyrin IX can be used as substrates. In contrast, protoporphyrin IX was not a viable substrate for the reaction, which supports the proposed mechanism requiring a metal center for catalysis.

The iron for the biosynthesis of siroheme and heme d_1 in *P. denitrificans* is proposed to be inserted into sirohydrochlorin by a homolog of CbiX, the cobaltochelatase from the cobalamin biosynthetic pathway. Clustered with the *cbiX* gene is *pden_2333*, which encodes a protein with a conserved domain of unknown function (DUF4202). In some species, these two gene are fused together which suggests a role for Pden_2333 in the biosynthesis of siroheme and heme d_1. In Chapter 4, we present size exclusion chromatography data that shows that Pden_2333 binds heme and may require it for structural stability and the formation of higher order oligomeric structures. We also were able to show that Pden_2333 is able to load iron into the core of the protein and mobilize it via reduction of the iron. Therefore, we propose that Pden_2333 may be a novel bacterioferritin that provides iron to CbiX for the biosynthesis of siroheme.

Acknowledgments

I would like to thank my advisor, Dr. Steven Mansoorabadi, for being ever so patient with me and molding me into the scientist I have become. You have been an amazing mentor and role model for me as both a person and as a scientist. I am extremely grateful for your support, encouragement, and guidance throughout my graduate career here at Auburn University. Your advice, knowledge, and wisdom that have been instilled in me will be useful throughout my career as a scientist and through life in general.

I would also like to thank my committee members, Dr. Douglas Goodwin, Dr. Evert Duin, and Dr. Sang-Jin Suh for their continued support, advice, and contributions towards my success as a scientist. I would especially like to thank Dr. Duin for assisting me with the use of his anaerobic glove box. I would like to thank Dr. Suh for his career and life advice and continued support of my graduate career.

I would like to thank the members of my lab, Phong Ngo, Trey Slaney, Kaiyuan “Ken” Zheng, Kenny Nguyen, Xingchen Huang, Shuxin Li, Patrick Donnan, Selam Ghebreamlak, and Eta Isiorho for your continuous help and discussions through my research. I would like to thank Auburn University Department of Chemistry and Biochemistry for the opportunity to pursue my dream of getting a Ph.D. in Chemistry and financially supporting me through these efforts.

To my best friend, Chasity, thank you for not allowing me to give up. You have been by my side in some of my darkest moments and always picked me up and brushed me off. You never judged me and always loved me for who I am. You always kicked my butt into gear when I needed it most with our famous “Get your life together” talks, and for this I could not be more grateful. I would not have made it

through graduate school without your support. Thank you for everything you have done and continue to do!!

Finally, I would like to thank my family for their continued support and help throughout my graduate career. My parents, Momma, Father, Sheri, Charles, Mr. Dale, and Mrs. April, you have been my rock and support through this and I would not have made it through without your continuous help, talks, and support. I did it. We did it. We finally did it! (Let's face it, guys, this has been a 6 year family affair). After being told many times that I never would never succeed, I proved them wrong and I did it! And I could not have done it without all of you. Thank you!

Ma, thank you for supporting me through both of my degrees and always going out of your way to make sure I had everything I needed or wanted. You have been a Godsend to Travis, Christopher, and I and we appreciate everything that you have ever done for us. There is no way that I would be where I am today without you!

To my amazing, supportive husband, Travis, you have gone far above and beyond your duties as husband to make sure that I fulfilled my dream of obtaining my Ph.D. in Chemistry. You have been more than supportive and always knew what to say when I needed it the most. I cannot wait to role reverse and support you in your dreams of getting your Masters and Ph.D. If there are two thing we have discovered together in the last 12 years together of life is 1) Life is tough but it is a lot easier together and 2) our hopes and dreams DO come true if we keep working on them and NEVER give up!

Last, but certainly not least, my amazing son, Christopher, to whom I dedicate this work and my career to. You have been the source of my motivation since the day you were born, and you continue to amaze me and inspire me daily. You give me hope and a sense of life that I never knew could exist prior to you being born. If you learn nothing else from me, I hope I have instilled in you a love for learning, to

always question why, and to never give up on your hopes and dreams! You, my son, are brilliant and can do anything you can set your mind to and I cannot wait to see what you aspire to be! I love you!

Table of Contents

List of Tables

List of Figures

List of Abbreviations

ALA	5-Aminolevulinic Acid
BIPY	2,2’-Bipyridal
BLAST	Basic Local Alignment Search Tool
BphO	Bacterial Phytochrome Heme Oxygenase
CNS	Central Nervous System
CO	Carbon Monoxide
CPR	Cytochrome P450 Reductase
CysG	Siroheme Synthase
DUF	Domain of Unknown Function
ESI	Electrospray Ionization
FPLC	Fast Protein Liquid Chromatography
Fur	Ferric Uptake Regulator
GSL	Genomic and Sequencing Lab
Has	Heme Assimilation System
HMB	Hydroxymethylbilane
HO	Heme Oxygenase

HPLC	High Pressure Liquid Chromatography
IMAC	Immobilized Metal Ion Affinity Chromatography
IPTG	Isopropyl β-D-Thiogalactoside
Isd	Iron –Regulated Surface Determinants
LMW	Low-Molecular Weight
MCR	Methyl-coenzyme M Reductase
MhuD	Mycobacterial Heme Utilization Degrader
MS	Mass Spectrometry
NAR	Nitrate Reductase
NCBI	National Center for Biotechnology Information
NIR	Nitrite Reductase
NirK	Copper Containing Nitrite Reductase
NirS	Cytochrome cd_1 Nitrite Reductase
NOR	Nitric Oxide Reductase
NOS	Nitrous Oxide Reductase
PBG	Porphobilinogen
PBGD	Porphobilinogen Deaminase
PCR	Polymerase Chain Reaction

Phu	*Pseudomonas* Heme Utilization
PigA	*Pseudomonas* Iron Induced Genes
PPIX	Protoporphyrin IX
ROS	Reactive Oxygen Species
SAH	S-Adenosyl-L-Homocysteine
SAM	S-Adenosyl-L-Methionine
SEC	Size Exclusion Chromatography
SUMT	S-Adenosyl-L-Methionine Uroporphyrinogen III Methyl Transferase
TIM	Triosephosphate Isomerase

Chapter 1: Literature Review

1.1 Introduction to the Nitrogen Cycle and the Reduction of Nitrite

Bacterial denitrification is one of the three major branches in the global nitrogen cycle, together with nitrate assimilation/ ammonification, denitrification, and dinitrogen fixation (Figure 1). Bacteria use the denitrification pathway, in which nitrate is used as a terminal electron acceptor, for energy generation.[1] This pathway consists of four major steps; nitrate reduction, nitrite reduction, nitric oxide reduction, and nitrous oxide reduction (Figure 2). These four steps are catalyzed by the enzymes nitrate reductase (NAR), nitrite reductase (NIR), nitric oxide reductase (NOR), and nitrous oxide reductase (NOS), respectively.[2] Bacteria can also reduce nitrate via the nitrate assimilation pathway to ammonia for incorporation into amino acids and other organic compounds needed for survival (Figure 3). In this pathway there are only two enzymatic steps, nitrate reduction to nitrite by NAS and nitrite reduction to ammonia by NIR. The first committed step within both of these pathways is catalyzed by NIR. Bacteria can therefore utilize two functionally distinct types of NIRs, ammonia forming or nitric oxide forming.[1]

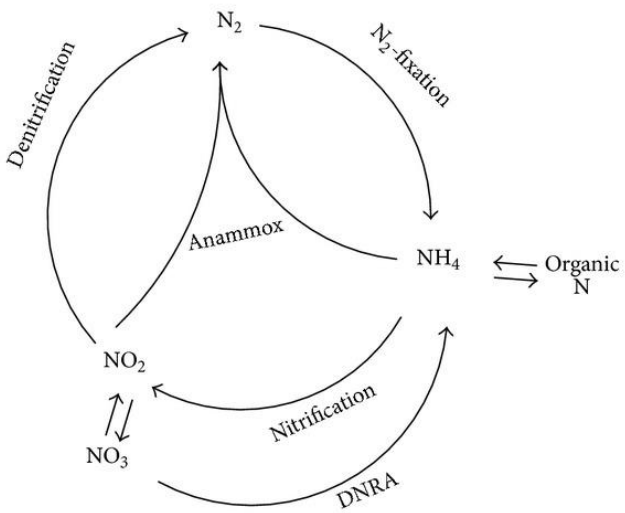

Figure 1: Global nitrogen cycle.[3]

Figure 2: Denitrification pathway from nitrate to dinitrogen gas.

Figure 3: Nitrate assimilation pathway from nitrate to ammonia.

1.2 Ammonia-forming Nitrite Reductases

The reduction of nitrite to ammonia is a six electron reduction (Equation 1) and can be performed by an enzyme containing a [4Fe-4S] cluster and siroheme as cofactors (ferredoxin-nitrite reductase, NirA) or can be achieved by one containing five to eight *c*-type hemes

(cytochrome *c* nitrite reductase, NrfA).[4–6] Some ammonia-forming nitrite reductases can also reduce sulfite to sulfide.[6]

$NO_2^- + 8H^+ + 6e^- \rightarrow NH_4^+ + 2H_2O$ (Equation 1)

Siroheme-containing Nitrite Reductase. Siroheme is a cofactor utilized in nitrite and sulfite reductases, both of which play major roles in nitrogen and sulfur assimilation.[7] Siroheme is arguably one of the most essential cofactors for life on earth. The assimilation of the majority of nitrogen and sulfur in the biosphere depends on the use of siroheme, the latter of which supplies reduced sulfur for the synthesis of the amino acid cysteine and methionine and for iron sulfur cluster biogenesis.[8] The siroheme-containing nitrite reductase contains an [4Fe-4S] cluster and siroheme as its cofactors (Figure 4).[9]

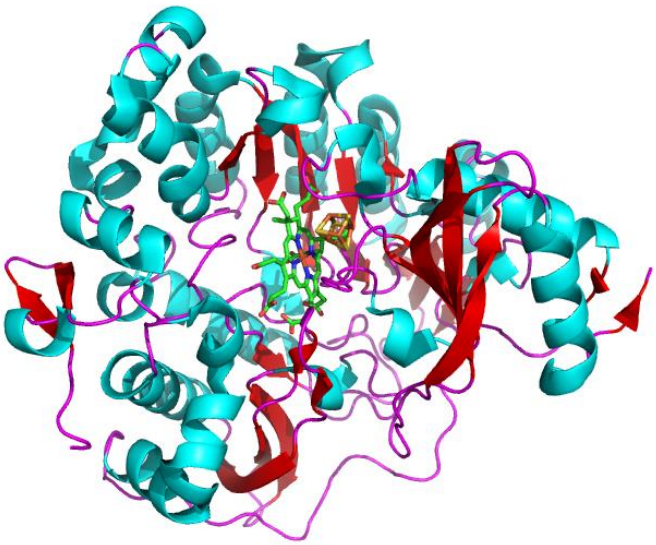

Figure 4: Spinach Nitrite Reductase with a Siroheme and [4Fe-4S] cluster as cofactors. PDB: 2AKJ

Multiheme Containing Nitrite Reductase. The multiheme-containing nitrite reductases are homodimeric, with each monomer-containing five to eight heme molecules (Figure 5).[10] In *Escherichia coli*, the multiheme nitrite-reductase has also been shown to not only perform the

six electron reduction of nitrite, but also the five electron reduction of nitric oxide to ammonia.[11]

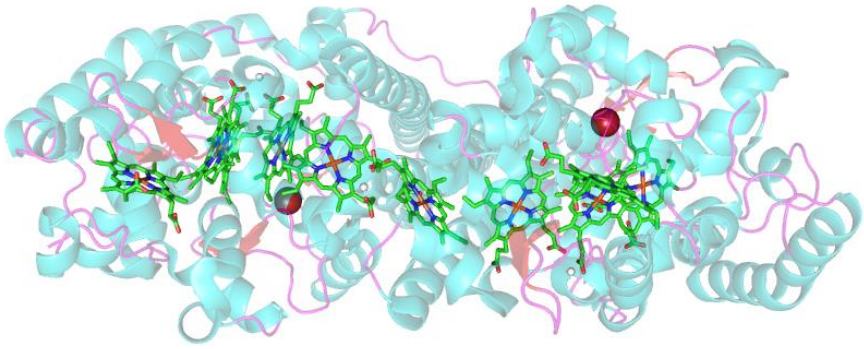

Figure 5: Multiheme nitrite reductase (PDB: 3TOR).

1.3 Nitric Oxide-forming Nitrite Reductases

The reduction of nitrite to nitric oxide is a one electron reduction (Equation 2) and can be performed by a copper-containing nitrite reductase (NirK) or a cytochrome cd_1 nitrite reductase (NirS).[6] Three examples of pathogenic bacteria that use these types of nitric oxide-forming NIRs are *Neisseria meningitidis*, *Neisseria gonorrhoeae*, and *Pseudomonas aeruginosa*.

$$NO_2^- + 2H^+ + e^- \rightarrow NO\cdot + H_2O \qquad \text{(Equation 2)}$$

Copper Containing Nitrite Reductase. Copper nitrite reductases (Cu-NIRs) are homotrimeric and contain six copper atoms/trimer. Each monomer contains one type I and one type II copper, where the nitrite binds (Figure 6).[12,13] The electrons for catalysis are donated by another copper-containing protein, pseudoazurin. The electrons are passed from pseudoazurin to the type I copper, to the type II copper, and then to nitrite, where it is reduced to nitric oxide.[12] The mechanism of the reduction of nitrite by Cu-NIRs is still not well understood.[14]

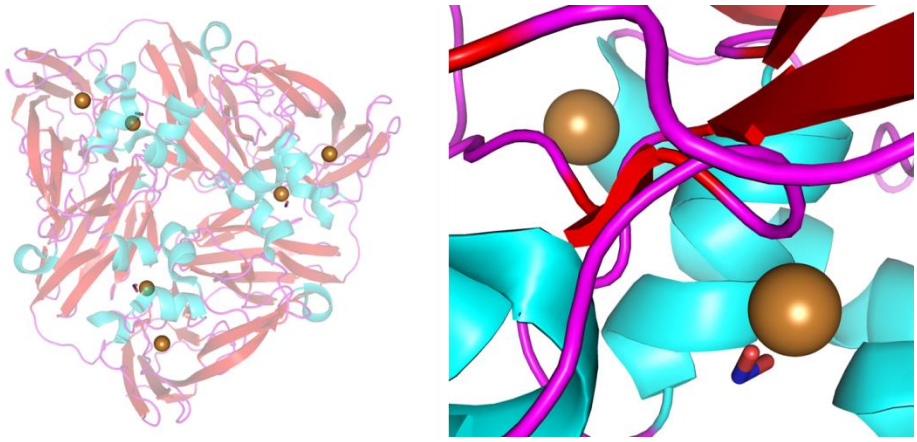

Figure 6: A) Crystal structure of Cu-NIR (PDB: 1KBV) from *N. gonorrhoeae*. B) The active site of Cu-NIR with nitrite bound to the type II Cu (PDB: 2DWS).

Cytochrome cd_1 Nitrite Reductase. Cytochrome cd_1 NIR is a homodimer (Figure 7A). Each subunit contains a covalently bound heme *c* in the alpha helical domain (Figures 7B and 7C) and a noncovalently bound heme d_1 in the beta propeller domain (Figures 7D and 7E).[15,16] Heme d_1 is a unique cofactor that is indigenous to denitrifying bacteria containing the cd_1 NIR. Electrons are passed from the heme *c* to the heme d_1 to reduce nitrite to nitric oxide.[15]

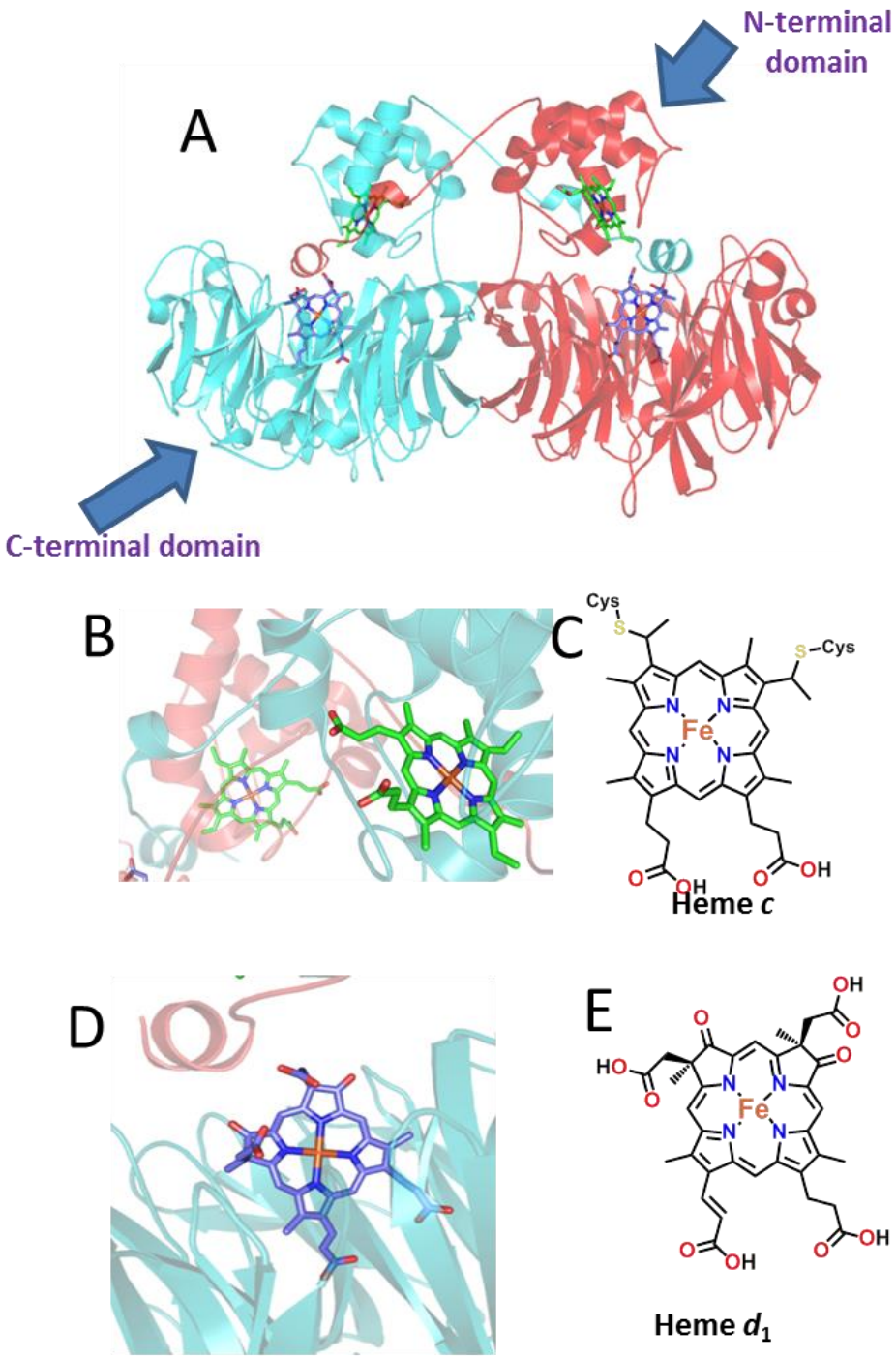

Figure 7: A) *Pseudomonas aeruginosa* nitrite reductase (NirS) (PDB 1GJQ). B) Alpha helical domain with covalently bound heme *c*. C) Structure of heme *c*. D) Beta propeller domain with noncovalently bound heme d_1. E) Structure of heme d_1.

The proposed mechanism of cytochrome cd_1 is shown in Figure 8. The heme *c* and heme d_1 are both initially in the 2+ oxidation state. Nitrite binds to the heme d_1 and is then doubly

protonated, and water leaves. The heme d_1 then donates an electron to NO forming a radical and converting heme d_1 to the 3+ oxidation state. Heme *c* then donates an electron to the heme d_1, oxidizing the heme *c* to the 3+ state and reducing heme d_1 back to the 2+ state. An electron donor then reduces the heme *c* back to the 2+ state, which results in release of the nitric oxide radical and completion of the catalytic cycle.[17]

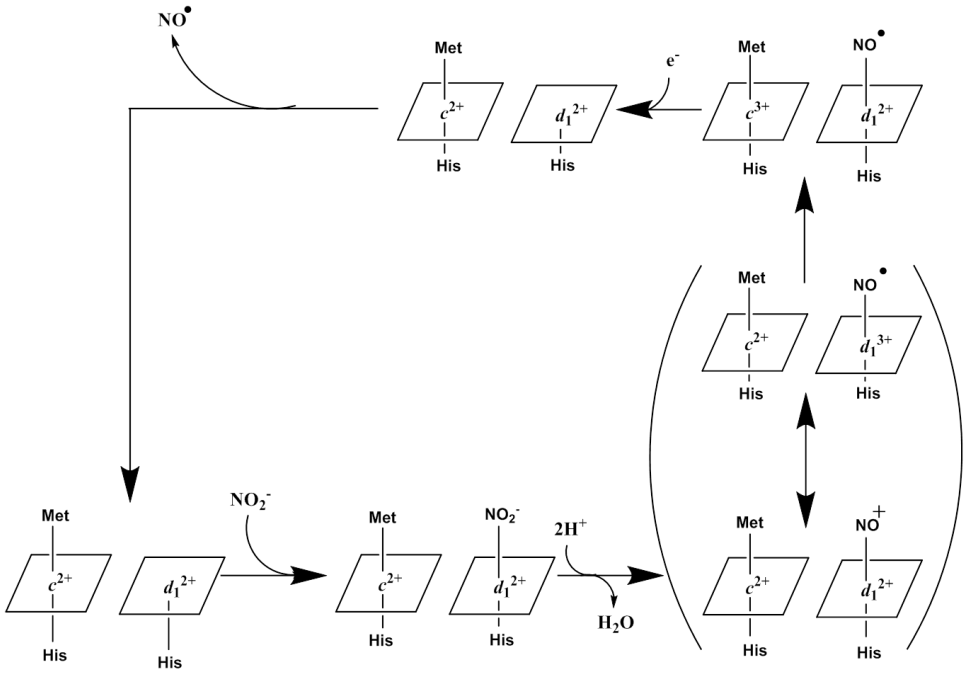

Figure 8: Proposed mechanism of cytochrome *cd*$_1$ nitrite reductase (NirS).

1.4 Nitrate-reducing Organisms

There are numerous pathogenic and nonpathogenic organisms that use either the denitrification or the nitrate assimilation pathways for the utilization of nitrate as an electron acceptor. A few notable examples of these organisms will be briefly discussed below.

Mycobacterium tuberculosis. *Mycobacterium tuberculosis* is a rod-shaped facultative anaerobe that is the leading cause of tuberculosis.[18] It has a slow generation time

(approximately 20 hours) and can form filaments and grow in clumps.[19] *M. tuberculosis* is an acid fast bacterium and contains a large amount of lipids (e.g., mycolic acid) within its cell envelope. The mycolic acid increases the virulence of this bacterium by resisting digestion by phagocytes, which can even multiply inside phagocytes. It is thought that these lipids may be responsible for their resistance to environmental stresses such as drying.[19] It has been shown that *M. tuberculosis* can survive for weeks in dried sputum and is resistant to chemical antimicrobials used as antiseptics and disinfectants.[19] This is due to the ability of *M. tuberculosis* to survive for extended periods of time in a dormant state. Dormancy is thought to be triggered by inhibition of aerobic respiration via hypoxia, nitric oxide, or carbon monoxide.[20] Nitrite reductase (NirBD) has been shown to be the most active in the host during anaerobic growth, which occurs during dormancy. Nitrite has been shown to be toxic to *M. tuberculosis* and needs to be exported or converted. The reduction of nitrite is required for detoxification.[20]

Klebsiella pneumoniae. *Klebsiella pneumoniae* is a Gram-negative bacterium that readily colonizes human mucoidal surfaces and has been shown to be responsible for a serious form of pneumonia in humans.[18,19,21] Some *Klebsiella spp.*, when invading the urinary tract, can be the underlying cause of kidney stones. This happens due to the fact that *Klebsiella spp.* reduce nitrite to ammonia under anaerobic conditions. The released ammonia can increase the pH of the urine, which causes insoluble Mg^{2+} and Ca^{2+} compounds to form.[22]

Neisseria meningitidis and *Neisseria gonorrhoeae*. *Neisseria meningitidis* and *Neisseria gonorrhoeae* are both aerobic Gram-negative cocci that usually inhabit the mucous membranes of mammals.[18,23] N. *meningitidis* is the major cause of meningococcal meningitis and *N. gonorrhoeae* is the major cause of gonorrhea. *N. gonorrhoeae* grows inside human epithelial

cells and leukocytes and uses fimbriae and Opa (an outer membrane protein) to attach to host cells. Once attached, the host cells take in the bacterium.[19] Denitrification in both *Neisseria spp.* are regulated by the amount of oxygen present, as well as the availability of nitrite and nitric oxide.[24] Nitrite reductase and nitric oxide reductase (AniA and NorB, respectively) were both shown to be required for their survival in both aerobic and microaerophilic conditions.[25]

Pseudomonas aeruginosa. *Pseudomonas aeruginosa* is a Gram-negative opportunistic human pathogen.[26,27] *P. aeruginosa* causes severe nosocomial infections and is the major pathogen in cystic fibrosis patients. It can colonize in the lungs and survive under low oxygen conditions using the denitrification pathway.[15] *P. aeruginosa* can survive and persist for years in the lungs of cystic fibrosis patients due to its adaptive mechanisms. It can form biofilms, develop mucoid phenotypes, and can lack membrane porins that are important to antibiotic diffusion.[28] A functional cytochrome cd_1 NIR is required for the virulence of *P. aeruginosa*.[26] *P. aeruginosa* biofilm dispersion and its regulation are triggered by nitric oxide, a signaling molecule and the product of NIR.[29] NO is also responsible for increased motility and the activation of genes for anaerobic metabolism and iron acquisition/metabolism.[30]

Paracoccus denitrificans. *Paracoccus denitrificans* is a Gram-negative, non-motile coccoid soil bacterium. *P. denitrificans* is a popular model organism for researchers due to its ease of genetic manipulation.[31] *P. denitrificans* grows well under aerobic conditions and expresses a respiratory chain very similar to that of the eukaryotic mitochondrion. It is a biochemically versatile organism, with a wide range of potential applications in bioremediation.[32] Some strains are capable of 'aerobic denitrification', the complete dissimilation of nitrate to dinitrogen (or nitrous oxide) under aerobic growth conditions. [32] *P.*

denitrificans also has the unusual ability to oxidize ammonia to nitrite during growth on organic energy sources ('heterotrophic nitrification').[32] This metabolic versatility allows *P. denitrificans* to survive under fluctuating (aerobic and anaerobic) conditions, using oxygen and nitrogenous oxide compounds as terminal electron acceptors.[33] Nitrite, an intermediate in the anaerobic pathway, generates a strong stress response within *P. denitrificans* causing inhibition of growth.[34]

Methanasarcina acetivorans. *Methanosarcina* is one of the most versatile and unique genera of methanogens. Most methanogens have one of the known pathways of methanogenesis and utilize no more than two substrates. However, *Methanosarcina* spp. contain all three pathways for methanogenesis (Figure 9) and are capable of utilizing no less than nine substrates, including acetate.[35] *M. acetivorans* is also unique in that no other known species from this genus contains a flagellum. Moreover, unlike other *Methanosarcina* spp. *M. acetivorans* is incapable of using H_2 to reduce CO_2 via the hydrogenotrophic pathway.[35]

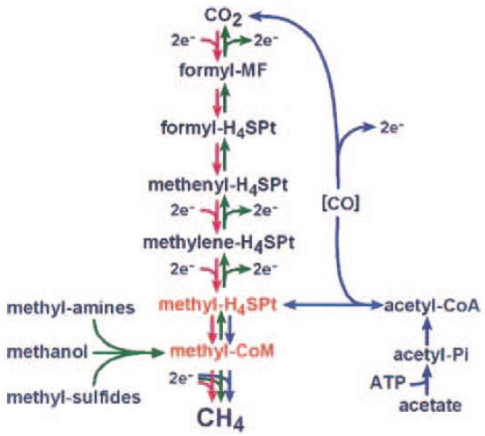

Figure 9: Three pathways for methanogenesis.[35]

It has been shown that most archaea do not possess a complete set of *hem* genes (i.e., *hemA, hemL, hemB, hemC, hemD, hemE, hemF,* and/or *hemN, hemY* or *hemG, hemH*) within

their genome to synthesize heme. However, most do have the genes required for uroporphyrinogen III formation (*hemALBCD*).[36] Many archaea contain cytochromes and other heme containing proteins, therefore it is thought they must be able to synthesize their own heme, if not via the traditional heme biosynthetic pathway, then by an alternative biosynthetic pathway. In a bioinformatics study by Storbeck *et*. *al*., they analyzed 59 archaeal genomes and found that 44 of them only possessed the genes responsible for uroporphyrinogen formation. Storbeck *et*. *al*. also noted 25 archaea were known to obtain heme containing proteins, 4 were known to produce heme d_1, and 26 possess siroheme-containing sulfite or nitrite reductases based on sequence homology.[36] It was later confirmed by Kühner *et*. *al*. that *Methanosarcina barkeri* does indeed produce heme via an alternative route, with siroheme as an intermediate.[37]

1.5 Introduction to Tetrapyrroles: The Pigments of Life

The siroheme, heme *c*, and heme d_1 coenzymes of the various types of nitrite reductase belong to the class of biomolecules known as the tetrapyrroles. Tetrapyrroles, "the pigments of life", play essential roles in multiple biological processes. These processes include, but are not limited to the aforementioned reduction of nitrite and sulfite (heme d_1 and siroheme, respectively), fatty and nucleic acid metabolism (cobalamin), oxygen and electron transport (heme), methanogenesis (coenzyme F430), and photosynthesis (chlorophyll and bacteriochlorophyll).[38]

Uroporphyrinogen III. Uroporphyrinogen III (Figure 10) is the last common precursor of all tetrapyrroles, and the first major branch point. Uroporphyrinogen III can go through four decarboxylations, two oxidative decarboxylations, and four dehydrogenations to form

protoporphyrin IX (PPIX), or it can undergo two methylations and a dehydrogenation to form sirohydrochlorin. From here, iron or magnesium can be inserted into PPIX to lead to the formation of heme and chlorophyll, or cobalt, iron, or nickel can be added to sirohydrochlorin to generate cobalamin, siroheme, or coenzyme F430, respectively.[39] One important fact about uroporphyrinogen III is that it is a light sensitive compound. An accumulation of it inside of the cell can cause photodamage and initiate the generation of reactive oxygen species (ROS) in cells and plastids.[8]

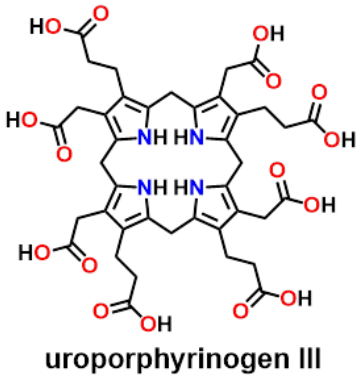

Figure 10: Structure of uroporphyrinogen III

Heme. Hemes are iron containing porphyrins that are cofactors widely found in nature (Figure 11). Heme-containing proteins vary in function, ranging from oxygen transport and storage, signal transduction, electron transfer, ligand binding, oxidative catalysis, and control of gene expression.[40] There are eight different types of hemes, designated *a*, *b*, *c*, *d*, *l*, *m*, *o*, and *s* (Figure 11).[41–44] The two most common types of hemes are heme *b* and heme *c*. Heme *b*, also known as iron-protoporphyrin IX, is commonly found in redox proteins such, as catalases and peroxidases. It is also commonly found in cytochrome *b*-type proteins (e.g., cytochrome b_5). Most proteins that contain a heme *c* are involved in electron transfer, where the heme is covalently bound by cysteine residues to the protein.[40]

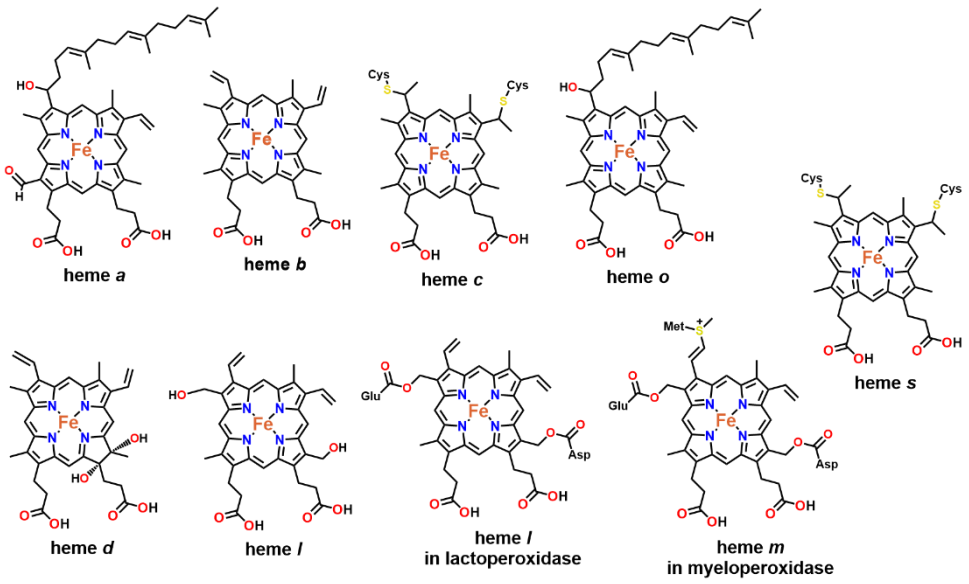

Figure 11: Structures of the known types of heme.

Siroheme. As discussed above, siroheme (Figure 12) is a cofactor in the assimilatory six electron reduction of both nitrite to ammonia and sulfite to sulfide, as well as the dissimilatory reduction of sulfite to sulfide, where siroheme is attached to a [4Fe-4S] cluster.[45] Siroheme is synthesized from uroporphyrinogen III in three steps involving methylation to form precorrin 2, dehydrogenation to form sirohydrochlorin, and ferrochelation to form the end product siroheme. In yeast, siroheme is produced by two enzymes, Met1p, a methyltransferase, and Met8p, a bifunctional dehydrogenase/ferrochelatase. Some bacteria use a trifunctional enzyme, CysG, to convert uroporphyrinogen III directly to siroheme.[46]

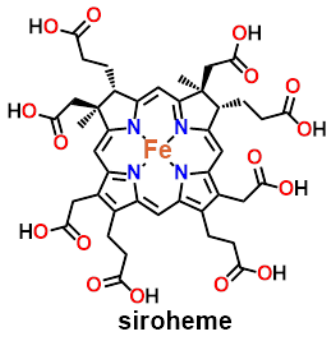

Figure 12: Structure of siroheme.

Chlorophyll. Chlorophyll is a magnesium-chelated tetrapyrrole that also contains a phytyl chain (Figure 13). This photopigment is the main component of the photosynthetic reaction center of green plants.[47] Chlorophyll biosynthesis starts off following the heme biosynthetic pathway (with uroporphyrinogen III, coproporphyrinogen III, protoporphyrinogen IX, protoporphyrin IX as common intermediates) and then branches at the metal insertion step. From protoporphyrin IX, Mg^{2+} is inserted, a methyl groups is added, an oxidative cyclization occurs to produce the exocyclic ring, the tetrapyrrole ring and a vinyl group are reduced, and the phytyl chain is added.[48,49] Chlorophyll is biosynthesized inside the chloroplast and most of the enzymes are membrane bound and form protein-protein interactions with one another.[50] As the biosynthesis progresses, the intermediates become increasingly non-polar and water insoluble with late stage intermediates being primarily protein bound in chloroplasts.[48]

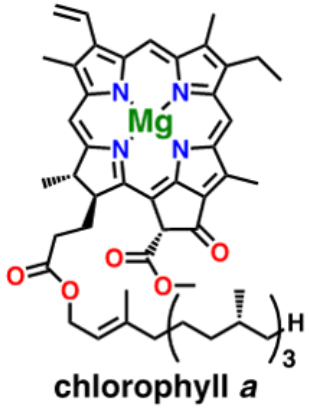

Figure 13: Structure of chlorophyll *a*.

Cobalamin. Cobalamin (Figure 14) is a complex cobalt-containing tetrapyrrole, and is one of three known coenzymes that contains a phosphodiester bond (the other two being methanopterin and coenzyme F420). Cyanocobalamin (vitamin B_{12}) is an essential nutrient for humans and animals and a deficiency in B_{12} leads to heath issues, such as pernicious anemia, stroke, dementia, and can even stunt brain and intellectual development in children.[51,52] Cobalamin can be synthesized via aerobic or anaerobic pathways.[53]

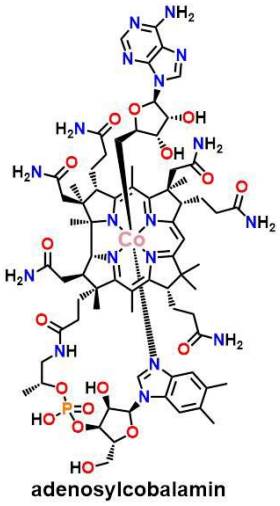

Figure 14: Structure of adenosylcobalamin (coenzyme B_{12}).

Coenzyme F430. Coenzyme F430 (Figure 15) is a nickel-containing tetrapyrrole that is an essential cofactor for the enzyme methyl-coenzyme M reductase (MCR). MCR is the key enzyme

in the biological production of methane by methanogenic archaea. All methanogenic species identified thus far have both MCR and F430,[54] suggesting its importance to the livelihood of these organisms. Until recently, the biosynthetic pathway of F430 was unknown.[55] This pathway starts from the same precursor, uroporphyrinogen III and proceeds down the sirohydrochlorin pathway, but instead of an iron or cobalt, nickel is inserted by a nickelochelatase, CfbA. This makes F430 unique, as well as the fact that it has two exocyclic rings and is the most highly reduced tetrapyrrole.[56] Many methanogens synthesize siroheme/heme and cobalamin in addition to coenzyme F430. However, some methanogens, like *M. acetivorans*, only contain a single canonical chelatase gene in their genome (i.e., *cfbA*) and it is unclear how iron and cobalt are inserted into sirohydrochlorin. In this dissertation, the possible involvement of a precorrin 2 dehydrogenase (SirC) in this process is investigated.

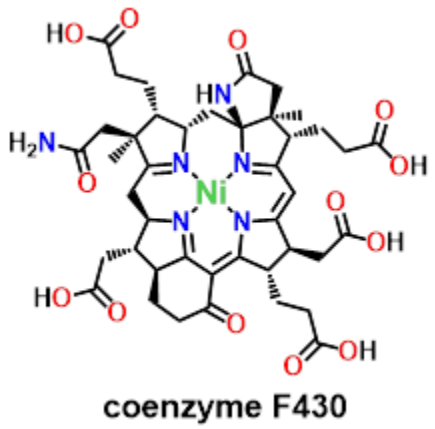

Figure 15: Structure of coenzyme F430.

Heme d_1. As previously noted, heme d_1 (Figure 16) is only made by denitrifying bacteria that contain a cytochrome cd_1 nitrite reductase (NirS) for which heme d_1 is an essential cofactor and the site of nitrite reduction.[57] Despite what the name implies, heme d_1 is not a true heme, but rather an iron-containing dioxo-isobacteriochlorin. True hemes are Fe-protoporphyrin IX

derivatives.[58] The complete biosynthetic pathway of heme d_1 is not currently known, but it has been established that siroheme is an intermediate within the pathway.[58]

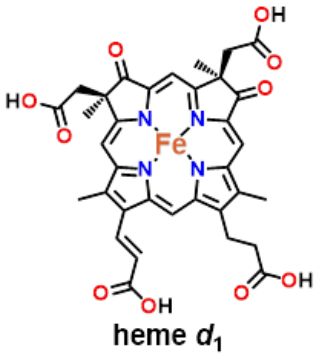

Figure 16: Structure of heme d1.

1.6 Tetrapyrrole Biosynthesis

As previously stated, uroporphyrinogen III is the last common intermediate in the biosynthesis of all tetrapyrrole biosynthesis.[39] In order to synthesize uroporphyrinogen III, 5-amino-levulinic acid (ALA), the first common intermediate in tetrapyrrole biosynthesis, is synthesized via one of two pathways. ALA may be generated from succinyl coenzyme A and glycine (the C_4 pathway) or from $tRNA^{Glu}$ (the C_5 pathway) (Figure 17). In the C_4 pathway only one enzyme,5-aminolevulinate synthase (ALAS), is required for the synthesis of ALA, while in the C_5 pathway, two enzymes, glutamyl-tRNA reductase (HemA) and glutamate-1-semialdehyde aminotransferase (HemL), are required.[58,59] The C_4 pathway is therefore comprised of a single step, the condensation of glycine and succinyl-CoA.[58] This pathway is found in fungi, animals, nonphotosynthetic eukaryotes, and members of the α subclass of the proteobacteria.[60] The C_5 pathway consist of the reduction of the glutamic acid residue on the glutamyl-tRNA, by NADPH, to form glutamate-1-semialdehyde (GSA) and the transamination of GSA to form ALA using PLP.[58] This pathway is found in plants, animals, and most bacterial species.[60,61]

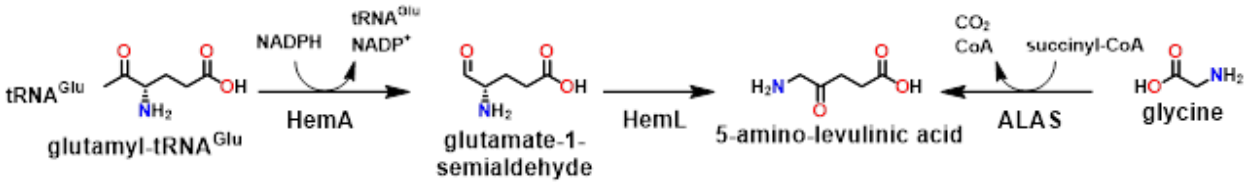

Figure 17: Biosynthetic routes for 5-Aminolevulinic acid (ALA).

HemB, 5-aminolevulinic acid dehydratase, catalyzes the condensation of two ALA molecules to form the pyrrole porphobilinogen (PBG) (Figure 18). This reaction is the first of three steps that converts ALA to the last common intermediate of all tetrapyrroles, uroporphyrinogen III (Figure 10). *E. coli* HemB is a magnesium activated zinc metalloenzyme. The zinc ion is coordinated by three cysteines within the active site of the enzyme, and is thought to help bind and activate the second ALA molecule.[62,63]

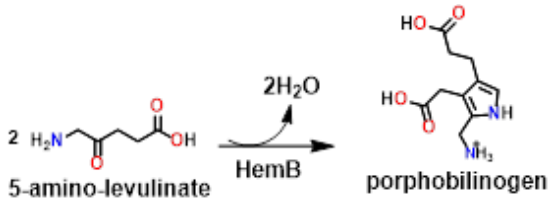

Figure 18: Conversion of 5-aminolevulinic acid to porphobilinogen by HemB.

Hydroxymethylbilane synthase, also known as HemC or porphobilinogen deaminase (PBGD), catalyzes the linkage of four porphobilinogens to form the open-chain tetrapyrrole hydroxymethylbilane (HMB) (Figure 19). HemC contains a unique cofactor, dipyrromethane, which consist of two PBG molecules linked together and covalently bound to the enzyme by Cys-242.[62,64] This cysteine residue is on a loop in domain 3 of the enzyme, and is housed within the active site in a highly conserved cleft between domains 1 and 2.[65]

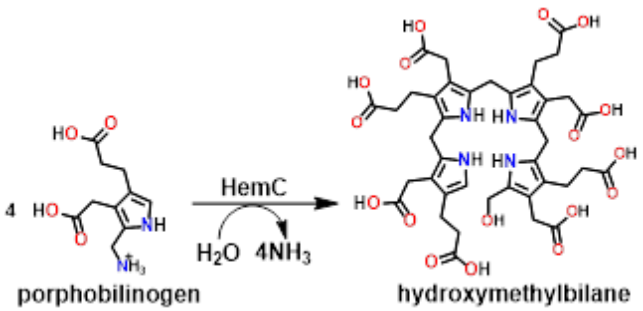

Figure 19: Conversion of porphobilinogen to hydroxymethylbilane by HemC.

The dipyrromethane cofactor is required for the correct folding and stability of the enzyme.[64] HemC uses the cofactor to initiate HMB synthesis and links four pyrroles to the end of it; HMB is then hydrolyzed off and is passed to the next enzyme in the pathway, uroporphyrinogen III synthase (HemD). HemD, catalyzes the rearrangement and cyclization of HMB to form uroporphyrinogen III (Figure 20).[39,62,66] HMB will spontaneously cyclize to uroporphyrinogen I in the absence of HemD.[39,62,67] Uroporphyrinogen I is not a precursor in any pathway and cannot be metabolized past this step. There is a human disease associated with HemD deficiency called congenital erythropoietic porphyria, where excess uroporphyrinogen I (and other oxidized derivatives such as coproporphyin I) build up in plasma, tissues, and red blood cells and leads to severe photosensitivity, with skin fragility, hypertrichois (excessive hair growth on the body, also known as werewolf syndrome), and lesions on light exposed areas.[67]

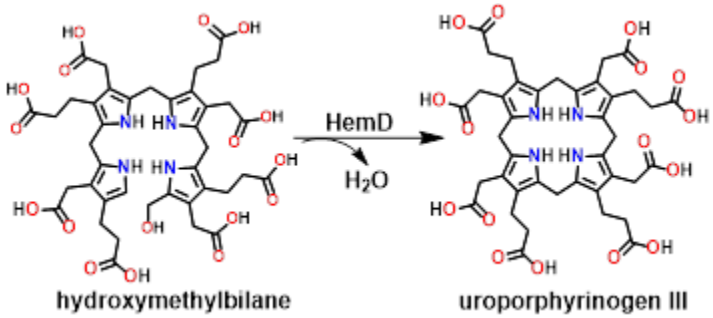

Figure 20: Conversion of hydroxymethylbilane to uroporphyrinogen III by HemD.

Heme d_1 Biosynthesis. Bacteria that contain cytochrome cd_1 nitrite reductase, NirS, have a gene cluster that is proposed to include the genes required to convert uroporphyrinogen III to heme d_1. These genes are organized similarly in the genomes of most denitrifiers as follows; *nirSECFD-LGHJN* (Figure 21).[59] The *nirDLGH* genes are all homologous to one another. In some organisms, such as *Paracoccus spp*., *nirD* and *nirL* are fused (*nirDL*) while in others, such as *Pseudomonas spp*., they are separate genes.[57] In another species, *Hydrogenobacter thermophilus*, there is a fused *nirD-L* homolog, but no *nirG* or *nirH* homolog.[68]

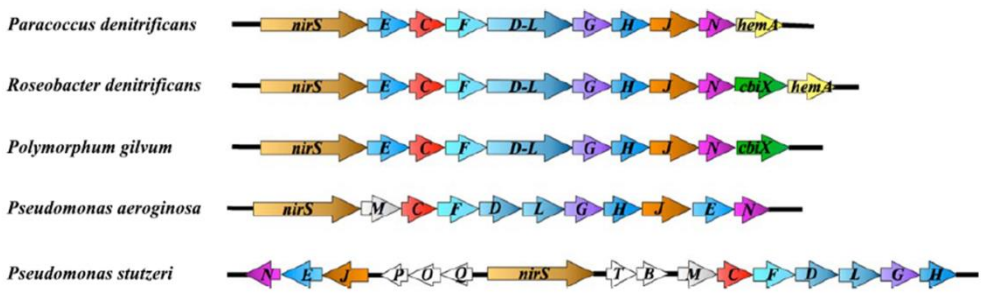

Figure 21: Comparison of the *nir* gene clusters encoding the heme d_1 biosynthetic enzymes.

Recently, siroheme has been identified as an intermediate in the heme d_1 biosynthetic pathway. In general, siroheme can be formed in several ways using additional genes not present in the *nir* cluster: 1) *cysG*, 2) *MET1* + *MET8*, or 3) *sirA* + *sirC* + *sirB* (Figure 22). These strategies differ in the use of a single, trifunctional enzyme (CysG), a monofunctional methyl transferase (Met1P) and a bifunctional dehydrogenase/ferrochelatase (Met8P), or three standalone enzymes (a methyltransferase (SirB), a dehydrogenase (SirC) and a ferrochelatase (SirB)) to carry out the methylation, dehydrogenation, and ferrochelation of uroporphyrinogen III to siroheme.

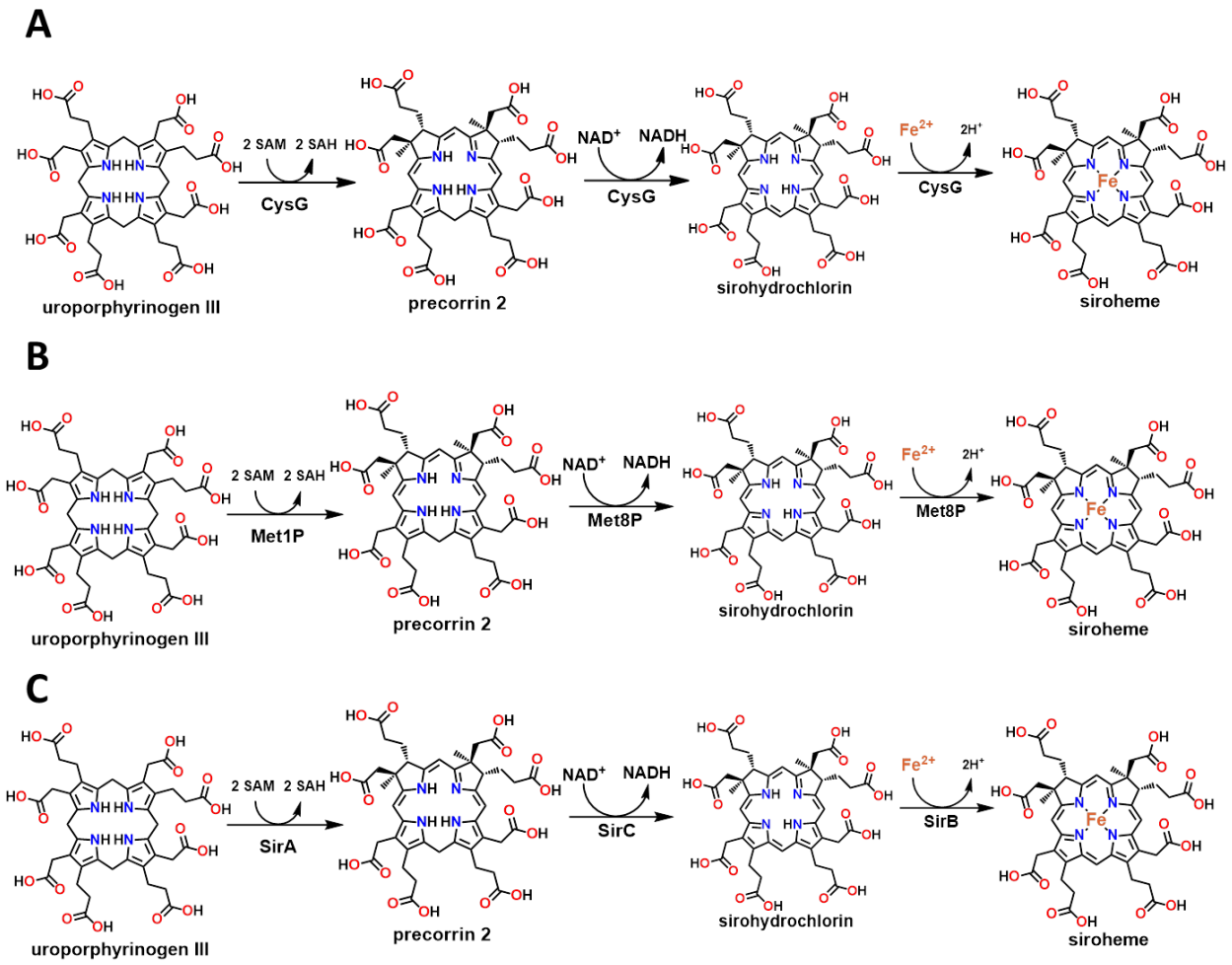

Figure 22: Different siroheme biosynthetic pathways. A) The trifunctional CysG converts uroporphyrinogen III all the way to siroheme. B) Met1P performs the methylation of uroporphyrinogen III to form precorrin 2 and the bifunctional Met8P converts precorrin 2 to siroheme. C) SirA methylates uroporphyrinogen III to precorrin 2, SirC performs the dehydrogenation to give sirohydrochlorin, and SirB inserts iron to form siroheme.

As noted, CysG is a trifunctional enzyme that uses a single polypeptide to catalyze: 1) methyl transfer to convert uroporphyrinogen III to precorrin 2, 2) dehydrogenation of precorrin 2 to sirohydrochlorin, and 3) iron insertion into sirohydrochlorin to give siroheme.[45] *E. coli* CysG contains the canonical GXGXG motif for a *S*-adenosyl-L-methionine (SAM)-binding domain. This SAM-binding motif is found in all *S*-adenosyl-L-methionine:uroporphyrinogen III methyltransferases (SUMTs) as well as in other methyltransferases. NAD^+ was also shown to be the preferred cosubstrate for the dehydrogenation reaction over $NADP^+$.[69] The N-terminal end

of CysG houses the dehydrogenases/ferrochelatase domain whereas the C-terminal end houses the methyltransferases domain (Figure 23). The dehydrogenase active site lies between the NAD^+ binding domain and the dimerization domain. It was also found that CysG is a phosphoprotein, where the phosphorylation state of a serine residue is thought to control the activity of the enzyme (Figure 23).[46]

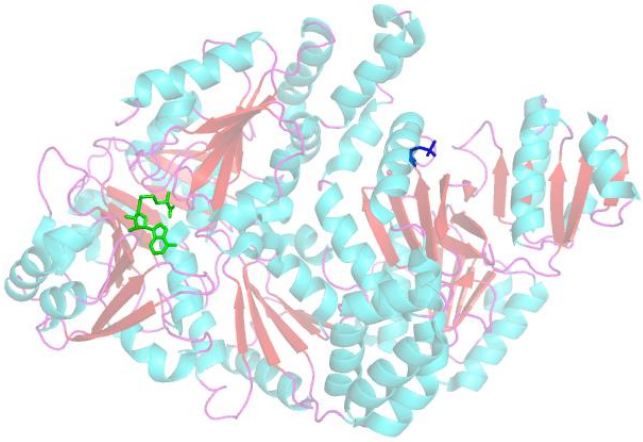

Figure 23: Crystal structure of CysG in complex with the product *S*-adenosyl-L-homocysteine (SAH bound in green) and phosphoserine shown in dark blue (PDB: 1PJQ).

Genetic analysis has shown that some species, such as *P. aeruginosa*, contain *cysG*, and if this gene is knocked out, the organism is incapable of growth under anaerobic conditions using NO_3^- or NO_2^- as a terminal electron acceptor.[70] However, other species, such as *P. denitrificans* and *Paracoccus pantotrophus*, that produce heme d_1 do not contain a homolog of *cysG* nor any homolog of a known precorrin 2 dehydrogenase (e.g., *sirC*, *MET8*) and it is unclear how they produce siroheme (Figure 24). The siroheme biosynthetic pathway in *P. denitrificans* will be investigated further in this dissertation.

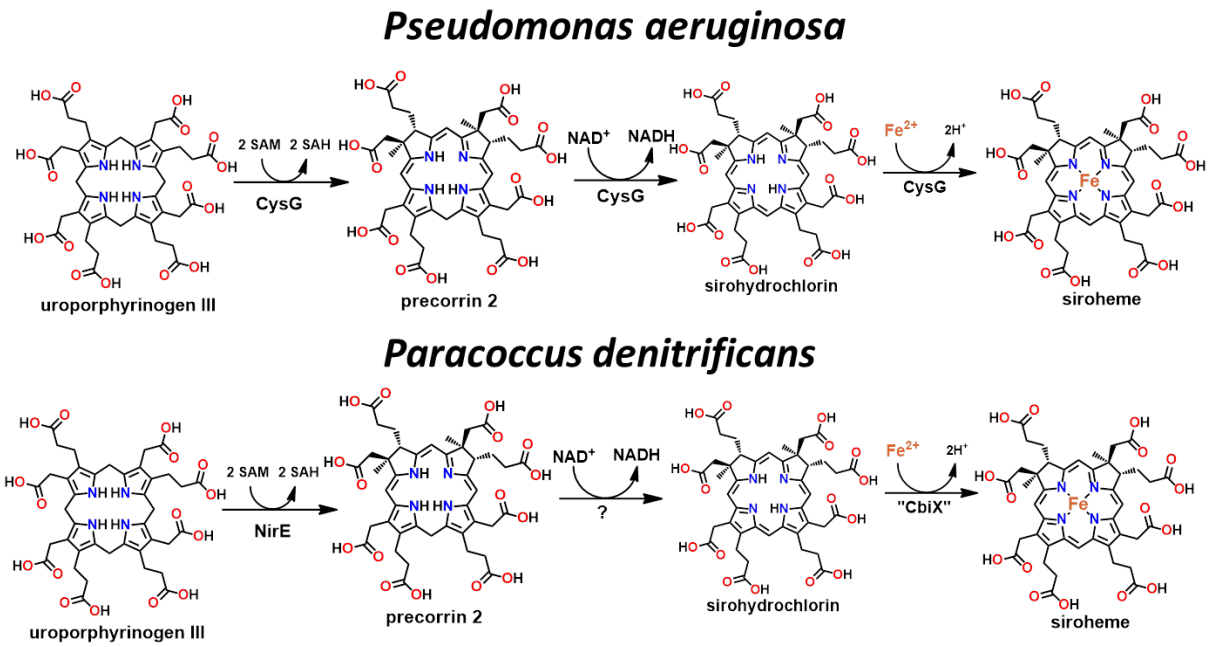

Figure 24: Biosynthetic pathways for siroheme in *Pseudomonas aeruginosa* and *Paracoccus denitrificans*.

NirE (Figure 25) is a SUMT that catalyzes the conversion of uroporphyrinogen III to precorrin 2 by the addition of two methyl groups at C2 and C7.[71] Structurally and functionally homologous enzymes are present in the cobalamin (CobA) and siroheme (SirA) biosynthetic pathways.[72] The methylation steps are kinetically slow (a k_{cat} of 38 h^{-1} has been reported[73]) and it has been shown that most SAM-dependent methylases are strongly inhibited by low concentrations of *S*-adenosyl-L-homocysteine (SAH), one of the coproducts of the reaction.[69]

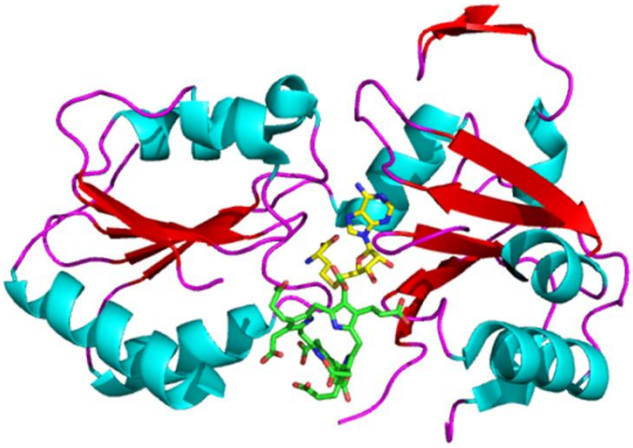

Figure 25: Crystal structure of NirE (PDB: 2YBQ).

Most SUMTs are homodimeric proteins and belong to one of two types. The first type is around 30 kDa and only has SUMT capabilities. The second type is larger and bifunctional, being capable of also catalyzing the previous or subsequent steps in the pathway (e.g., HemD + CobA or CobA + SirC). Some SUMTs show an over methylation activity and catalyze a third methylation at the C12 position, making a trimethylpyrrocorphin.[71]

SirC (Figure 26) plays an important role in siroheme and cobalamin biosynthesis. As mentioned previously, SirC catalyzes the dehydrogenation of precorrin 2 to form sirohydrochlorin. *Bacillus megaterium* SirC binds metal ions such as Co(II) and Cu(II) with the same geometry and type of ligands as in Met8p, which were found to be required for the latter's chelatase activity. Electron paramagnetic resonance (EPR) spectroscopy suggests that both *B. megaterium* Met8P and SirC bind Cu^{2+} with at least two nitrogen and two oxygen ligands. Unfortunately, the residues responsible for metal binding were not identified.[46]

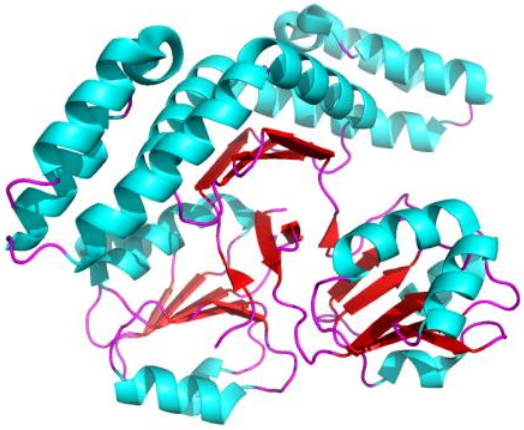

Figure 26: Crystal structure of *Bacillus megaterium* SirC (PDB: 3DFZ)

Tetrapyrrole chelatases fall into three broad categories designated Class I, Class II, and Class III. Class I chelatases require three subunits for activity as well as ATP. Class II chelatases exist as monomers or homodimers and do not require ATP. Class III chelatases are multifunctional proteins within siroheme biosynthesis (e.g., CysG and Met8p), and are homodimers that do not require the use of ATP. Sirohydrochlorin ferrochelatase (SirB), as well as its homologs in the cobalamin (CbiX) and coenzyme F430 (CfbA) biosynthetic pathways, are class II chelatases.[55,74] There are two types of CbiX, a long monomeric chelatase ($CbiX^L$) and a short homodimeric ($CbiX^S$) chelatase. $CbiX^L$ often contains a histidine rich C-terminal end that may be important for metal storage and/or metal insertion and may also contain an Fe-S cluster.[8] CbiX from *Bacillus megaterium* contains a [4Fe-4S] cluster that was detected via EPR spectroscopy.[75] A homolog of CbiX from *Paracoccus pantotrophus* (Figure 27) has been implicated in catalyzing iron insertion during the biosynthesis of siroheme and heme d_1.[45]

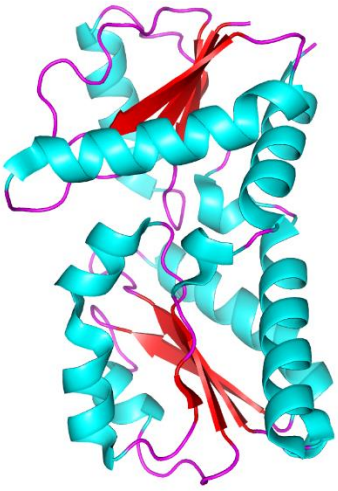

Figure 27: Crystal structure of *Paracoccus pantotrophus* CbiX (PDB: 4CCS).

The *nirDLGH* genes were initially annotated as transcriptional regulators and the encoded proteins show pairwise homology to one another. However, when *E. coli* cell lysates over producing *P. pantotrophus* NirD-LGH were incubated with sirohydrochlorin, the solution turned from purple to blue green. This reaction mixture was separated using high-performance liquid chromatography (HPLC) and was shown to contain monodecarboxysiroheme and didecarboxysiroheme as products of the reaction.[57] Therefore, NirD-LGH was proposed to be a siroheme decarboxylase (Figure 28).

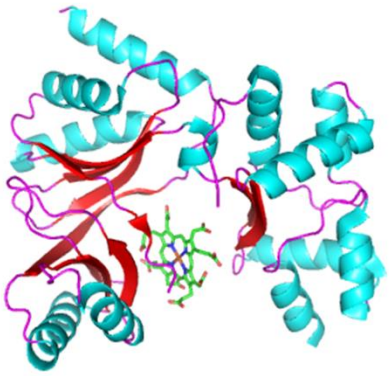

Figure 28: Structure of *H. thermophilus* NirD-L with iron-uroporphyrin III bound (PDB: 4CZC)

The exact function of NirJ is unknown; however, it is known that NirJ is a member of the radical *S*-adenosyl-L-methionine (SAM) superfamily.[76] Radical SAM enzymes carry out a wide variety of biological functions and catalyze a diverse range of chemistries.[77] All radical SAM enzymes generate a 5'-deoxyadenosyl radical that initiates catalysis.[78] Radical SAM enzymes have been structurally characterized as triosephosphate isomerase (TIM) barrels (Figure 29), and all contain at least one [4Fe-4S] cluster and SAM as a cofactor.[77,78] The [4Fe-4S] cluster is generally bound by three cysteines in a CXXXCXXC motif, which allows the 'unique' iron to bind to SAM directly via the amino group nitrogen and carboxylate oxygen.[77] Two other binding motifs have been reported; CXXCXXXXC and CXXXXXCXXC.[77]

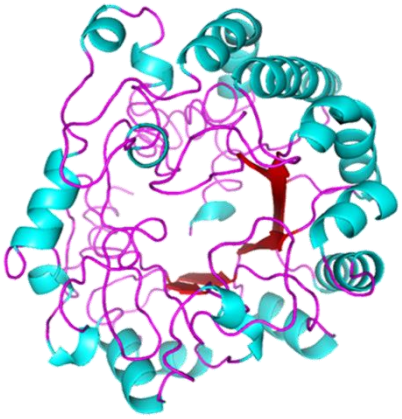

Figure 29: Predicted structure of NirJ.[79–81]

The proposed mechanism for the common initial steps of catalysis by radical SAM enzymes can be seen in Figure 30. A reduced flavodoxin/ferredoxin is thought to serve as the physiological reductant to convert the $[4Fe\text{-}4S]^{2+}$ cluster to the $[4Fe\text{-}4S]^{1+}$ state.[78,82] The $[4Fe\text{-}4S]^{1+}$ then donates an electron to the sulfonium group of SAM, which cleaves giving methionine and the highly reactive 5'-deoxyadenosyl radical. The radical then can abstract a hydrogen atom from the substrate, yielding a substrate radical and 5'-deoxyadenosine.[78]

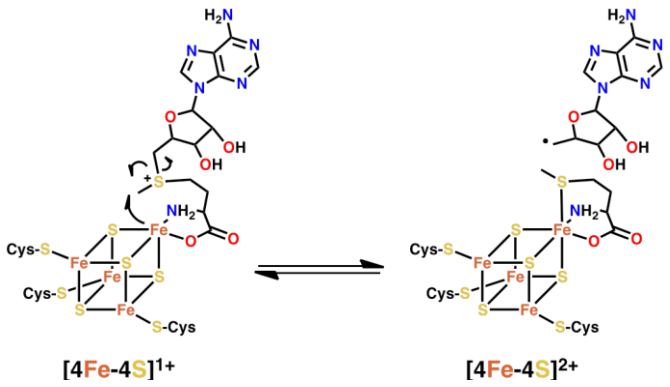

Figure 30: Reaction mechanism for the initial step of radical SAM enzymes.

In the NirJ protein, there are two possible iron-sulfur cluster binding sites. There is the traditional CXXXCXXC site in the N-terminal domain of the protein,[83] and a CXXCXXXXXC motif at the C- terminal end of the protein (Figure 31). It is proposed that the first binding site is for the [4Fe-4S] cluster and the binding of SAM.[76] Recently, evidence has been obtained that the second iron-sulfur cluster exists and is required for structural stability. The exact function this second iron-sulfur cluster plays in catalysis is unknown, but it is hypothesized that it may interact with the substrate directly, and/or may play a role in electron transfer.[84] It has been proposed that NirJ installs the ketones at C3 and C8, which would be a novel enzymatic reaction.[57] Another possibility is that NirJ performs similar chemistry as the alternative heme biosynthetic enzyme AhbD, which performs an oxidative decarboxylation of the propionate side chains of iron-coproporphyrin III to make heme, because of their high sequence similarity (57.0%).[37] Although the exact reaction that NirJ catalyzes is still unknown, evidence was recently reported that favors an O-atom insertion over the decarboxylation reaction.[84]

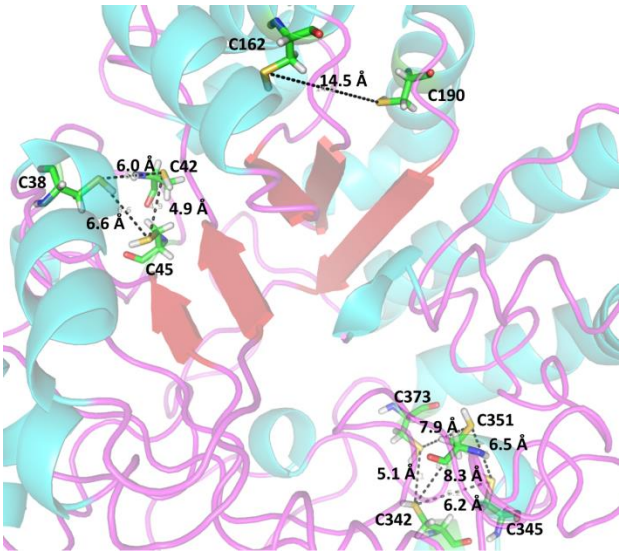

Figure 31: Predicted NirJ active site structure.[79–81]

NirF shows homology to NirS, but its function is unknown. In some organisms, NirF is predicted to be a lipo-protein potentially attached to the cytoplasmic side of the inner membrane via a lipid anchor.[85] In all NirF sequences, a highly conserved N-terminal glycine rich $GxGX_2GX_7G$ motif has been identified. This motif has also been found in other dehydrogenases involved in tetrapyrrole biosynthetic pathways, such as CysG and SirC in the siroheme pathway. Given this, it was initially proposed that NirF performs the last step in heme d_1 biosynthesis, the dehydrogenation of the propiated side chain at carbon 17,[86] but recently NirN has been shown to perform this function (*vide infra*).[87] Being one of the last enzymes in the *nir* cluster without a known function, it is probable that NirF functions as either a dehydrogenase to convert the hydroxyls installed by NirJ to ketones, or as an oxygenase to insert the ketones if NirJ functions as an oxidative decarboxylase. Based on the predicted structure (Figure 32),[79–81] NirF appears to contain a single tetrapyrrole binding site. Given this and its homology to NirS, it is possible that NirC, a cytochrome *c* protein that can accept electrons from NirS, may function as the physiological electron acceptor of NirF.

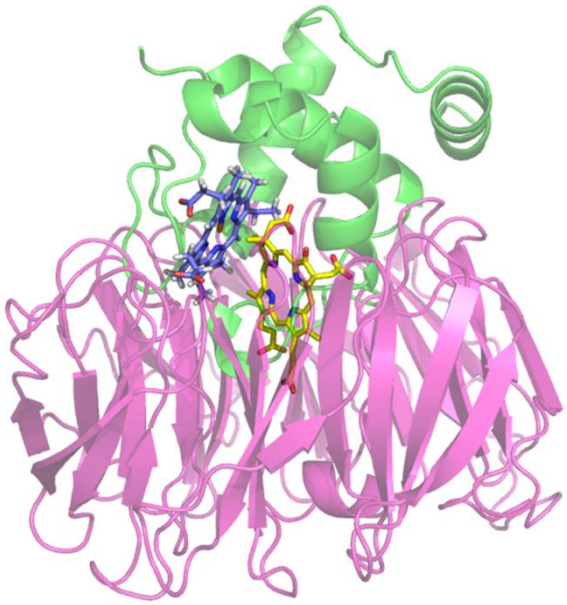

Figure 32: Predicted structure of the complex between heme d_1 (yellow) bound NirF (pink) and heme c (blue) bound NirC (green).

NirN is a soluble, periplasmic cytochrome *c* protein that contains a heme *c* cofactor and is also homologous to NirS.[85,87] It is an unusual dehydrogenase because it does not require any cofactors such as NAD^+ or FAD/FMN. It was shown that the iron of heme d_1 was reduced during the conversion of dihydro-heme d_1 to heme d_1 (Figure 33). It was also shown that the covalently bound heme *c* was also reduced, suggesting that NirN catalyzes the formation of the acrylate side chain at carbon 17 using an electron bifurcation mechanism. When NirN was knocked out, the double bond was not inserted. NirN has also been shown to bind heme d_1 *in vitro* and transfer it to NirS.[87]

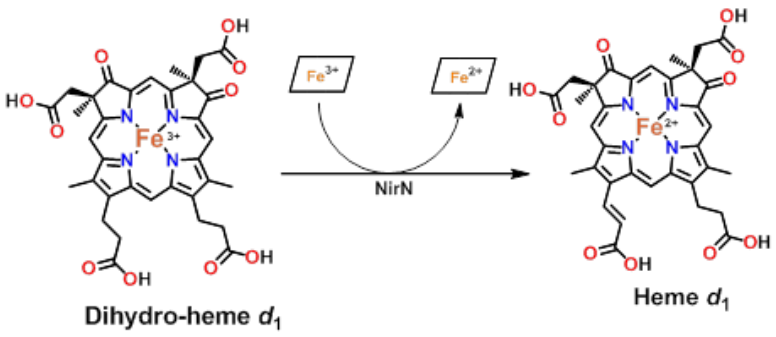

Figure 33: Conversion of dihydro-heme d_1 to heme d_1 by NirN.

1.7 Brief Introduction to Chapters

Chapter 2: An investigation into the Potential Dual Role of SirC in the Biosynthesis of Heme and Siroheme in Methanosarcina acetivorans C2A. Metal ions are inserted into tetrapyrroles by different chelatase enzymes and sometimes by different classes of chelatases depending on the pathway.[74] *M. acetivorans* contains only one class II chelatase, yet produces three different metallated tetrapyrroles (heme/siroheme, cobalamin, and coenzyme F430).[74] The SirC from *M. acetivorans* shows homology to the bifunctional dehydrogenase/ferrochelatase domain of *E. coli* CysG. Therefore, we investigated the potential dual function of this enzyme.

Chapter 3: Determining the function of Pden_1323. As previously mentioned, the genome of *P. denitrificans* lacks a precorrin 2 dehydrogenase although it synthesizes siroheme and heme d_1. Also, heme d_1 biosynthesis starts inside the cytoplasm and is completed in the periplasm, and it is unclear how the intermediate is transported from one to the other.[58] When looking at potential enzymes in *P. denitrificans* that could perform either/both of these tasks, Pden_1323 looked to be a potential target. Pden_1323 is a protein of unknown function that is annotated as a pyridoxamine 5'-phosphate oxidase-related, FMN-binding protein and has

homology to the heme utilization protein HutZ. Moreover, the gene encoding Pden_1323 is found within a gene cluster containing ABC transporter proteins, which have been shown to be capable of transporting tetrapyrroles such as cobalamin and heme. However, in this chapter we show that Pden_1323 is actually a non-canonical heme oxygenase.

Chapter 4: Determining the function of Pden_2333. In some denitrifying organisms, such as *Paracoccus denitrificans*, a CbiX homolog is needed for heme d_1 biosynthesis and catalyzes the ferrochelation of sirohydrochlorin to form the intermediate siroheme. In *P. denitrificans*, the *cbiX* gene is found clustered with a gene encoding a hypothetical protein, Pden_2333, that is sometimes fused with CbiX in other organisms. In this chapter, we investigate several proposed functions for Pden_2333 and present data that suggests it is a novel bacterioferritin that can bind heme and store and release iron ions.

Chapter 2: An Investigation into the Potential Dual Role of SirC in the Biosynthesis of Heme and Siroheme in *Methanosarcina acetivorans* C2A

2.1 Introduction

Methanogens play an important role in the environment due to their capability of performing methanogenesis, a major part of the global carbon cycle. They are also important in waste treatment plants and can be used to produce alternative fuel sources.[88] This can be done by the production of methane from one of three different methanogenic pathways. Methane can be produced via carbon dioxide reduction, from acetate, or from methylated compounds such as methyl-amines. *Methanosarcina acetivorans* C2A is a metabolically diverse methanogen that contains all three pathways.[35] Contributing to global warming and climate change, methane is a damaging greenhouse gas whose production needs to be fully studied and understood.[88]

Methanogens use tetrapyrroles as enzymatic cofactors in their energy production reactions. These tetrapyrroles include coenzyme F430 and corrinoids as the major components, as well as heme and siroheme in smaller amounts in some methanogens. These four cofactors are derived from uroporphyrinogen III, which is the last common biosynthetic precursor of all tetrapyrroles (Figure 34). Uroporphyrinogen III is then converted to sirohydrochlorin, which serves as a branch-point intermediate within the coenzyme F430, corrinoid, siroheme, and alternative heme biosynthetic pathways (Figure 34).[46,57,74] It is generally thought that there is a

unique chelatase performing each metal insertion (i.e., one for Ni, Co, and Fe, respectively).[74] After searching the genome of *M. acetivorans*, only one canonical chelatase homolog was found, a 'small' class II chelatase with homology to sirohydrochlorin cobaltochelatase (*cbiX*). This gene was recently shown to be part of the coenzyme F430 biosynthesis (*cfb*) gene cluster and to catalyze the insertion of Ni into sirohydrochlorin.[55] The question then arose, does this class II chelatase homolog chelate multiple metals to make each of the needed cofactors, or are there other unidentified genes that are involved in these processes? Like bacteria, some methanogens cluster their genes, and after looking at several gene clusters within *M. acetivorans*, a precorrin 2 dehydrogenase (*sirC*) homolog stood out.

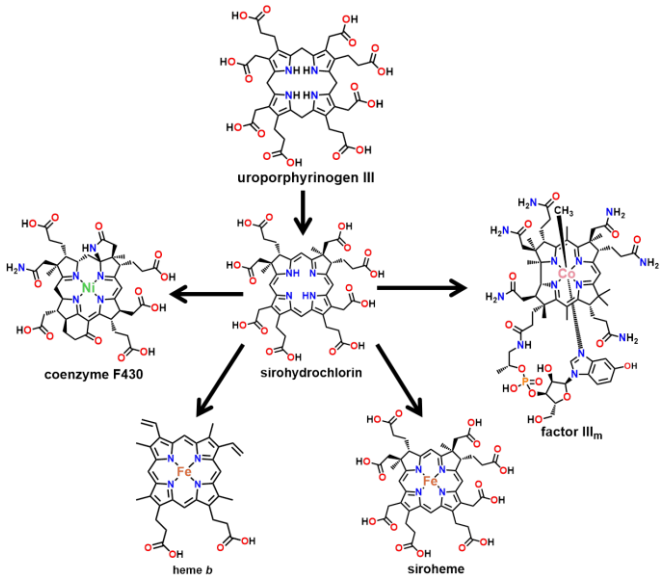

Figure 34: Sirohydrochlorin is the branch point to different metallated tetrapyrroles in methanogens.

M. acetivorans contains two gene clusters for the alternative heme biosynthesis (*ahb*) pathway, which contain a *sirA* and a *sirC* homolog (Figure 35). SirA homologs in other organism have been shown to be *S*-adenosyl-L-methionine (SAM)-dependent uroporphyrinogen III methyl transferases (SUMTs), and the function of SirA in *M. acetivorans* was recently confirmed by

Zheng et. al.[55] There is not a chelatase homolog within this alternative heme biosynthetic gene cluster. However, SirC is homologous to the N-terminal end of *Escherichia coli* CysG, which is a multifunctional dehydrogenase/ferrochelatase domain. It was also recently confirmed by Zheng et al, that SirC is indeed a NAD(P)$^+$-dependent precorrin 2 dehydrogenase.[55] Therefore, this study will investigate whether SirC plays a dual role as a bifunctional dehydrogenase/ferrochelatase enzyme in the biosynthesis of heme and siroheme in *M. acetivorans*.[55]

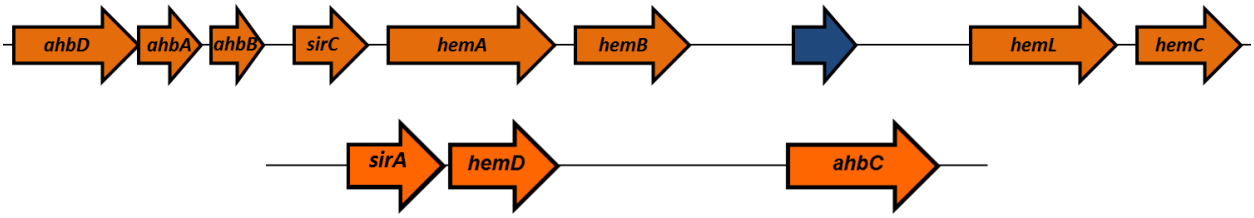

Figure 35: Alternative heme biosynthesis (*ahb*) gene clusters, from *M. acetivorans*. The first cluster contains heme synthase (*ahbD/MA_0573*), siroheme decarboxylase (*ahbA/MA_0574* and *ahbB/MA_0575*), precorrin 2 dehydrogenase (*sirC/MA_0576*), 5'-aminolevulinic acid synthase (*hemA /MA_0577*), porphobilinogen synthase (*hemB/MA_0578*), glutamate-1-semialdehyde aminotransferase (*hemL/MA_0581*), and hydroxymethylbilane synthase (*hemC /MA_0582*). *MA_0579* (in blue) is annotated as an integrase and is not thought to be a part of the alternative heme biosynthetic pathway. The second cluster contains uroporphyrinogen III methyltransferase (*sirA /MA_3033*), uroporphyrinogen III synthase (*hemD /MA_3034*), and Fe-coproporphyrin synthase (*ahbC /MA_3035*).

2.2 Methods and Materials

Expression Vector Construction. The genes *hemCD* were amplified via polymerase chain reaction (PCR) from the genomic DNA of *E. coli* BL21 (DE3) (New England Biolabs). The genes *sirAC* as well as *cfbA* were amplified from the genomic DNA of *M. acetivorans* C2A (DSM-2834). The primers for *hemCD* and *sirAC* were from Sigma-Aldrich and were designed to incorporate a NdeI restriction site at the 5' end and a XhoI restriction site at the 3' end of the gene. The *cfbA* primers were designed to incorporate a NdeI and a BamHI site at the 5' and 3' ends of the gene, respectively. The genes were amplified using Phusion High-Fidelity DNA Polymerase according

to manufacturer's protocol. The PCR products as well as the pET-28b(+) vector were subjected to restriction enzyme digestion according to the manufacturer's protocol. The genes were purified using a Lonza FlashGel™ DNA Cassette (Basel, Switzerland) and recovered with an Omega BIO-TEK E.Z.N.A.® Gel Extraction Kit (Norcross, Georgia) following the protocol provided by the manufacturer. The linearized pET-28b(+) vector was purified using an Omega BIO-TEK E.Z.N.A.® Cycle Pure Kit following the protocol provided in the manual. The genes were individually ligated with the digested pET-28b(+) using T4 DNA Ligase (NEB) following the manufacturer's protocol. The ligated mixtures were then transformed into *E. coli* TOP10 cells and plated on Lysogeny Broth(LB) agar plates containing 50 μg/mL kanamycin. Colonies were picked, grown in liquid LB medium, and plasmids were isolated using the Omega BIO-TEK E.Z.N.A.® Plasmid Mini Kit. The purified expression vectors were then sequenced verified by the Genomics and Sequencing Laboratory (GSL) at Auburn University or by Eurofins Genomics (Louisville, KY).

Expression and Purification of Enzymes. Each expression vector was overexpressed in *E. coli* BL21(DE3) cells. HemC was grown at 37 °C until an OD_{600} ~ 0.5 was reached and then the temperature was lowered to 15 °C. The culture was then induced with 40 μM isopropyl β-D-1-thiogalactopyranoside (IPTG) and 10 μM 5-aminoleculinic acid (ALA). The cells were incubated at 15 °C for 8 hours. HemD was incubated at 37 °C until and OD_{600} ~ 0.6 was reached and was then induced with 40 μM IPTG and incubated for 8 hours at 18 °C. SirAC and CfbA were grown at 37 °C until an OD_{600} ~ 0.5 was reached. SirAC was then induced with 100 μM IPTG and CfbA was induced with 400 μM IPTG. The cultures were then incubated for 12 hours at 18 °C.

The cells were then centrifuged at 15,970 x g at 4 °C. The HemC purification took place in a Coy anaerobic chamber using degassed buffers. The supernatant was decanted and the cells were re-suspended in 500 mM sodium phosphate buffer, pH 8.0, containing 300 mM NaCl, 5 mM imidazole, lysozyme (1 mg/mL), and Ameresco's Protease Inhibitor Cocktail. The cells were then sonicated and centrifuged at 104,600 x g for 20 minutes at 4 °C. The supernatant was applied to a Bio-Rad Econo-Pac Column, packed with Ni-charged Profinity Immobilized Metal Affinity Chromatography (IMAC) Resin. HemCD and SirAC were washed with 50 mM sodium phosphate buffer, pH 8.0, containing 300 mM NaCl and 5 mM imidazole, and the wash was collected. The protein was then eluted from the column using 50 mM sodium phosphate buffer, pH 8.0, containing 300 mM NaCl and 500 mM imidazole. The protein was then spin concentrated/buffer exchanged into 100 mM Tris buffer, pH 8.0. CfbA was washed with 100 mM Tris-HCl buffer, pH 8.0, and then thrombin (80 units/mL IMAC resin) was applied to the column. The column was capped at the top and bottom and incubated at 25 °C while shaking for 16 hours. CfbA was then eluted from the column by passing 100 mM Tris-HCl buffer, pH 8.0, through the column. The eluate was then applied to a Benzamidine Sepharose 4 Fast Flow column (GE Healthcare) to remove the thrombin. The protein was then spin concentrated/buffer exchanged into 100 mM Tris buffer, pH 8.0.

SirC Ferrochelation Assay. The ferrochelation activity of SirC was examined by performing an anaerobic reaction in a MBRAUN LABmaster glove box. The initial reaction mixture contained the following components: HemC (1.77 µM), HemD (2.16 µM), SirA (4.33 µM), SirC (0.364 mg/mL), porphobilinogen (PBG) (884 µM), *S*-adenosyl-L-methionine (SAM) (1 mM), $NAD(P)^+$ (1mM), $MgCl_2$ (40 µM), and made to 1 mL with 50 mM Chelex-treated Tris-HCl

buffer, pH 8.0. After 12 hours, the reaction was split into 13 smaller reactions. Reactions 1-6 contained constant enzyme concentration and increasing iron concentrations, and reactions 7-13 contained constant iron concentration and increasing SirC concentrations. The final iron concentrations of reactions 1-6 are as follows: 0 μM, 10 μM, 20 μM, 30 μM, 40 μM, and 50 μM, respectively. Reactions 7-13 contained 30 μM iron and the following SirC concentrations: 0 mg/mL, 0.5 mg/mL, 1 mg/mL, 1.5 mg/mL, 2 mg/mL, 2.5 mg/mL, and 3 mg/mL, respectively. Bovine serum albumin (BSA) was also added to these reactions to make the final concentration of SirC + BSA 3 mg/mL. The reactions mentioned above were performed at different temperatures as follows: 1) 37 °C initial 12-hour reaction followed by four additional hours at 37 °C, 2) 37 °C initial 12-hour reaction followed by four additional hours at 25 °C, and 3) 25 °C initial 12-hour reaction followed by four additional hours at 25 °C.

Uroporphyrinogen III Spontaneous Metal Chelation Assay. An initial HemCD reaction was performed to produce uroporphyrinogen III. The initial reaction contained the following components: HemC (1.77 μM), HemD (2.16 μM), $MgCl_2$ (40 μM), and PBG (884 μM) in Chelex-treated 50 mM Tris-HCl buffer, pH 8.0 buffer. After incubating at 37 °C for 12 hours, the reaction was boiled at 95 °C for 20 minutes and then centrifuged for 20 minutes to pellet the denatured proteins. The reaction was then split into six different reactions where the spontaneity of metal chelation was examined. One of the six reactions was a control reaction without metal, while the other five tested the chelation of nickel sulfate, iron sulfate, cobalt chloride, zinc sulfate, and copper sulfate by uroporphyrinogen III with the final concentration of each metal being 123 μM. The reaction mixtures were analyzed by UV-visible absorption

spectroscopy, and then the reactants and products of each sample were extracted with methanol and analyzed using high-performance liquid chromatography (HPLC).

Precorrin 2 Spontaneous Metal Chelation Assay. An assay was also used to investigate the spontaneous chelation of metals by precorrin 2. The initial reaction conditions were as follows: HemC (1.77 µM), HemD (2.16 µM), SirA (4.33 µM), PBG (884 µM), SAM (1 mM), and $MgCl_2$ (40 µM), in Chelex-treated 50 mM Tris-HCl buffer, pH 8.0. After incubating at 37 °C for 12 hours, the reaction was boiled, centrifuged, and split into six different reactions, one being a control reaction and the other five testing for the chelation of nickel, iron, cobalt, zinc, and copper by precorrin 2, with the final concentration of each metal being 123 µM. The reaction mixtures were analyzed by UV-visible absorption spectroscopy, and then the reactants and products of each sample were extracted with methanol and analyzed using HPLC.

Sirohydrochlorin Spontaneous Metal Chelation Assay. A SirC reaction was performed to produce sirohydrochlorin. The reaction mixture contained the following components: HemC (1.77 µM), HemD (2.16 µM), SirA (4.33 µM), SirC (15 µM), PBG (884 µM), SAM (1 mM), $NAD(P)^+$ (1mM), $MgCl_2$ (40 µM), and made to 1 mL with 50 mM Chelex-treated Tris-HCl buffer, pH 8.0. The mixture was incubated at 37 °C for 12 hours. The reaction was then boiled at 95 °C for 20 minutes, centrifuged for 20 minutes to precipitate the denatured proteins, and split into seven reactions, one being a control reaction and the other six testing for the spontaneous chelation of iron, nickel, cobalt, zinc, manganese, and copper. The final concentration of each metal in the assay was 123 µM. The reaction mixtures were analyzed by UV-visible absorption spectroscopy, and then the reactants and products of each sample were extracted with methanol and analyzed using HPLC.

Spontaneous Chelation Assay of Metals at Physiological Concentration. A SirC reaction was performed as described above to produce sirohydrochlorin. The solution was then split into five reactions, one being a control, and the other four being mixed with a metal ion solution, such that the final concentration of each metal ion was at its estimated cytosolic value (Table 1).[89,90] In the first of the latter reactions, only the metal ion solution was added to the SirC reaction in Chelex-treated 50 mM Tris-HCl buffer, pH 8.0. In the second reaction, the metal ion solution and additional purified SirC (15.2 µM) were added. In the third, the metal ion solution and purified CfbA (the recently identified sirohydrochlorin nickelochelatase from *M. acetivorans*) (6.6 µM) were added. In the final reaction, the metal ion solution and purified SirC and CfbA (15.2 µM and 6.6 µM, respectively) were added.

Table 1: Concentration of metal ions in the cytoplasm of a cell.[89,90]

Metal Ions	Cytoplasmic Ion Concentration (M)
Ca^{2+}	5×10^{-8}
Mg^{2+}	1×10^{-3}
Mn^{2+}	1×10^{-7}
Fe^{2+}	5×10^{-6}
Cu^{2+}	1×10^{-15}
Zn^{2+}	1×10^{-11}
Ni^{2+}	1×10^{-9}
Co^{2+}	1×10^{-8}

High-performance Liquid Chromatography Analysis. High-performance liquid chromatography (HPLC) analysis was performed on an Agilent Infinity 1260 HPLC with an Agilent Poroshell 4.6 x 150 mm C18 column and data were analyzed using the Agilent ChemStation Software. The method consisted of a gradient of solvent A (water + 0.5% formic acid) and solvent B (acetonitrile + 0.5% formic acid) with a flow rate of 1.0 mL/min. The column

was equilibrated with 100% A and remained isocratic for 2 minutes after sample injection. Solvent B was increased to 20% over 3 minutes and remained isocratic for 5 minutes. Solvent B was then increased to 25% over 5 minutes and remained isocratic for 5 minutes. Solvent B was then increased to 30% over 5 minutes and subsequently to 100% over 2 minutes. Finally, solvent B remained isocratic for an additional 1 minute. Solvent B was then decreased to 0% over 1 minute. The total run time of the solvent gradient program was 30 minutes. A detection wavelength of 400 nm was selected on the diode array detector.

Mass Spectrometry Analysis. Samples were also subjected to mass spectrometry (MS) analysis on a Waters Acquity UPLC Q-TOF Premier mass spectrometer equipped with an identical Agilent Poroshell 4.6 x 150 mm C18 column and the data were analyzed using the Waters MassLynx software. The method utilized an identical solvent A and B as described above for HPLC analysis with a 0.2 mL/min flow rate. The method consisted of a linear gradient from 100% solvent A to 100% solvent B over the course of 15 minutes. The electrospray ionization (ESI) mass detector was configured to positive ion mode with scanning between 800 and 1000 *m*/*z*. The inline Waters TUV detector was also engaged at 400 nm to verify that the peaks detected by MS analysis corresponded to the same peaks observed in the above HPLC analysis.

2.3 Results

When incubating SirA and SirC with SAM, $NAD(P)^+$, and uroporphyrinogen III (prepared in situ using HemCD and PBG), the reaction mixture turned a deep purple color (Figure 36). This purple color is indicative of sirohydrochlorin formation.[57] After methanol extraction of the assay mixture, the tetrapyrrole intermediates were separated via reverse phase HPLC using a C18 column. A large peak at 15.9 minutes and a smaller peak at 16.9 minutes were detected (Figure

36) and further analyzed by mass spectrometry. Both species were found to have a *m*/*z* of 863.30 (Figure 37), which corresponds to the predicted mass of sirohydrochlorin.[62,91] The formation of sirohydrochlorin confirms the function of the SirA and SirC homologs from *M. acetivorans* as a SUMT and a precorrin 2 dehydrogenase, respectively.

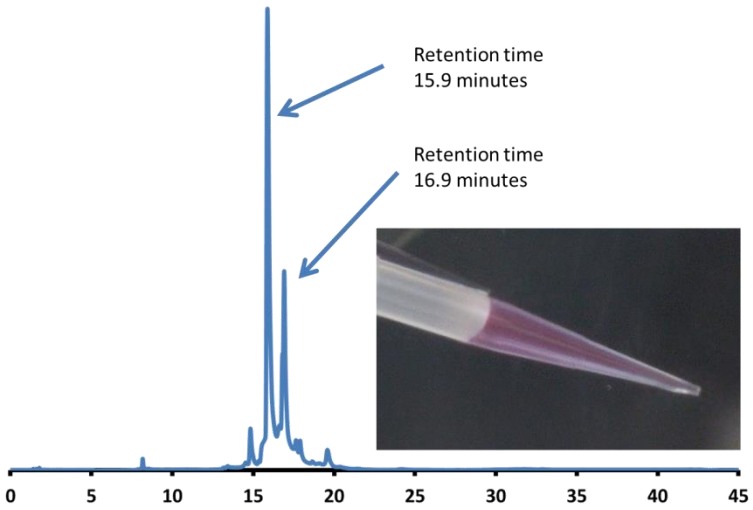

Figure 36: HPLC trace of enzymatically synthesized sirohydrochlorin. Inset: Picture of the sirohydrochlorin reaction mixture.

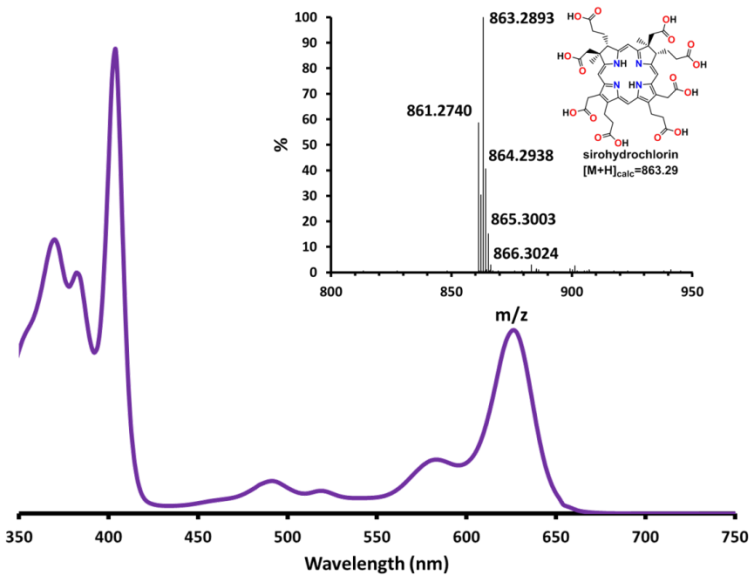

Figure 37: UV-visible absorption spectrum of HPLC purified sirohydrochlorin. Inset: Mass spectrum of purified sirohydrochlorin.

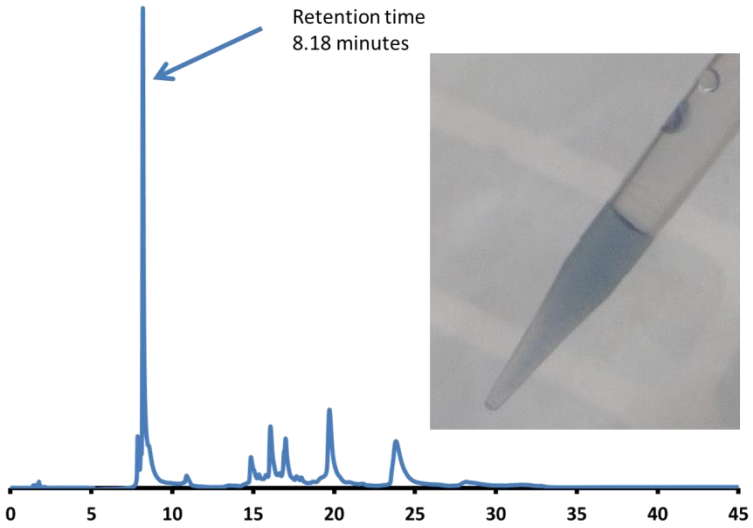

Figure 38: HPLC trace of siroheme generated via the ferrochelation of sirohydrochlorin. Inset: Picture of the siroheme reaction mixture.

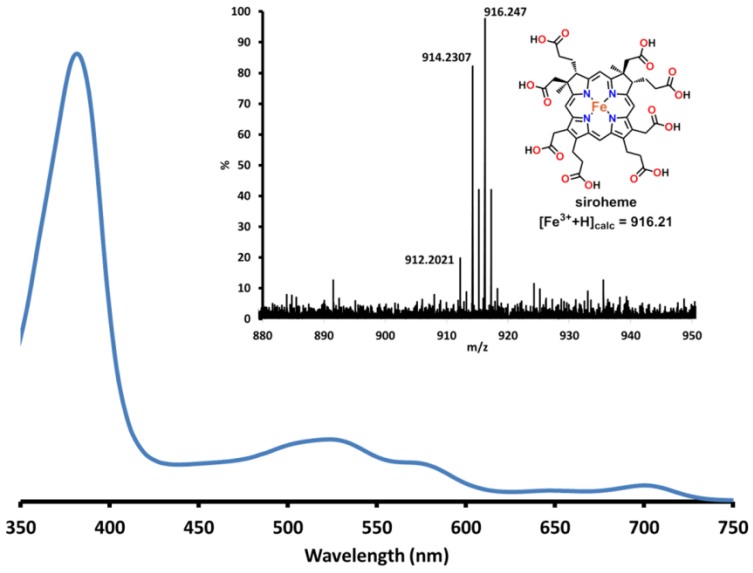

Figure 39 UV-visible absorption spectrum of HPLC purified siroheme. Inset: Mass spectrum of purified siroheme.

After a 12-hour reaction to produce sirohydrochlorin, the assay mixture was incubated with different concentrations of iron. As the iron concentration increased, the peak at 15.9 minutes diminished and a new peak at 8.2 minutes formed (Figure 40A). The peak at 8.2 minutes was further analyzed by UV-visible spectrophotometry and MS and was confirmed to be siroheme (i.e., Fe-sirohydrochlorin, Figure 39).[62,91]

To distinguish between spontaneous or enzyme catalyzed chelation, sirohydrochlorin was generated and the iron concentration was kept constant while varying the SirC concentration. Surprisingly, as the SirC concentration increased, the yield of siroheme diminished (Figure 40B).

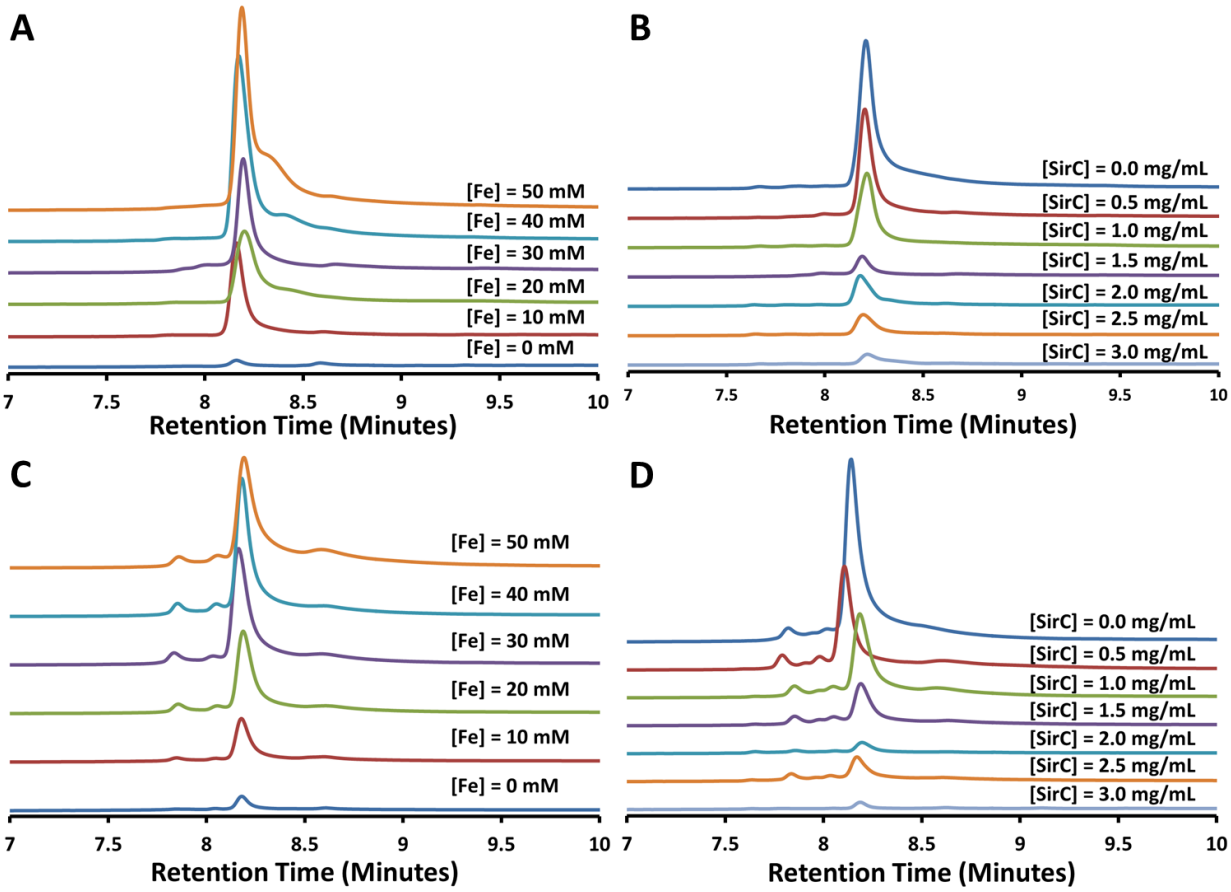

Figure 40: HPLC analysis of the effects of iron and SirC concentration on siroheme formation. Sirohydrochlorin was enzymatically synthesized and the reaction mixture was incubated with increasing concentrations of iron A) or SirC B). The sirohydrochlorin reaction was also boiled and centrifuged to inactivate and remove the biosynthetic enzymes and the ferrochelation assays were repeated with increasing concentration of iron C) or SirC D).

To control for the possible formation of additional sirohydrochlorin during the 4-hour chelation reaction, the 12 hour sirohydrochlorin reaction was boiled and centrifuged to remove all of the enzymes present in the assay mixture. The remaining assay mixture was then split into subsequent reactions and analyzed as above for enzymatic and non-enzymatic ferrochelation (Figure 40C and 40D). Similar trends were observed as with the non-boiled sirohydrochlorin samples.

The concentration of siroheme and sirohydrochlorin in each of the aformentioned assays was calculated. It was noted that at 10 mM iron, the concentration of siroheme and

sirohydrochlorin was appoximately equal (Figure 41 A and C). It was also noticed that at 83.4 µM and 104.3 µM SirC concentration, the siroheme and sirohydrochlorin concentrations were approximately the same (Figure 41 B and D). Also, at a SirC concentration of 83.4 µM, it appears that the concentration of siroheme and sirohydrochlorin remain fairly constant. At this concentration, the SirC:siroheme:sirohydrochlorin ratio is approximately 2:1:1, suggesting that SirC binds one molecule or siroheme or sirohydrochlorin.

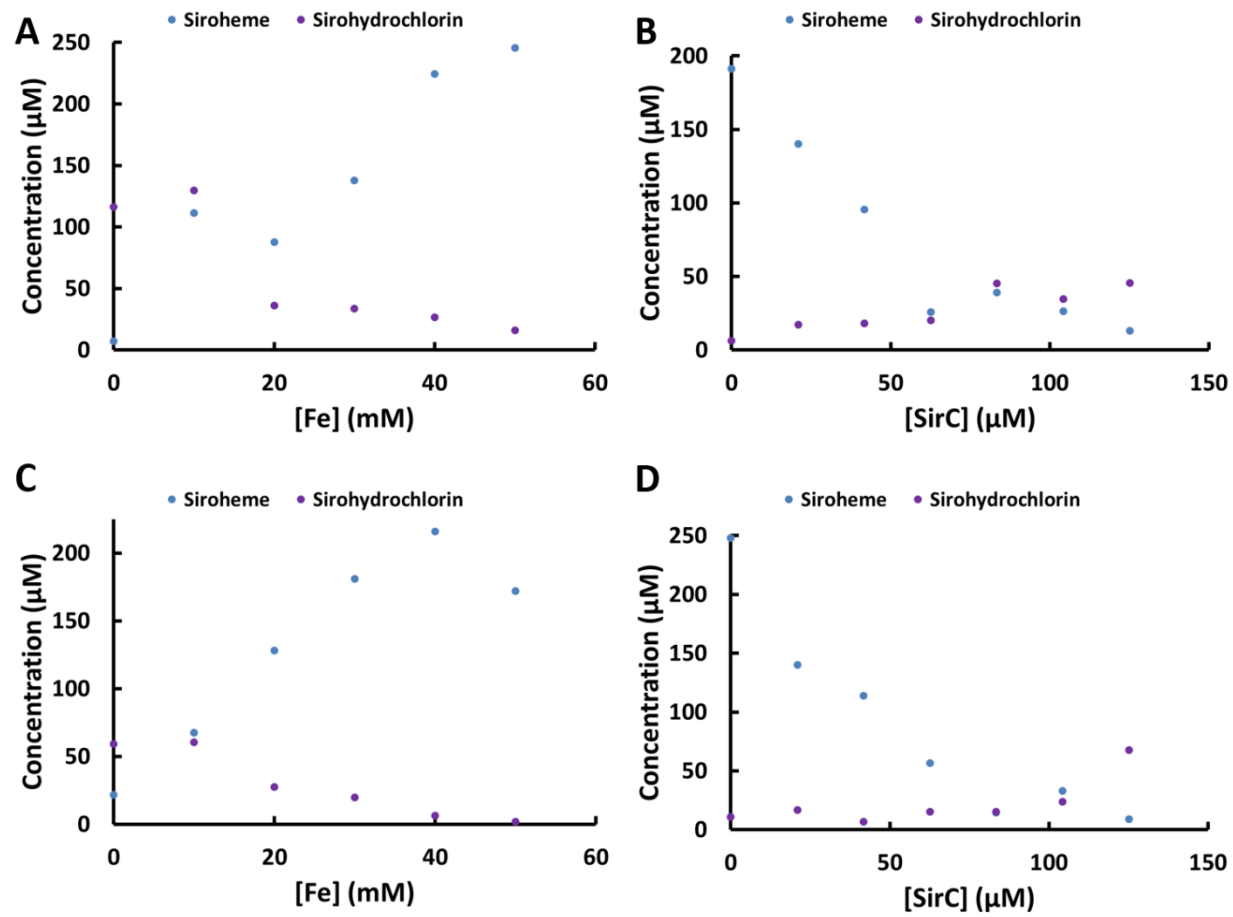

Figure 41: Siroheme and sirohydrochlorin concentration graph.

From the uroporphyrinogen III spontaneous chelation data presented in Figure 42, it suggests that iron, copper, zinc, and cobalt spontaneously chelate uroporphyrinogen III but

nickel does not. The data also suggests that zinc and copper seem to be the best chelators of uroporphyrinogen III under the assay conditions. Each of the metal/uroporphyrinogen III mixtures have a distinct UV-visible spectrum, as well as a unique retention time. However, uroporphyrinogen III is oxygen and light sensitive, therefore the spectrum could be indicative of an metallated oxidation product.

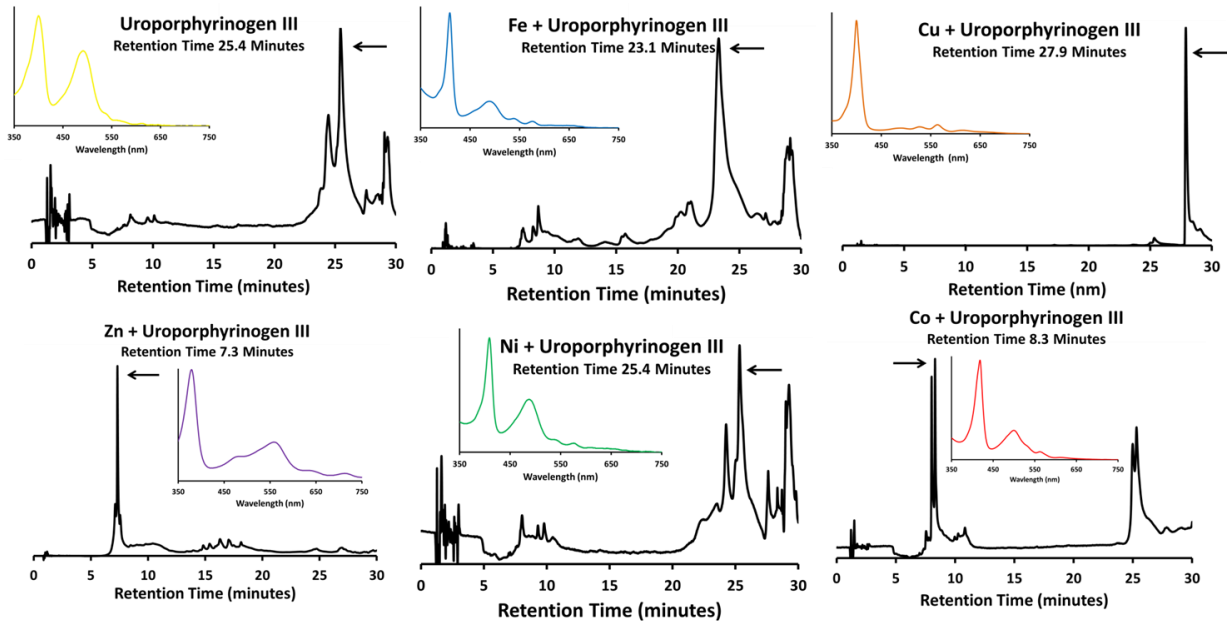

Figure 42: HPLC and UV-visible spectrophotometric analysis of uroporphyrinogen III and its metallated variants.

Precorrin 2 is highly unstable and can be easily photo-oxidized. The HPLC data in Figure 43 suggests that iron, copper, zinc, and cobalt spontaneously chelate precorrin 2 when incubated under anaerobic conditions in the dark. When exposed to light, the retention times of the resulting metallated tetrapyrroles shift and their UV-visible spectra change due to the photo-oxidation (Figure 44).

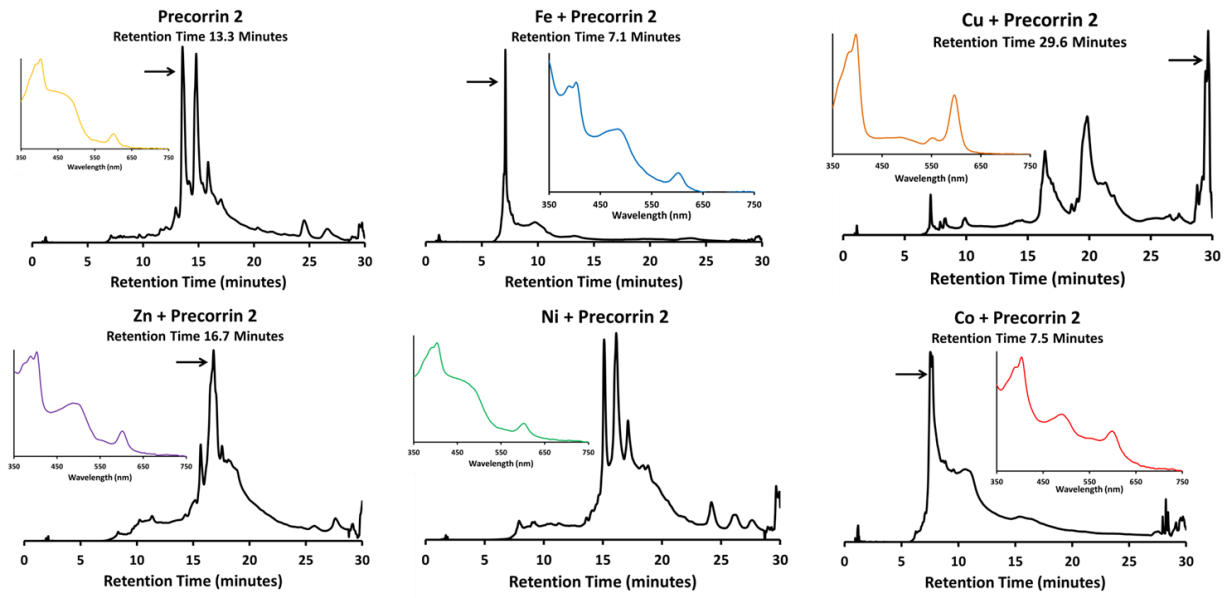

Figure 43: HPLC UV-visible spectrophotometric analysis of precorrin 2 and its metalated variants when kept in the dark.

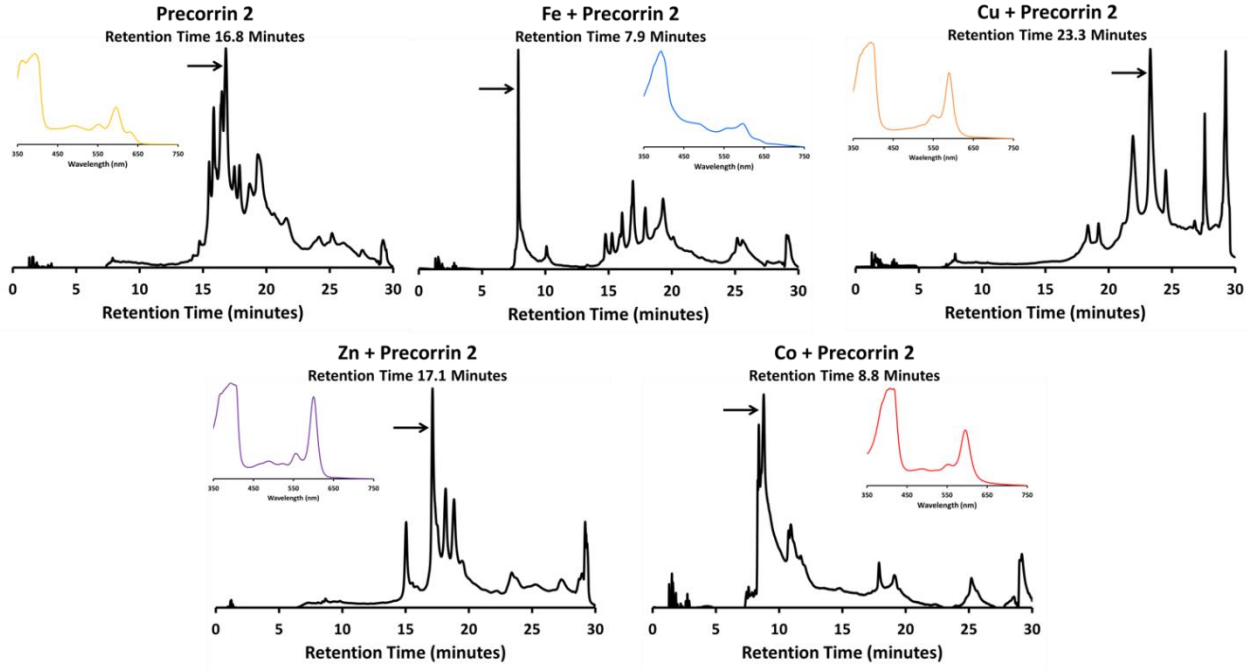

Figure 44: HPLC UV-visible spectrophotometric analysis of precorrin 2 and its metalated variants when exposed to light.

When sirohydrochlorin was mixed with different metals, it was found to spontaneous chelate with iron, cobalt, zinc, manganese, and copper, but again was not found to bind nickel under the reaction conditions. Each metallated sirohydrochlorin has a distinct UV-visible

spectrum and HPLC retention time (Figure 45). Although nickel is not spontaneously chelated by sirohydrochlorin, we showed that CfbA is a nickelochelatase and catalyzes the insertion of nickel into sirohydrochlorin; therefore, we know the HPLC retention time and UV-visible spectrum of Ni-sirohydrochlorin.[55]

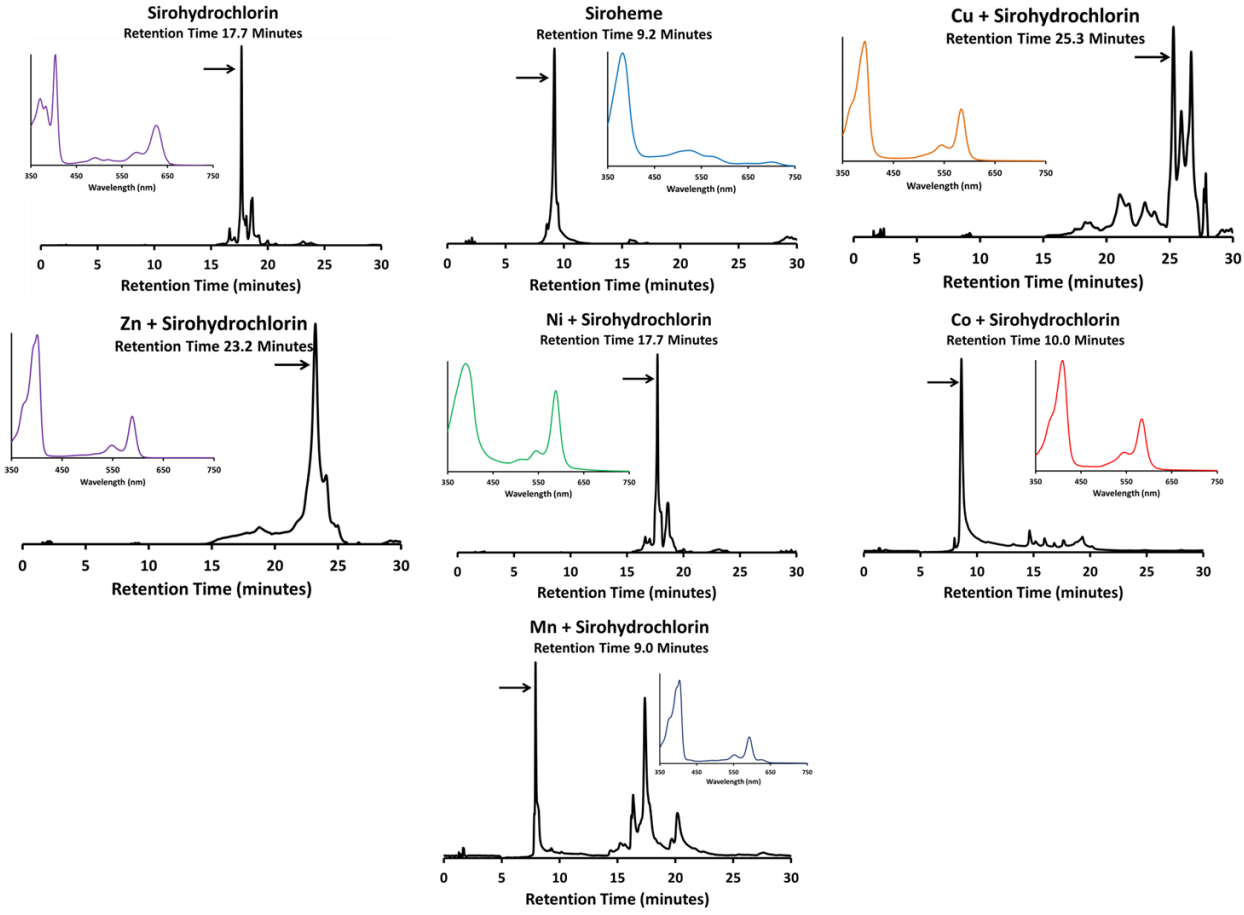

Figure 45: HPLC and UV-visible spectrophotometric analysis of sirohydrochlorin and its metallated variants.

We then simulated the cytoplasmic environment of a cell by combining each of the metal ions together at their estimated physiological concentrations (Table 1) and tested for spontaneous and enzyme-catalyzed chelation of sirohydrochlorin. When the SirC reaction is mixed with the metal solution, siroheme formation was observed. When additional SirC is

added to the reaction mixture, a decrease in siroheme formation is observed, as was observed before. Interestingly, when CfbA is added to the reaction, even less siroheme formation than with SirC is observed. When both SirC and CfbA are added to the reaction, the yield of siroheme is similar to that of SirC alone, approximately half of the amount produced in the metal solution spontaneous chelation assay (Figure 46).

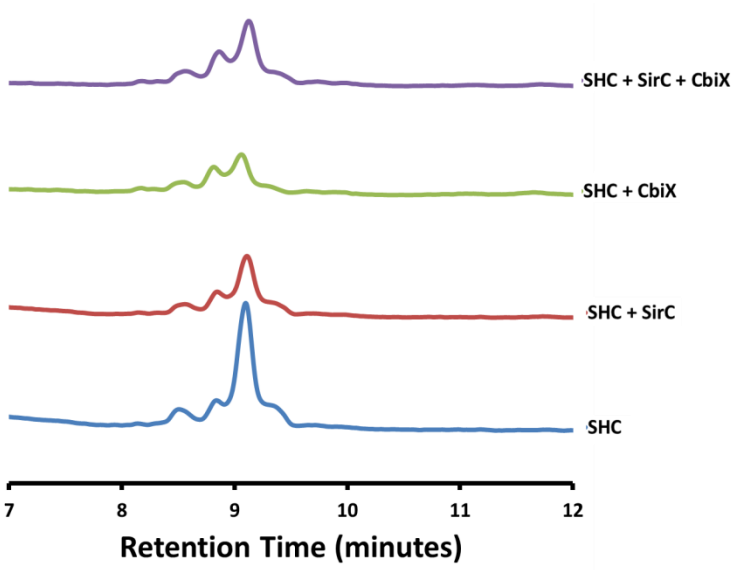

Figure 46: HPLC analysis of the ferrochelation of sirohydrochlorin by a metal ion mixture at physiological concentrations.

2.4 Discussion

Methanogens, such as *M. acetivorans*, synthesize a number of tetrapyrroles with distinct metals, including Ni (coenzyme F430), Co (corrinoids), and Fe (siroheme, heme). However, the genome of *M. acetivorans* contains only one gene encoding a canonical class II chelatase (*cfbA*), which has been shown to catalyze Ni insertion into sirohydrochlorin.[55] Sirohydrochlorin is biosynthesized via a precorrin 2 dehydrogenase (*sirC*), which is part of the alternative heme biosynthesis (*ahb*) gene cluster in *M. acetivorans*. Homologs of SirC have been shown in some species to act as a multifunctional dehydrogenase/ferrochelatase. This

investigation was therefore focused on determining whether SirC from *M. acetivorans* is capable of catalyzing the ferrochelation of sirohydrochlorin.

We investigated the ability of tetrapyrroles (i.e., uroporphyrinogen III, precorrin 2, and sirohydrochlorin) to spontaneously chelate various divalent transition metals (i.e., iron, cobalt, nickel, copper, and zinc). Interestingly, under the assay conditions tested, each of the tetrapyrroles were able to spontaneously chelate all the metals except for nickel (Figures 42-45). This observation correlates with the smaller ionic radius and weaker Brønsted acidity of nickel compared to the other metal ions. Unsurprisingly, the yield of siroheme (Fe-sirohydrochlorin) in spontaneous ferrochelation assays increases with increasing Fe concentration (Figure 40A and 40C).

If SirC is a multifunctional dehydrogenase/ferrochelatase that catalyzes the insertion of Fe into sirohydrochlorin, it is expected that the rate of siroheme formation should increase with increasing enzyme concentration. However, in an assay where the concentration of SirC was varied, it was found that with increasing concentration of SirC, the yield of siroheme decreased (Figure 40B and 40D). The results suggest that the observed siroheme is generated via spontaneous ferrochelation of sirohydrochlorin and instead of catalyzing this process, SirC prevents sirohydrochlorin from spontaneously complexing with Fe. This effect can also be observed in assays with multiple metals present at physiological conditions.

One explanation for this phenomenon is that SirC binds sirohydrochlorin tightly in its active site and protects it from spontaneous ferrochelation. Indeed, it has been observed that intermediates in tetrapyrrole biosynthesis often remain tightly bound to their cognate enzyme

and are transferred to the next pathway enzyme by substrate channeling.[92] Alternatively, the decrease in siroheme formation with increasing concentration of SirC might be due to its ability to bind iron. It has been shown that homologs of SirC can bind to several different metals, although iron was not explicitly tested.[46] We have shown that Mg^{2+} enhances SirC activity, therefore eluding to a possible metal binding site at or near the active site (Figure 47). In either case, increasing the SirC concentration increase the number of active sites available to bind free sirohydrochlorin and/or iron ions in solution, thereby preventing their spontaneous association and lowering the yield of siroheme synthesis.

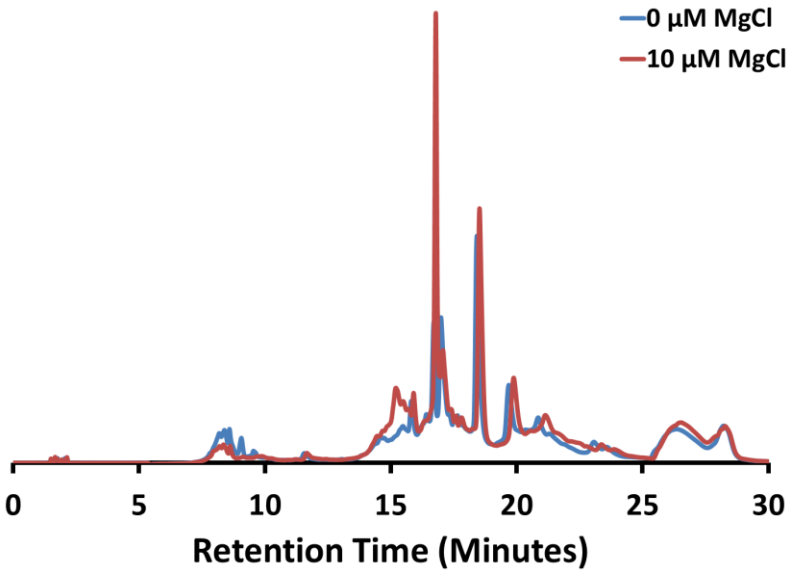

Figure 47: Sirohydrochlorin formation with 0 µM and 10 µM MgCl.

The question then remains: how is *M. acetivorans* able to catalyze the insertion of multiple metals (Ni, Co, or Fe) into sirohydrochlorin? It is possible that the lone class II chelatase, CfbA, is promiscuous and able to catalyze the insertion of Fe and Co into sirohydrochlorin in addition to Ni.

M. acetivorans also contains several genes that are annotated as class I, ATP-dependent, chelatases. Class I chelatases include the cobaltochelatase, CobNST, from the aerobic cobalamin biosynthetic pathway, and the magnesium chelatase, ChlHID, from chlorophyll biosynthesis. CobN/ChlH is the catalytic substrate (tetrapyrrole and metal)-binding subunit, while CobST/ChlID are the AAA^+ motor subunits and are responsible for the ATP hydrolysis used to drive the chelation reaction.[74,93] All three enzyme subunits are required for tetrapyrrole chelation activity.[94] *M. acetivorans* has multiple *cobN* homologs within its genome; however, it does not contain any genes with significant homology to *cobS* or *cobT*. Therefore, it is unlikely that these genes function as cobalto- or ferrochelatases in *M. acetivorans*. Interestingly, the genome of *M. acetivorans* contains a large (433 kDa) hypothetical, transmembrane protein that has three putative class II chelatase domains (MA3471). This gene is uniquely found in *Methanosarcina spp*. and its function is unclear, but it is tempting to speculate that it could play a role as a novel multi-functional tetrapyrrole chelatase in *M. acetivorans*.

Chapter 3: Pden_1323 is a Non-canonical Heme Oxygenase Involved in Iron Assimilation in *Paracoccus denitrificans*

3.1 Introduction

Iron regulation is an important part of bacterial survival.[95] The intracellular levels of iron are regulated and maintained under strict control.[96] Most of the 'free' iron within the cell is found in iron binding proteins such as transferrin and lactoferrin.[97] Siderophores are often used in pathogenic bacteria for iron acquisition, while others can acquire iron using systems for the binding, uptake, and degradation of heme (iron-protoporphyrin IX, Fe-PPIX).[96–99] Some pathogens uptake heme through a heme specific outer membrane receptor.[100,101] The heme is then transported via a periplasmic heme binding protein to the cytoplasmic membrane, where it is further transported into the cytoplasm.[97,102–105] Once in the cytoplasm, a heme oxygenase enzyme can then degrade the heme to release the iron.[105]

The concentration of free iron in a cell is low relative to the amount of iron that is needed for survival. This is due to two factors: 1) the low solubility of ferric iron (~10^{-18} M) at physiological pH, and 2) the sequestration of ferrous iron into porphyrins and iron carrier/storage proteins. Heme iron accounts for ~95% of iron in animal hosts; therefore, heme is the dominant source of iron for pathogenic bacteria.[106]

Iron is critical for establishing and maintaining bacterial infections. During infection, the genes that encode heme transporters are often upregulated.[106] *P. aeruginosa* has two sets of heme transporters, Has (heme assimilation system, Figure 48) and Phu (*Pseudomonas* heme utilization).[106,107] These systems are responsible for bringing heme into the periplasm and

cytoplasm, respectively. Both Gram-negative and Gram-positive cells have been shown to accept and import antimicrobial porphyrins (porphyrins with antimicrobial properties).[106]

Figure 48: Structure of the Has heme transporter (PDB: 3CSL).

ABC-transporters are used by bacteria to uptake heme inside the cell. The ABC transporter is composed of a ligand (e.g., heme) binding protein, a membrane permease, and an ATPase. Heme is captured by the heme binding protein and transferred to the permease. The ATPase supplies the energy needed for transportation though the cell membrane. Inside the host, hemoproteins are used to help solubilize the heme by binding it in a hexacoordinated form using two axial ligands from amino acid side chains.[108]

Heme oxygenase (HO) catalyzes the first and rate-limiting step of the heme degradation pathway. HO degrades heme to produce carbon monoxide (CO), iron, and biliverdin.[109] The HO catalyzed opening of the heme macro cycle requires three oxygen molecules and seven

electrons.[110] This cleavage reaction can yield four possible isomers of biliverdin: α, β, γ, δ. Biliverdin can then further be reduced to bilirubin by biliverdin reductase.[111]

HOs can be found in a wide variety of organism, such as mammals, higher plants, insects, and photosynthetic and non-photosynthetic bacteria. In mammals, HOs Play important roles in heme catabolism, iron homeostasis, antioxidant defense, cellular signaling, and oxygen sensing. In bacteria, they are responsible for acquiring iron from heme, and in plants and cyanobacteria, they are involved in the production of a light-sensing chromophore.[112] Another potential role for HOs is to prevent cellular heme toxicity.[105]

The HO enzyme is unusual in that it uses heme as both a substrate and a cofactor. One mechanism for heme degradation is ferric heme forms a complex with HO and is then reduced by a NADPH-dependent cytochrome P450 reductase (CPR).[113] Then molecular oxygen binds to the heme-HO complex, forming a ferric-superoxide intermediate (Figure 49). A hydroperoxide intermediate is then formed by the transfer of another electron from the CPR and a proton from solvent. The terminal oxygen of the hydroperoxide intermediate then attacks a carbon on the porphyrin ring to form the hydroxyheme intermediate. This intermediate then reacts with molecular oxygen to form ferrous verdoheme and CO. The conversion of verdoheme to ferric biliverdin is not well understood, although to release the iron from ferric biliverdin, CPR must reduce the ferric iron to ferrous (Figure 49).[109] It has been shown that the rate-limiting step of the heme degradation process is the release of biliverdin from HO.[114]

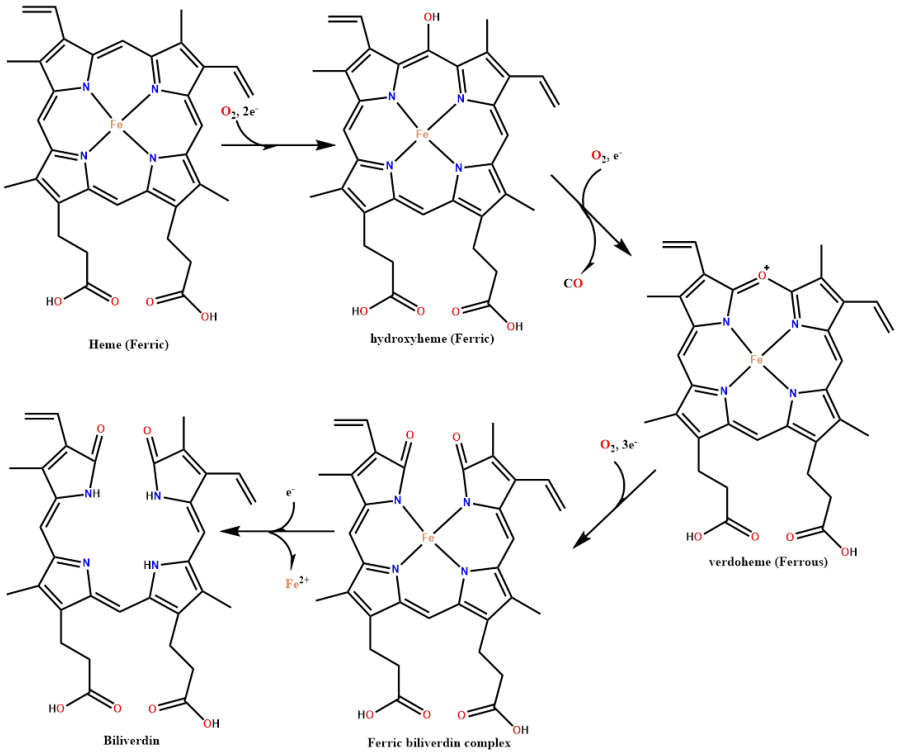

Figure 49: Heme Oxygenase Mechanism.

The CPR complex can be substituted with ascorbic acid as the electron donor to HO for the initiation of heme degradation. When adding reducing equivalents of ascorbic acid under predominantly CO_2 atmospheric conditions, heme degradation is inhibited by CO after forming verdoheme, resulting in an accumulation of ferrous verdoheme-CO complex, and preventing biliverdin formation. However, under physiological conditions when the CO concentration is much less than the O_2 concentration, CO does not inhibit the reaction.[115]

In bacteria, several different types of HO have been found that yield products that are different but similar to biliverdin (Figure 50). The HO homolog IsdG forms staphylobilins and MhuD forms mycobilins. The linear tetrapyrrole product is not the only difference in the reaction: IsdG yields formaldehyde instead of CO, and MhuD does not yield a C_1 product.[116] A novel heme degradation product was discovered from *Rhodnius prolixus*, a blood sucking

insect, where the heme is modified before the oxidative cleavage resulting in dicyseinyl-BV IXγ.[117]

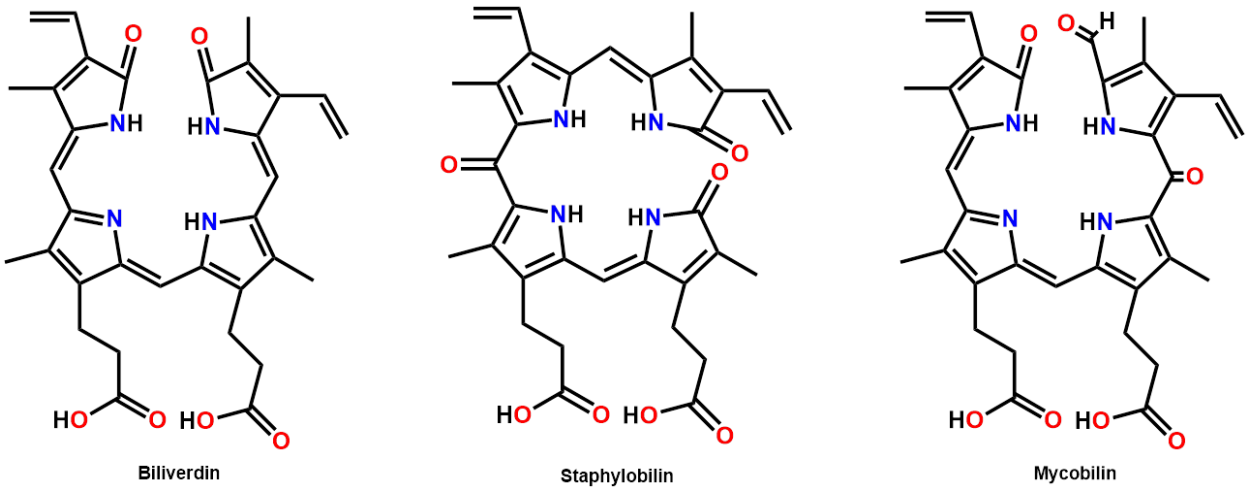

Figure 50: Heme oxygenase products.

There are 5 branches of bacterial HO proteins: cyanobacterial HO-1 and HO-2, IsdG (iron-regulated surface determinants), HmuO, PigA (*Pseudomonas* iron induced genes), and BphO (bacterial phytochrome heme oxygenase).[105,112,118] HOs can also be classified into three structural families: the HO-like family, the ChuS family, and the IsdG family. HmuO was the first bacterial heme oxygenase identified and is structurally classified with PigA and HemO.[117]

It has been shown that *pigA* is regulated by the ferric uptake repressor Fur (ferric uptake regulator) and depressed when iron is limiting.[112,119] Gisk et. al. looked at the genomes of different *Pseudomonas* species and noted that there were four typical combinations of HO in the genome: 1) a single BphO, 2) a single PigA, 3) both BphO and PigA, and 4) two PigAs. They also noted that cells overproducing BphO were green in color while cells overproducing PigA

are not. This is thought to be due to PigA targeting the β or δ bridging carbon of heme instead of the α carbon leading to the formation of β or δ biliverdin instead of α biliverdin.[112]

HemO and PigA are structurally similar and fall into the same branch of HO homologs. PigA targets the β and δ bridging carbon and leaves a 30:70 β biliverdin:δ biliverdin product ratio, respectively. The importance of these isomers is not known, but it has been speculated that it may be related to the fact some pathogenic bacteria, such as *Pseudomonas aeruginosa* contain a second HO homolog, BphO, that targets the α bridging carbon, suggesting that each heme oxygenase in *P. aeruginosa* has a distinct function. It has been proposed that the heme used in the PigA reaction is extracellular heme.[105]

Less is known about the BphO family of HOs. They show characteristics of a bacterial two component system, and therefore often have a response regulator in close genomic proximity. It is proposed that the heme used in the BphO reaction is biosynthesized intracellular heme.[105]

IsdGI from *Staphylococcus aureus* contains two active sites that degrade heme in the presence of CPR or ascorbate.[120] It has been shown that heme adopts a "ruffled" conformation in the active site of *S. aureus* IsdG. It has been proposed that this ruffling of heme inside the active site is important for the regulation of the O_2 activation and leads to the production of the distinct product, staphylobilin, which has an extra oxygen insertion at the *meso* carbon.[121] Reniere et al. was able to obtain the crystal structure of the IsdGI-product complex, providing crystallographic evidence that staphylobilin is indeed produced by IsdGI.[122]

IsdGI forms formaldehyde as a coproduct instead of CO like canonical HOs. It has been proposed that neither the staphylobilin nor the mycobilin pathway precedes through a

verdoheme intermediate due to the lack of CO production. Furthermore, it is thought that the heme ruffling suppressed CO production and aids in the formation of the aldehyde.[121]

A study revealed that IsdGI was unable to degrade Co-PPIX, Ga-PPIX, Mn-PPIX, or Zn-PPIX, although it was shown that Co-PPIX, Ga-PPIX, and Zn-PPIX undergo spectral changes in the presence of ascorbate.[120]

Another branch of HOs is characterized by the IsdG homolog MhuD (mycobacterial heme utilization degrader).[123] The structure of MhuD from *Mycobacterium tuberculosis* has been determined and shown to be a homodimer and binds two heme molecules per monomer (Figure 51).[124] There is only one other protein structure in the PDB with a similar diheme planar stacked conformation in the active site, NapB, which is a cytochrome unit of nitrate reductase and is involved in electron transfer.[124] It has been shown that MhuD degrades heme but does not produce CO. Instead, the carbon atom at the site of the ring cleavage is retained as an aldehyde group, producing a new product, mycobilin.[121] Another IsdG homolog, HmuQ, from *Bradyrhizobium japonicum* has been shown to have heme oxygenase activity and its product is thought to be biliverdin.[120]

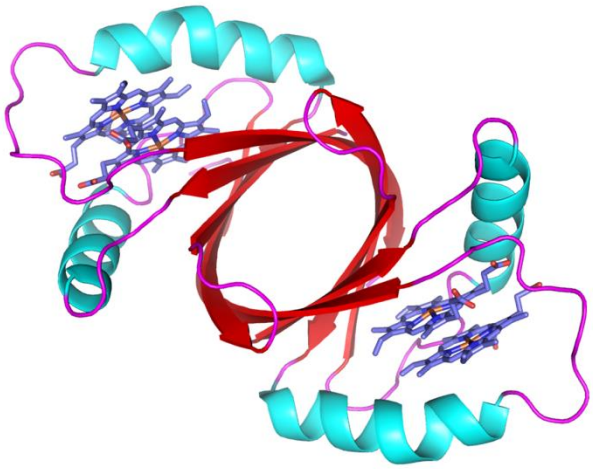

Figure 51: Crystal structure of MhuD from M. tuberculosis (PDB: 3HX9).

Paracoccus denitrificans has a gene cluster (*pden_1323 – pden_1328*) containing ABC transporter homologs that are similar to those involved in heme transport (Figure 52). Within this cluster is a gene, *pden_1323*, that is annotated in the National Center for Biotechnology Information (NCBI) database as a pyridoxamine 5'-phosphate (PMP) oxidase related, Flavin mononucleotide (FMN)-binding protein. When Pden_1323 is submitted to the Basic Local Alignment Search Tool (BLAST), it returns with a conserved domain of HutZ which is a putative heme iron utilization protein that is found and used in inorganic ion transport and metabolism, and is homologous to HugZ and domain of unknown function 2471 (DUF2470) superfamily members (Figure 53). The DUF2470 superfamily is also a putative heme-iron utilization family and many are annotated as PMP oxidase-related, FMN-binding protein. The HugZ crystal structure from *Helicobacter pylori* showed it is a dimer that forms a split barrel fold, similar to that found in FMN binding proteins.[108]

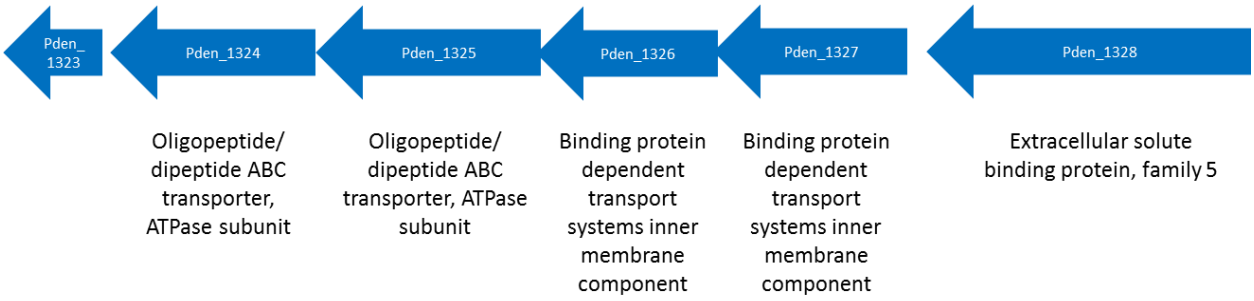

Figure 52: A putative heme-iron utilization gene cluster from *P. denitrificans*.

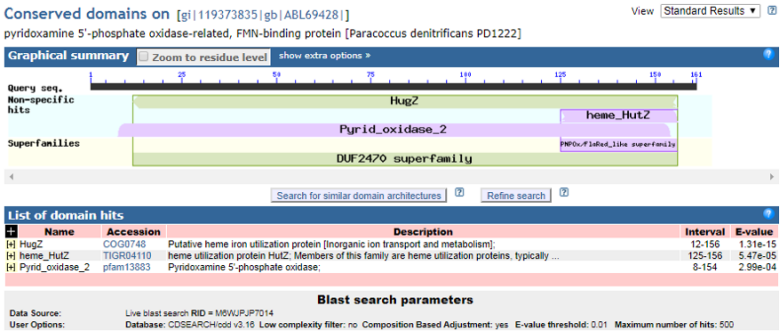

Figure 53: Conserved domain search results of Pden_1323.

None of the functions of the proteins encoded by the identified gene cluster have been confirmed. One possibility is that the transporter genes are used to import heme and Pden_1323 is a non-canonical HO. However, *P. denitrificans* is a denitrifying bacterium that produces heme d_1, whose biosynthetic pathway has yet to be fully elucidated. In particular, the gene(s) responsible for the dehydrogenation of precorrin 2 to sirohydrochlorin, and for the transport of heme d_1 precursor from the cytosol to the periplasm, have yet to be identified Thus, another possibility is that *pden_1323* encodes a novel precorrin 2 dehydrogenase and the transporter genes are used to export an intermediate in heme d_1 biosynthesis. In this chapter, the function of Pden_1323 is investigated to help distinguish between these two hypotheses.

3.2 Methods and Materials

All chemicals were purchased from Frontier Scientific, Inc. (Logans, UT), Sigma-Aldrich (St. Louis, MO), or Biorad unless otherwise stated. Primers were ordered from Sigma-Aldrich and the synthesized *pden_1323* gene was purchased from GeneArt, A Thermo Fisher Scientific Company, (Waltham, MA).

Expression Vector Construction. The *pden_1323* gene was codon optimized for expression in *E. coli* with the NdeI and XhoI restriction enzyme sites included at the 5' and 3' ends, respectively, for use in restriction enzyme cloning.

The plasmid containing codon optimized *pden_1323*, as well as an empty pET-28b(+) vector, were subjected to restriction enzyme digestion using the following protocol: 1 µg plasmid, 5 µL 10x CutSmart Buffer, 1 µL NdeI, 1 µL XhoI, and the reaction was made to volume (50 µL) with water. The reaction was incubated at 37° C for 1.5 hours, and then heat inactivated at 65 °C for 20 minutes. The *pden_1323* product was purified via a Lonza FlashGel™ DNA Cassette (Basel, Switzerland) and then recovered using an Omega BIO-TEK E.Z.N.A.® Gel Extraction Kit (Norcross, GA) following the protocol provided by the manufacture. The linearized pET-28b(+) vector was purified using an Omega BIO-TEK E.Z.N.A® Cycle Pure Kit following the protocol provided in the manual. The *pden_1323* product and the digested pET-28b(+) vector were then ligated together using T4 DNA Ligase (NEB) using the manufacturer's protocol. The ligated mixture was then transformed into *E. coli* TOP10 cells and plated on Lysogeny Broth(LB) agar plates containing 50 µg/mL kanamycin. Colonies were picked, grown in liquid LB medium, and plasmid preparations were made using the Omega BIO-TEK E.Z.N.A.® Plasmid Mini Kit. The purified plasmid was then submitted for sequencing at Eurofins Genomics

(Louisville, KY). After sequence verification, the plasmid was transformed into *E. coli* BL21 (DE3) cells.

Expression and Purification of Pden_1323. The pET-28b(+):*pden1323* plasmid was overexpressed in *E. coli* BL21-(DE3) cells. The cells were grown at 37 °C until the OD_{600} reached 0.6. The cultures were then induced with isopropyl β-D-1-thiogalactopyranoside (IPTG) at a final concentration 400 µM and incubated for an additional 4 hours.

The cells were centrifuged at 15,900 x g for 45 minutes. The supernatant was decanted and the cells were re-suspended in 50 mM sodium phosphate, 300 mM NaCl, 5 mM imidazole, pH 8.0 buffer. The cells were sonicated and centrifuged at 15,900 x g for 1 hour. The supernatant was then loaded onto a Bio-Rad Econo-Pac column loaded with nickel-charged Profinity IMAC resin and the flow-through was collected. The column was then washed with 50 mM sodium phosphate, 300 mM NaCl, 5 mM imidazole, pH 8.0 buffer, and this wash fraction was collected. The protein was then eluted from the column by adding 50 mM sodium phosphate, 300 mM NaCl, 500 mM imidazole, pH 8.0 buffer and collected in 1 mL fractions. The protein was combined and spin-concentrated/buffer exchanged into 100 mM Tris, pH 8.0 buffer and aliquoted into 100 µL increments.

Size Exclusion Chromatography. Size exclusion chromatography (SEC) was performed using either an Agilent 1260 Infinity high-performance liquid chromatography (HPLC) or an ÄKTA™ Start fast protein liquid chromatography (FPLC) instrument. Two different columns were used for HPLC: an Agilent Bio SEC-3, 3 µm, 100 Å, 7.8 x 300 mm column and an Agilent Bio SEC-3, 3 µm, 300 Å, 7.8 x 300 mm column. The run was a 25 minute, isocratic method using 100 mM

Tris buffer, pH 8.0. When performing FPLC, a GE HiLoad Superdex 200 pg column was used. The run was a 120 minute, isocratic method using 50 mM Tris, 200 mM NaCl buffer, pH 7.5.

Precorrin 2 Dehydrogenase Activity Assay. Pden_1323 was tested for dehydrogenase activity in a MBRAUN anaerobic chamber. First a positive precorrin 2 dehydrogenase (SirC) control reaction was performed by adding porphobilinogen (PBG) deaminase (HemC, 1.77 µM), uroporphyrinogen III synthase (HemD, 2.16 µM), uroporphyrinogen III methyltransferase SirA (4.33 µM), SirC (15.2 µM), PBG (884 µM), *S*-adenosyl-L-methionine (SAM 1 mM), nicotinamide adenine dinucleotide (NAD^+ 30 µM), and $MgCl_2$ (40 µM) in Chelex-treated 50 mM Tris-HCl, pH 8.0 buffer (250 µL total volume). The reaction was incubated at 37 °C for 12 hours. A SirA reaction was also performed by adding HemC (1.77 µM), HemD (2.16 µM), SirA (4.33 µM), PBG (884 µM µM), SAM (1 mM), and $MgCl_2$ (40 µM) in Chelex-treated 50 mM Tris-HCl, pH 8.0 buffer (250 µL total volume). The reaction was incubated at 37 °C for 12 hours. Pden_1323 was substituted for SirC and NAD^+, FMN, and Flavin adenine dinucleotide (FAD), cofactor F420, and 8-hydroxy-5-deazaflavin (Fo) were all tested as cosubstrates. F420 and Fo were generous gifts from Dr. Kayunta Johnson-Winters (University of Texas, Arlington). Reaction conditions were as follows: HemC (1.77 µM), HemD (2.16 µM), SirA (4.33 µM), Pden_1323 (15.2 µM), PBG (884 µM), SAM (1 mM), NAD+/FMN/FAD/F420/Fo (30 µM), and $MgCl_2$ (40 µM) Chelex-treated 50 mM Tris-HCl, pH 8.0 buffer (250 µL total volume). The reaction was incubated at 37 °C for 12 hours. A Pden_1323 control was also performed with no cofactor as follows: HemC (1.77 µM), HemD (2.16 µM), SirA (4.33 µM), Pden_1323 (15.2 µM), PBG (884 µM), SAM (1 mM), $MgCl_2$ (40 µM) in Chelex-treated 50 mM Tris-HCl, pH 8.0 buffer (250 µL total volume). The reaction was also incubated at 37 °C for 12 hours.

PMP Oxidase Activity Assay. Pden_1323 was tested for PMP oxidase activity using 5 different cosubstrates, FAD, FMN, NAD^+, F420, and Fo. The reactions conditions were as follows: Pden_1323 (5 µM), FAD/FMN/NAD^+/F420/Fo (10 µM), and PMP (50 µM) in 50 mM Tris-HCl buffer, pH 8.0 (1 mL total volume). The assays using NAD^+, FMN, and FAD as cofactors were performed both aerobic and anaerobically. The assays where Fo and F420 were used as cosubstrates were only performed aerobically.

Heme Oxygenase Activity Assay. The heme oxygenase activity of Pden_1323 was examined by incubating 10 µM enzyme, 9 µM hemin, and 30 µM ascorbic acid in a cuvette containing 100 mM potassium phosphate buffer, pH 7.6. The reaction mixture was heated to 37 °C and incubated with stirring. UV-visible absorption spectra were acquired every 15 seconds for 5 minutes and then every two minutes for up to one hour using a Nanodrop 2000C (Thermo Fisher). Three control reactions were also performed that omitted Pden_1323, hemin, or ascorbic acid individually. Other substrates were also tested, including deuteroheme, protoporphyrin IX (PPIX), and Mn-protoporphyrin IX (Mn-PPIX) using the same assay conditions described above for hemin.

HPLC Analysis. The Pden_1323 reaction mixtures were analyzed via reverse phase chromatography using an Agilent 1260 Infinity HPLC equipped with an Agilent Poroshell 120 EC-C18 (4.6 x 150 mm, 2.7 µm column. The solvents used were 20 mM formic acid (solvent A), and acetone (solvent B). The method started with 0% B for 2 minutes. Solvent B was then increased to 25% over 3 minutes and increased again to 75% over 20 minutes. Solvent B was then increased to 100% over five minutes and then held constant for 10 minutes before returning back to 0% B over 10 minutes.

Mass Spectrometry Analysis. The Pden_1323 reaction mixtures were also subjected to mass spectrometry (MS) analysis on a Waters Acquity UPLC Q-TOF Premier mass spectrometer equipped with an Aeris™ 3.6 µm WIDEPORE C4 200 Å, 50 x 2.1mm LC column. All MS data were analyzed using the Waters MassLynx software. The method utilized 95% water, 5% acetonitrile, 0.1% formic acid as solvent A and 95% acetonitrile, 5% water, and 0.1% formic acid as solvent B with a 0.3 mL/min flow rate. The method started with 90% A and decreased to 62% over 20 minutes. Over the next 2 minutes, solvent A was decreased further to 10% where it then remained constant for 3 minutes before increasing back to 90 % A over 2 minutes and being held there for 13 minutes. The electrospray ionization (ESI) mass detector was configured to positive ion mode with scanning between 800 and 1000 *m*/*z*. The inline Waters TUV detector was also configured to 400 nm to verify that the peaks detected by MS analysis corresponded to the same peaks observed in the above HPLC analysis.

3.3 Results

Size Exclusion Data. The theoretical molecular weight for the monomeric form of Pden_1323 is approximately 17.3 kDa and that of the dimeric form is 34.7 kDa. All three size exclusion chromatographic runs yielded a calculated molecular weight for Pden_1323 (using the molecular weight standards shown in Table 2) of approximately 35 kDa, indicating that Pden_1323 is a homodimer in solution (Figure 54).

Table 2: Protein standards and their molecular weights.

Protein Standard	Molecular Weight (Da)
Thyroglobulin	670,000
γ- globulin	158,000
ovalbumin	44,000
myoglobin	17,000
vitamin B_{12}	1,350

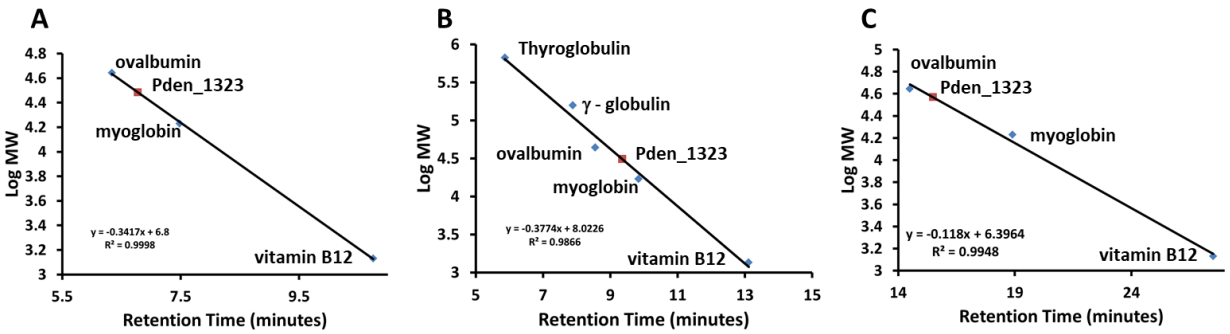

Figure 54: Size exclusion chromatographic data of Pden_1323 obtained using A) HPLC and an Agilent Bio SEC-3 100 Å column B) HPLC and an Agilent Bio SEC-3 300 Å column C) FPLC and a GE HiLoad Superdex 200 pg column.

Pden_1323 Dehydrogenase Assay. The UV-visible spectroscopic and HPLC analysis suggest that Pden_1323 is not a precorrin 2 dehydrogenase. The Soret band of the SirC assay is more blue shifted than any of the other assays (Figure 55), however, all the UV-visible spectra are more similar to photo-oxidized precorrin 2 than sirohydrochlorin (Figure 56). The HPLC traces show the 22.1 minute peak in the SirC trace has almost completely disappeared and the 20.7 minute peak is larger than the reactions with F420, Fo, FMN and FAD (Figure 57). Both the 22.1 and the 20.7 minute peak have UV-visible spectra consistent of that of sirohydrochlorin, and it is thought that the two peaks are isomers of one another.

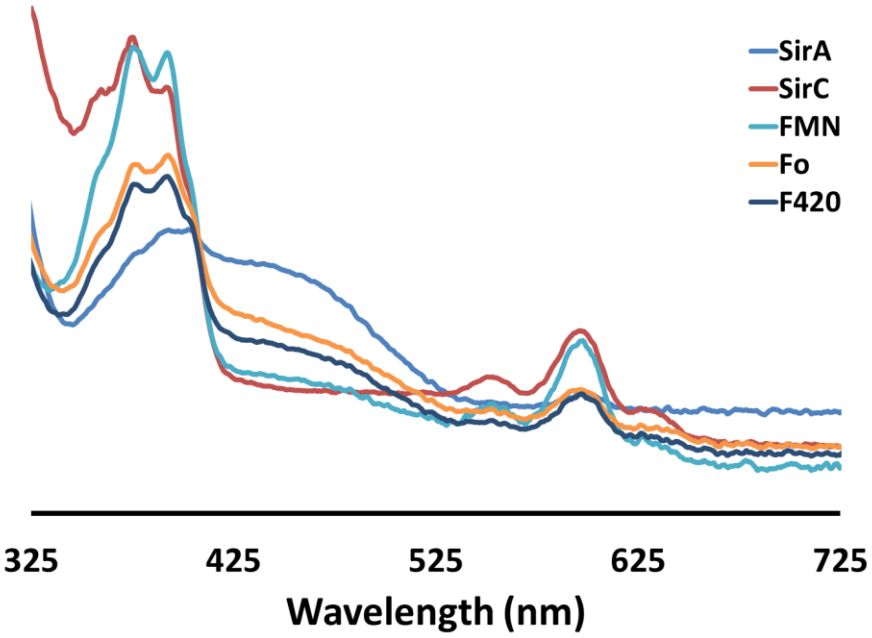

Figure 55: UV-Visible spectra of the Pden_1323 precorrin 2 dehydrogenase assay.

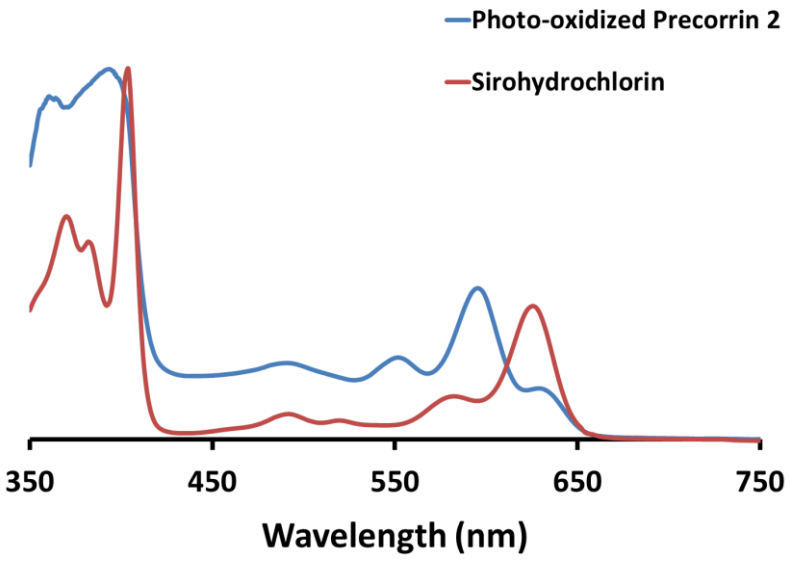

Figure 56: UV-Visible spectra of photo-oxidized precorrin 2 and sirohydrochlorin

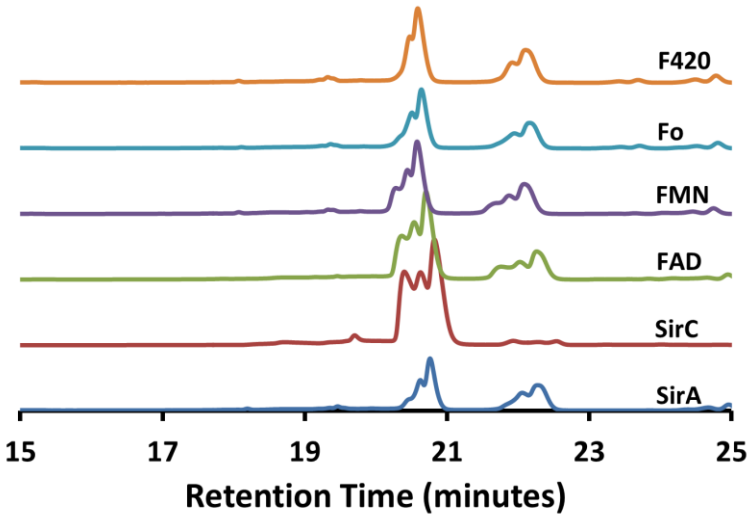

Figure 57: HPLC traces of the Pden_1323 precorrin 2 dehydrogenase assay.

Pden_1323 P(M/N)P Oxidase Assay. Pden_1323 was tested for P(N/M)P Oxidase activity both anaerobically and aerobically using a variety of cofactors. Aerobically, Pden_1323 was tested using NAD^+, FAD, FMN, and F420, however there was no change in any of the spectrum (Figure 58). Anaerobically, Pden_1323 was tested with NAD^+, FAD, and FMN, but again there was no change in the spectrum (Figure 59).

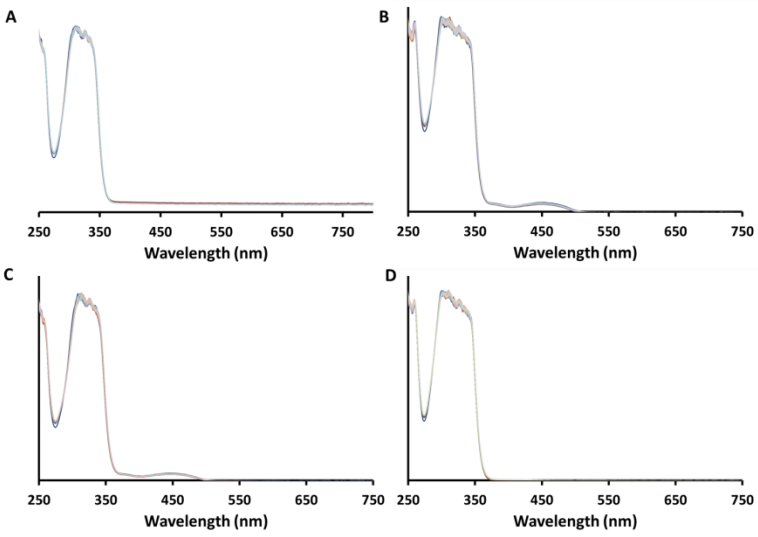

Figure 58: Aerobic Pden_1323 PMP Oxidase Assays with A) NAD, B) FAD, C) FMN, and D) F420 as cosubstrates.

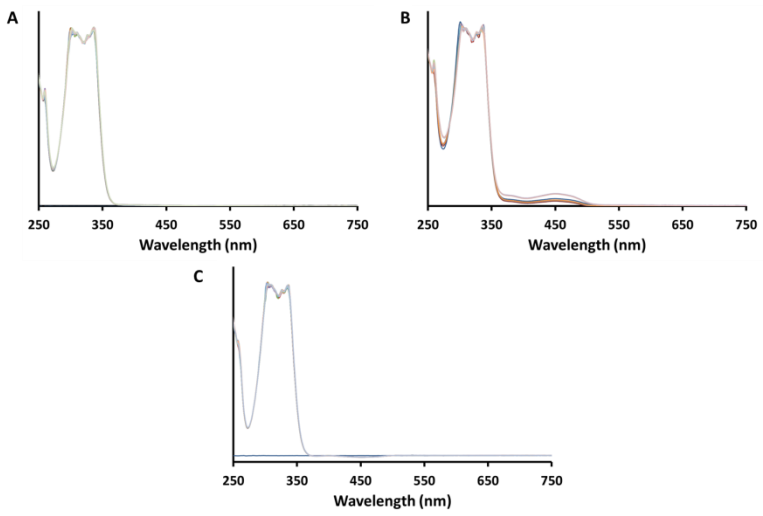

Figure 59: Anaerobic Pden_1323 PMP oxidase assays with A) NAD, B) FAD, and C) FMN as cosubstrates.

Pden_1323 Shows Heme Oxygenase Activity. Pden_1323 was incubated with a mixture of hemin and ascorbic acid to determine if this enzyme is responsible for the degradation of heme. After the addition of Pden_1323 to the assay mixture to initiate the reaction, there was an initial shift in the Soret band from 380 nm to 386 nm. The peak at 386 nm then decreases over time and a new peak with a λ_{max} of 343 nm is formed (Figure 60). The initial observed rate of the reaction was determined to be 0.04 min^{-1} (initial velocity of 4.11 x 10^{-7} M/min). This was calculated using the decrease in absorbance at 386 nm and an extinction coefficient of 58.44 mM^{-1} cm^{-1}.[125]

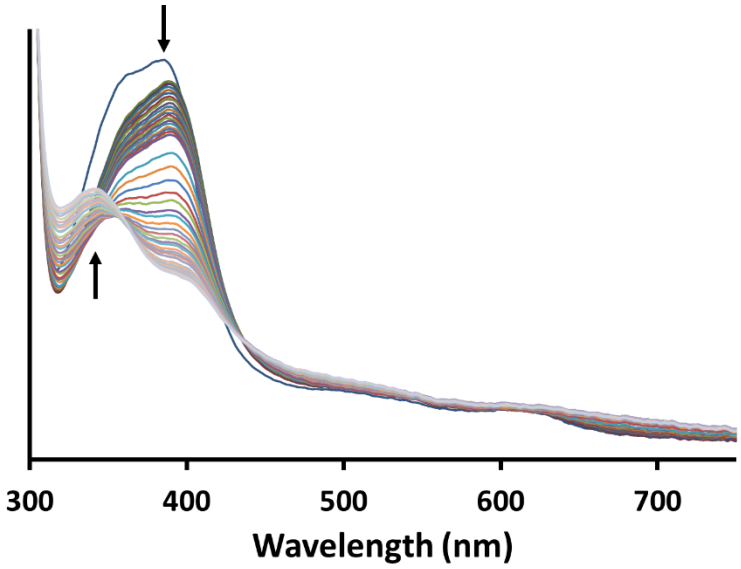

Figure 60: UV-visible spectra of the Pden_1323 heme oxygenase reaction.

When Pden_1323 is omitted from the assay mixture a similar trend is observed, but there is not as much degradation (Figure 61 A). This is consistent with data reported in the literature that ascorbic acid can facilitate the degradation of heme by itself.[120] When ascorbic acid is left out of the reaction mixture, there are no spectral shifts in the UV-visible spectrum, suggesting that no reaction is taking place (Figure 61 B). Also, when looking at the absorbance at 386 nm between the Pden_1323 reaction and its controls, there is an obvious rate enhancement when enzyme is present (Figure 62). The initial observed rate of the reaction with no enzyme is 0.02 min^{-1}, half of when the enzyme is present.

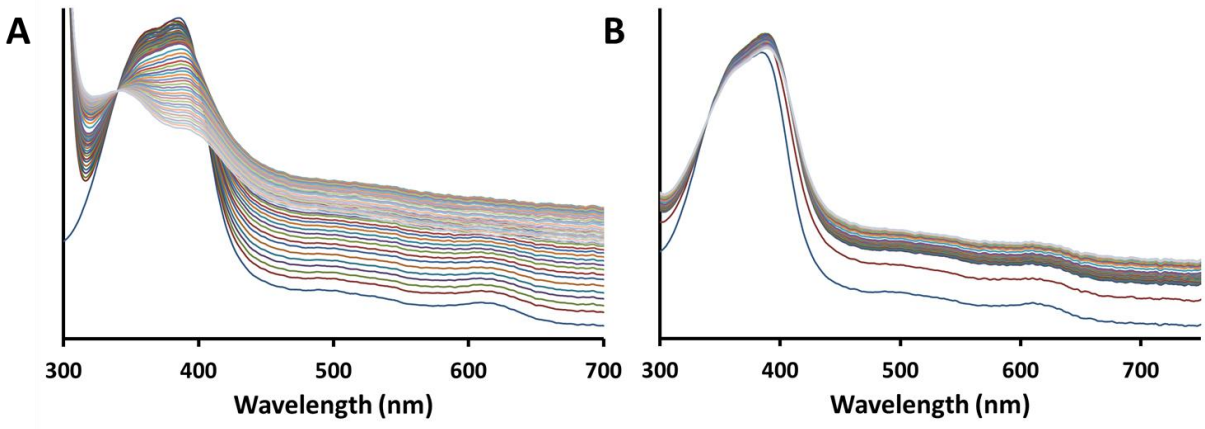

Figure 61: A) UV-visible spectra of Pden_1323 control reactions lacking A) Pden_1323 or B) ascorbic acid.

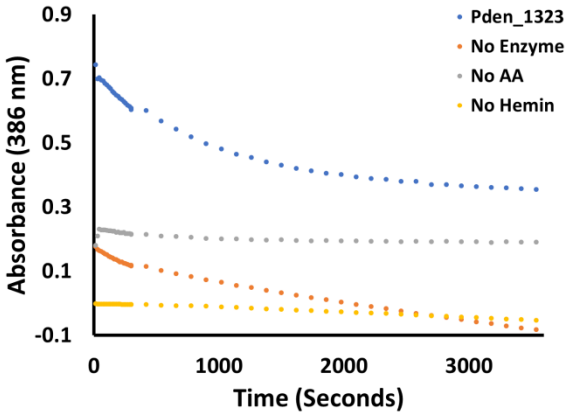

Figure 62: Change in absorbance at 386 nm during the Pden_1323 heme oxygenase reactions.

When hemin in the assay is substituted with deuteroheme, there is a shift in the Soret band upon addition of Pden_1323 and then a similar decrease and shift in the Soret band as the reaction progresses (Figure 63 A). However, when protoporphyrin IX (PPIX) was substituted for hemin, similar spectral changes are not observed (Figure 63 B) which is not surprising as the iron atom is an essential part of the reaction. The slight variation in spectral features is attributed to a small amount of metal ion contamination/spontaneous chelation. Interestingly, when Mn-PPIX was substituted for hemin, there was a slight change in the UV-visible spectrum, suggesting that it is also a substrate of Pden_1323 (Figure 63 C).

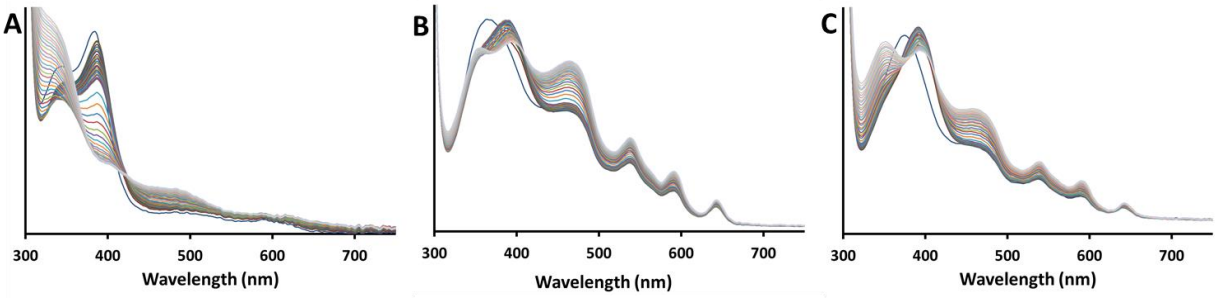

Figure 63: UV-visible spectra of Pden_1323 heme oxygenase reactions using A) deuteroheme B) protoporphyrin IX, and C) Mn-protoporphyrin IX as substrates.

These assays were then analyzed using HPLC and LC-MS to verify that new products had been formed and to confirm their identity. The hemin standard had a retention time of 16.6 minutes and the biliverdin product standard had a retention time of 17.7 minutes (Figure 64). The two standards were analyzed using MS and peaks with the appropriate *m*/*z* (616.17*m*/*z* and 583.25 *m*/*z*, respectively) were observed (Figure 65). The Pden_1323 heme oxygenase reaction was then submitted for MS analysis and both substrate and product could both be seen in the sample (Figure 66). When the no enzyme control was analyzed using MS, neither substrate nor

product was found. However, substrate could be seen via HPLC for both control assays, and a small amount of product could be seen in the no enzyme control assay (Figure 67).

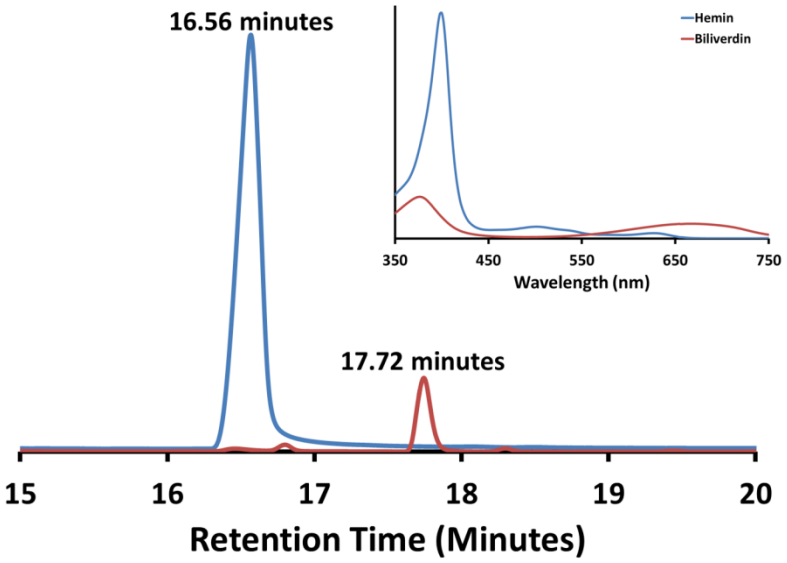

Figure 64: HPLC analysis of hemin and biliverdin standards. Inset: UV-visible spectra of both standards.

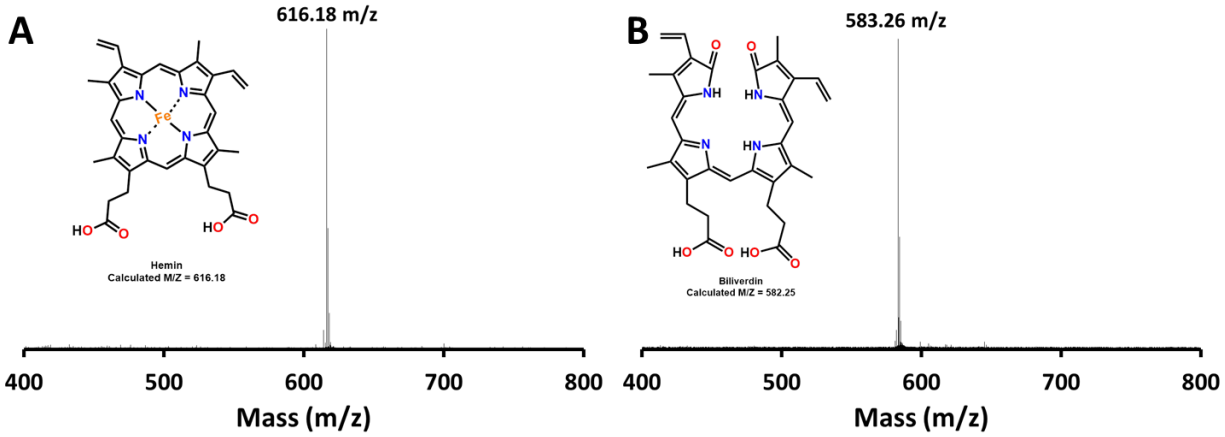

Figure 65: Mass spectra of hemin and biliverdin standards.

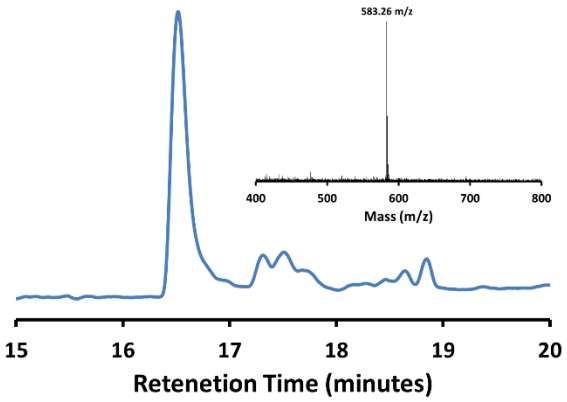

Figure 66: HPLC analysis of the Pden_1323 heme oxygenase reaction and the mass spectrum of 17.7 min peak corresponding to the biliverdin product.

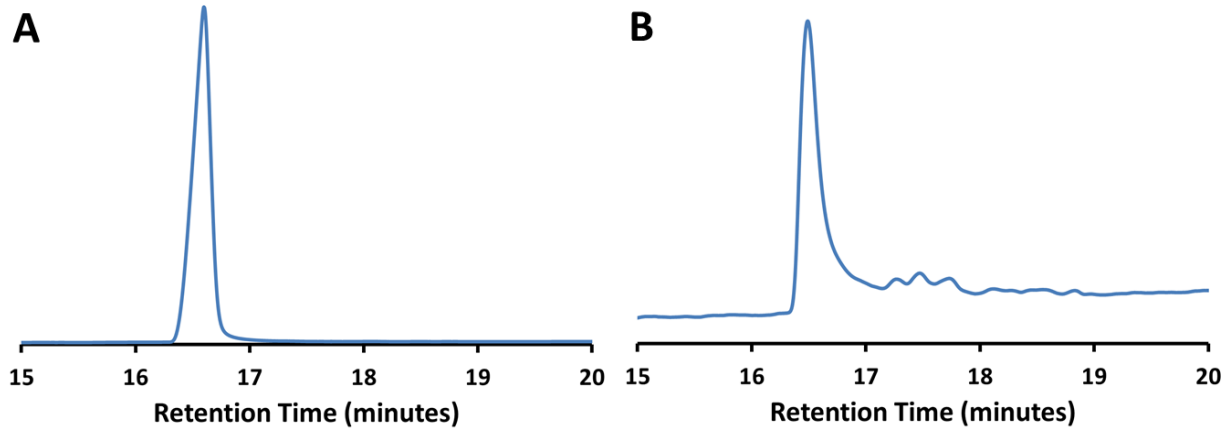

Figure 67: HPLC analysis of Pden_1323 heme oxygenase control reactions containing A) no ascorbic acid and B) no enzyme.

Next, the deuteroheme standard and the Pden_1323 deuteroheme reaction were analyzed using HPLC and MS. Deuteroheme has a HPLC retention time of 6.5 minutes, and in the Pden_1323 deuteroheme oxygenase assay, this peak is replaced with a new peak with a retention time of 19.5 minutes, indicative of substrate conversion (Figure 68). When the standard sample was analyzed via MS, a peak with a 564.14 *m/z* was found, which matches the theoretical value for deuteroheme exactly (Figure 69). We expected to see an analogous 530.22 *m/z* peak in the deuteroheme oxygenase reaction, but instead we saw neither substrate nor product peaks.

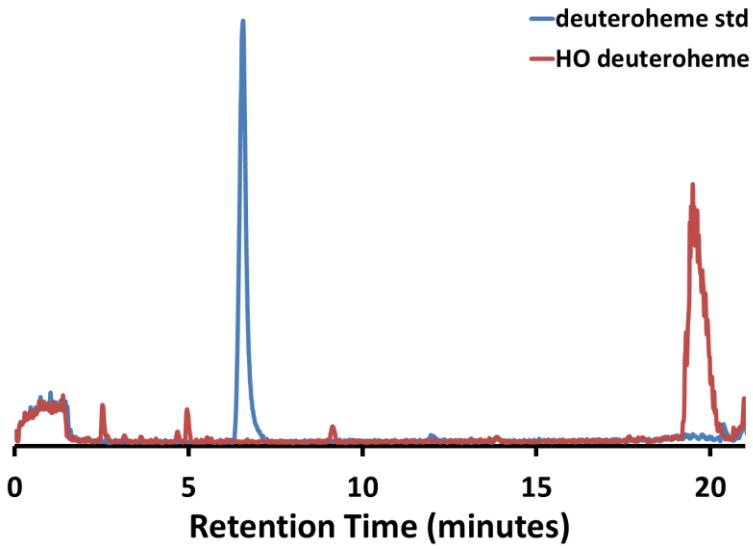

Figure 68: HPLC analysis of the deuteroheme standard and the Pden_1323 deuteroheme oxygenase reaction.

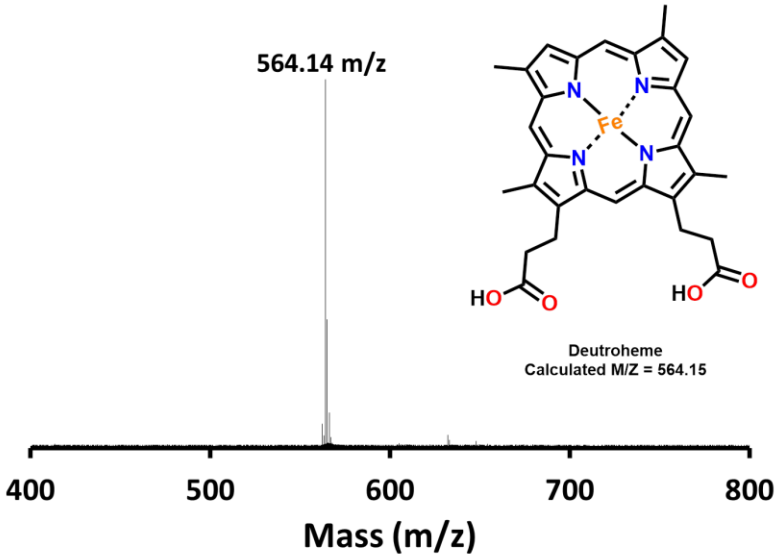

Figure 69: Mass spectrum of the deuteroheme standard.

We then submitted the PPIX and Mn-PPIX standards and their corresponding Pden_1323 reactions for HPLC and MS analysis. The PPIX has a HPLC retention time of 26.3 minutes, which can be seen in both the standard and the Pden_1323 reaction (Figure 70). There is a new peak formed in the reaction with a retention time of 28 minutes, which is attributed to spontaneous metal ion insertion (Figure 70). In the MS spectrum of the PPIX standard, there was a peak with a 563.27 *m/z*, which matches the calculated value for the protonated molecular ion exactly (Figure 71). In the HPLC traces of Mn-PPIX and the Mn-PPIX Pden_1323 reaction, Mn-PPIX has a retention time of 25.8 minutes and a new peak is formed at 27.5 minutes in the reaction. (Figure 72). When analyzed by MS, the Mn-PPIX standard results showed a 563.27 *m/z* peak, suggesting that the Mn^{2+} ion might not have been chelated by PPIX or it may have fallen out during the MS analysis. The only peaks detected in the mass spectrum of both the PPIX and Mn-PPIX Pden_1323 reactions were the 563.27 *m/z* peak corresponding to PPIX.

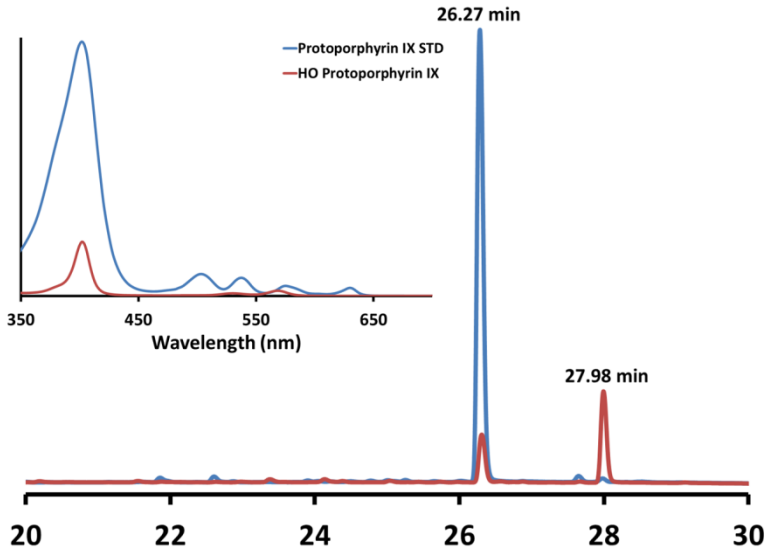

Figure 70: HPLC and UV-visible spectra of the protoporphyrin IX standard and its reaction with Pden_1323.

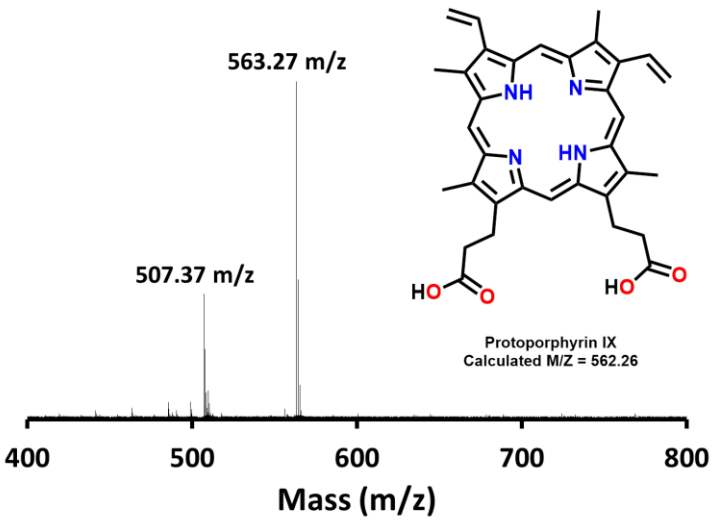

Figure 71: Mass spectrum of protoporphyrin IX standard.

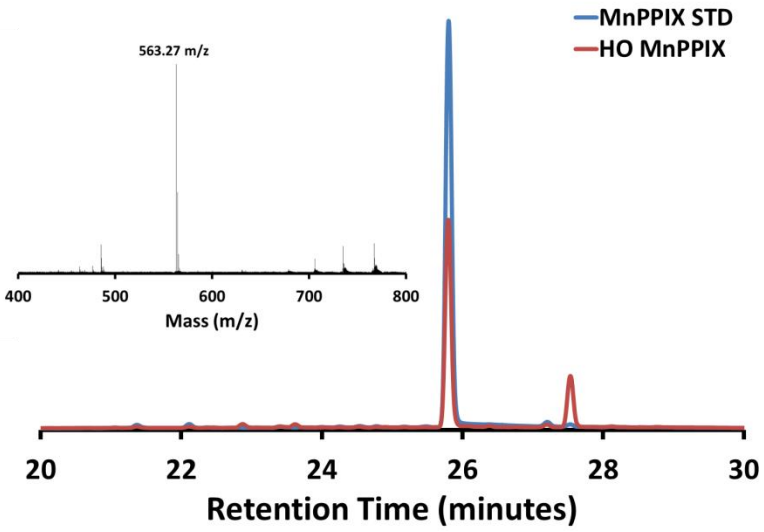

Figure 72: HPLC analysis of the Mn-Protoporphyrin IX standard and its reaction with Pdem_1323. Inset: MS data from the Pden_1323 reaction.

3.4 Discussion

Despite the annotation as a P(M/N)P oxidase, the data suggest that Pden_1323 is most likely a non-canonical heme oxygenase that is capable of converting of heme to biliverdin. This process would provide the iron needed to support the metabolism of *P. denitrificans*. As

reported in literature, it was also observed that ascorbic acid alone could partially degrade hemin to biliverdin.[126] Although the UV-visible traces indicated that deuteroheme and Mn-PPIX could also be used as substrates for the Pden_1323 reaction, the MS data could not confirm this. However, the substrate could also not be found in either case, which suggests that a reaction occurred, even though no product was found. This is attributed to the excess iron and reducing agents in the reaction and it being carried out aerobically, which, in combination, can lead to Fenton chemistry and the production of reactive oxygen species that could degrade both the substrate and product. It was also determined that PPIX was not a substrate for Pden_1323, which supports the currently proposed heme oxygenase mechanism that requires that the metal center of the heme molecule helps to facilitate its own degradation.

Chapter 4: Pden_2333 is a Potentially Novel Bacterioferritin That Provides Iron for the Biosynthesis of Siroheme and Heme d_1 in *Paracoccus denitrificans*

4.1 Introduction

Denitrifying bacteria use tetrapyrroles such as heme, siroheme, and heme d_1 in their energy metabolism.[1] Heme and siroheme are cofactors in two types of ammonia forming nitrite reductases, and heme d_1 is used in one type of nitric oxide forming nitrite reductase.[4–6] In many organisms, the biosynthesis of heme and siroheme is well understood, but the biosynthetic pathway for heme d_1 has yet to be fully characterized.[58,127] It has been shown that siroheme is an intermediate in the heme d_1 pathway and there are multiple enzymes, monofunctional or multifunctional, that can perform the methylation, dehydrogenation, and ferrochelation reactions required for the conversion of uroporphyrinogen III to siroheme.[57,58]

In *P. denitrificans* the enzyme responsible for the dehydrogenation step of siroheme biosynthesis is unknown. A homolog of CbiX, a cobaltochelatase involved in cobalamin biosynthesis, has been implicated in the ferrochelation of sirohydrochlorin in *P. denitrificans*. Clustered with *cbiX* is a gene, *pden_2333*, encoding a hypothetical protein with a conserved domain of unknown function (DUF4202, Figure 73). Proteins of this class are usually between 187 and 202 amino acids in length and have two conserved amino acid motifs: LED and KMS. The importance of these conserved amino acids as well as the function of these proteins are unknown, and many are incorrectly annotated as glutamyl tRNA synthetases (Figure 74). In some organisms the DUF4202 superfamily member is fused with *cbiX*, which supports the hypothesis that it could be involved in for the formation of siroheme, possibly serving as the missing precorrin 2 dehydrogenase.

Figure 73: Gene cluster containing *cbiX* and *pden_2333* in *P. denitrificans*.

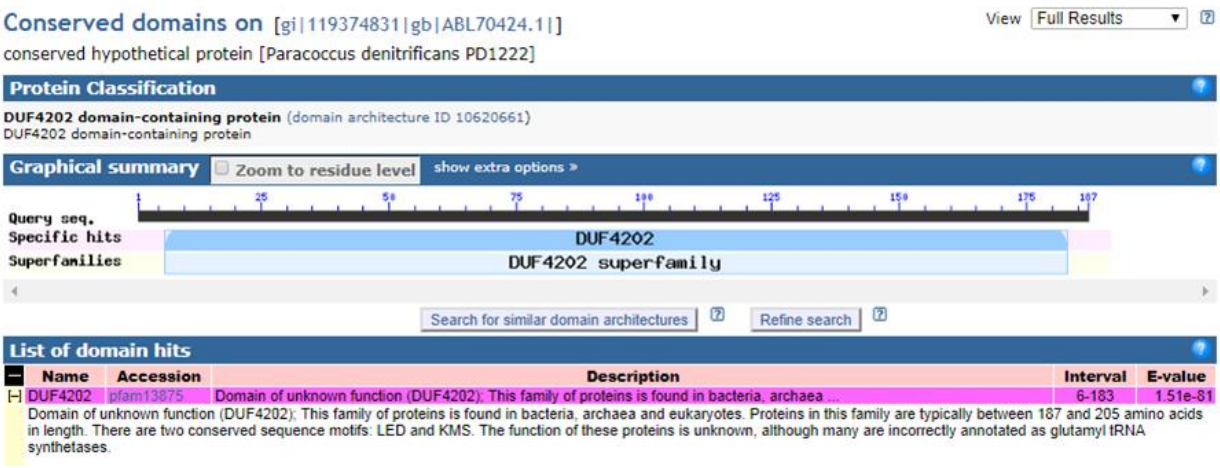

Figure 74: Conserved domain structure of Pden_2333.

Structure prediction analysis was performed using the Iterative Treading ASSEmbly Refinement (I-Tasser) server and the predicted structure shows a helical fold containing eight α-helices (Figure 75).[80,81,128] This fold is similar to that observed in the ferritin and bacterioferritin superfamily, which are iron storage proteins (Figure 76). I-Tasser also predicts a metal ion binding site inside the protein as well as the position of potential ligands that could coordinate a heme molecule (Figure 75).

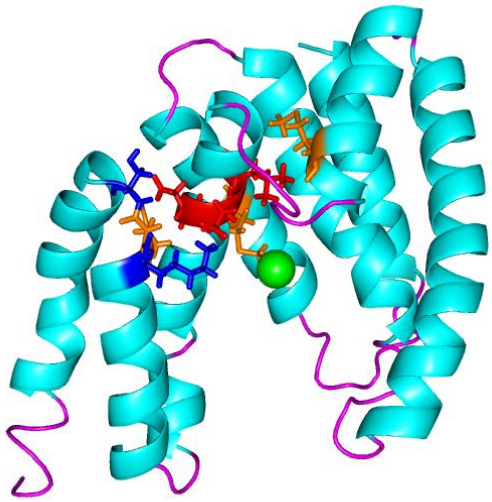

Figure 75: I-Tasser structure prediction of Pden_2333 with magnesium bound. Methionine-orange, LED – red, KMS – dark blue.

Iron is required for nearly all organisms to survive and grow but it is toxic, has low solubility, and has low availability. This is resolved in part through the use of iron storage proteins. Bacteria contain two types, bacterioferritins and ferritins, the former of which is heme-dependent and the latter of which is not (Figure 76). These two iron storage proteins are distantly related but are similar in structure and functional properties. Both are composed of 24 subunits that form a spherical ball with a hollow center. This hollow center is where the iron is stored. In most ferritins, the active site of each subunit is a ferroxidase center that is able to mediate the iron uptake, oxidation, and core formation process. Bacterioferritin genes are often clustered next to a small [2Fe-2S] ferredoxin protein, Bfd. Bfd could interact directly with bacterioferritin and aid in the release/delivery of iron by donating/accepting electrons to/from the core.[129]

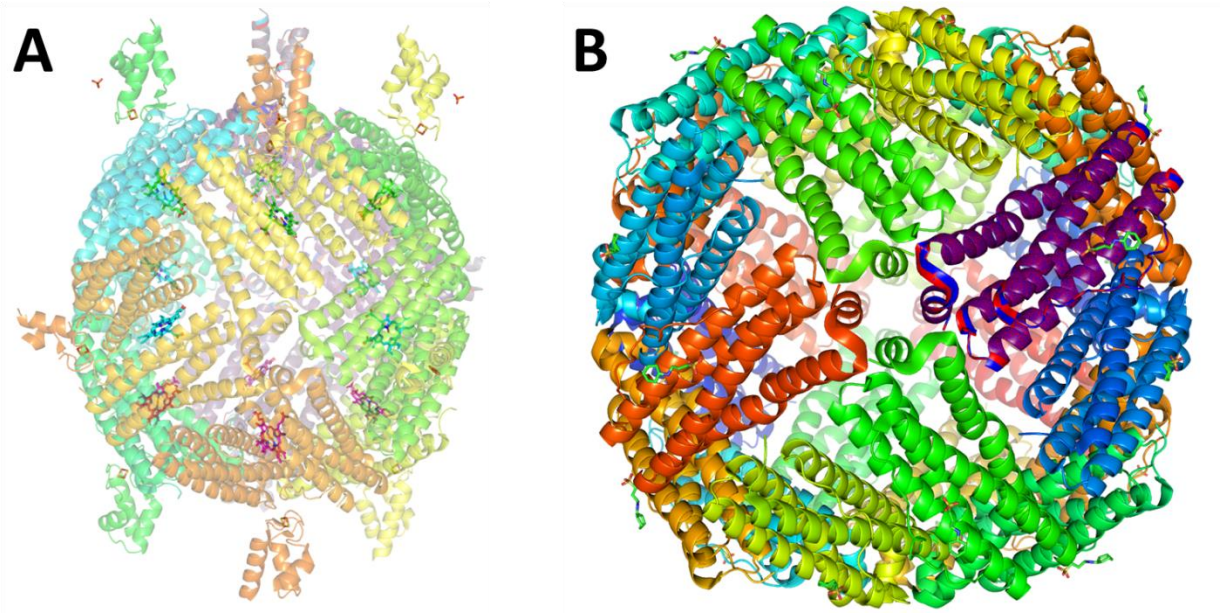

Figure 76: Structures of A) bacterioferritin (BfrB) in complex with bacterioferritin associated ferredoxin (Bfd) and B) bacterial ferritin (FtnA) from *Pseudomonas aeruginosa*.

Iron can be incorporated into proteins in several different forms, such as: heme, iron-sulfur clusters, iron-nickel complexes, and mono- and dinuclear iron centers. There are numerous biological processes that require iron-containing proteins including respiration, oxygen binding and activation, peroxide and oxygen degradation, amino acid and pyrimidine biosynthesis, the citric acid cycle, DNA synthesis, nitrogen fixation, carbon fixation, photosynthesis, aromatic compound degradation, and gene regulation.[129]

Iron taken in by the cell is primarily incorporated into hemoproteins or iron storage proteins. There is a low concentration "free" iron within the cell that forms in a low-molecular weight (LMW) iron pool. The function and details of the iron pools is currently under debate.[129] Most of the free ferrous iron is located within the cytosol of bacteria and the mechanism of keeping the iron in the reduced state, especially under aerobic conditions is unknown.[129]

Ferritin-like molecules play an important role in cell homeostasis by storing large amounts of Fe^{3+}, which is highly insoluble, and by oxidizing toxic Fe^{2+} form so it does not react with O_2 to generate reactive oxygen species. Ferritins and bacterioferritins form a polymeric (24-mer) hollow ball-like structure in which the iron is stored inside. When the iron is needed for metabolism, iron in the ferric mineral core is reduced, solubilizing it, and it exits the complex via channels at the three-fold symmetry axis of the multimer.[130] Mammals have a ferritin homolog that is comprised of two different (heavy and light) subunits that self-assembles in various ratios depending on the type of tissue to form the hollow 24-mer.[131]

The difference between bacterioferritin and bacterial ferritin is that the former contains heme within the dimer interfaces, whereas the latter does not. The heme plays an important role in the electron transfer used to reduce the ferric iron in the core to the ferrous form.[132] Thus, bacterioferritin functions as both an electron transfer protein and an iron storage protein. In addition to heme, bacterioferritin contains one binuclear iron binding site (the ferroxidase center) per subunit. The occupancy of the binuclear sites is dependent on pH. At high pH (pH ~8.0) both of the binuclear sites are filled and at low pH (pH ~5.3) both sites are empty.[133]

Excess iron in the cell is stored by ferritin and bacterioferritin as a ferric mineral. When iron concentrations in the cell drop, the iron stored inside the ferritin and bacterioferritin spheres can be mobilized to fulfill the needs of the cell.[134] Ferritin and bacterioferritin differ in that ferritin has a crystalline ferrihydrite core, whereas bacterioferritin contains a ferric-hydroxyphosphate core.[135]

It has been shown that a ferritin dimer is the first intermediate in the assembly of the 24-mer. It can spontaneously self-assemble in the presence of high salt concentrations. It has also

been shown that it disassembles at low pH and reassembles at high pH, allowing different size iron nanoparticles to be formed inside it. Purified assembled ferritin molecules can incorporate a variety of metal ions in the center (e.g., Fe, Au, Pd, Rh, Pr, Ni, Cr, Cd, Ti, Tb, Co, Cu).[136]

In addition to iron storage proteins, other bacteria such as *Helicobacter pylori* contain a histidine rich, nickel storage proteins, Hpn, that is 60 amino acids long, 28 of which are histidine residues. There are two separate stretches of six to seven histidines in a row, as well as several other amino acid patterns that suggest tight binding of metal ions.[137] It has been shown that *H. pylori* Hpn binds five nickel ion per monomer at pH 7.4 and under physiological conditions it is a 20-mer. *In vivo* Hpn has preferential binding affinity for $Ni^{2+} > Bi^{3+} > Cu^{2+} \approx Zn^{2+}$.[138]

In this chapter, the potential involvement of Pden_2333 in the biosynthesis of siroheme and heme d_1 (as either a precorrin 2 dehydrogenase or a novel type of bacterioferritin) is investigated.

4.2 Methods and Materials

All chemicals were purchased from Frontier Scientific, Inc. (Logans, UT), Sigma-Aldrich (St. Louis, MO), or Bio-Rad (Hercules, CA) unless otherwise stated. Primers were ordered from Sigma-Aldrich and the synthesized *pden_2333* gene was purchased from GeneArt, A Thermo Fisher Scientific Company (Waltham, MA). *Spinacia oleracea* (spinach) ferredoxin and ferredoxin reductase were purchased from Sigma-Aldrich.

Expression Vector Construction. The *pden_2333* gene was codon optimized for *Escherichia coli* including restriction enzyme sites at the 5' (NdeI) and the 3' (XhoI) end of the gene for use in restriction enzyme cloning.

The plasmid containing the codon optimized *pden_2333* gene and the pET-28b(+) vector were subjected to restriction enzyme digestion, separately as follows: 1 µg plasmid, 5 µL 10x CutSmart Buffer, 1 µL NdeI, 1 µL XhoI, and the reaction was made to volume (50 µL) with water. The reaction was incubated at 37 °C for 1.5 hours, and then heat inactivated at 65°C for 20 minutes. Restriction enzyme digested *pden_2333* was purified via a Lonza FlashGel™ DNA Cassette (Basel, Switzerland). The product was then recovered with an Omega BIO-TEK E.Z.N.A.® Gel Extraction Kit (Norcross, GA), following the protocol provided in the manual. The pET-28b(+) reaction was treated with the Omega BIO-TEK E.Z.N.A® Cycle Pure Kit following the protocol provided in the manual. The digested *pden_2333* product and pET-28b(+) vector were then ligated together using T4 DNA Ligase (NEB) following the manufacture's protocol. The ligated mixture was then transformed into *E. coli* TOP10 cells and plated on Lysogeny Broth(LB) agar plates containing kanamycin (50 µg/mL). Colonies were picked, grown in liquid LB medium, and the resulting plasmid was prepared using an Omega BIO-TEK E.Z.N.A.® Plasmid Mini Kit. The purified plasmid was then submitted to Eurofins Genomics (Louisville, KY) for sequencing. After sequence verification, the plasmid was transformed into *E. coli* BL21 (DE3) cells.

Protein Expression and Purification. The pET-28b(+):*pden_2333* plasmid was overexpressed in *E. coli* BL21-(DE3) cells. The cultures were grown at 37 °C until the OD_{600} reached 0.6, after which they were induced with isopropyl-β-D-1-thiogalactopyranoside (IPTG) at a final concentration of 400 µM and grown for 4 hours.

The cells were centrifuged at 15,900 x g for 45 minutes. The medium was decanted, and the cells were re-suspended in 50 mM sodium phosphate, 300 mM NaCl, 5 mM imidazole, pH 8.0 buffer. The cells were sonicated and centrifuged at 15,900 x g for 1 hour. The supernatant was

then loaded onto a Bio-Rad Econo-Pac column containing Ni-charged Profinity IMAC resin and the flow-through was collected. The column was then washed with 50 mM sodium phosphate, 300 mM NaCl, 5 mM imidazole, pH 8.0 buffer, and the wash fraction were collected. Then the protein was eluted, and 1 mL factions were collected after adding 50 mM sodium phosphate, 300 mM NaCl, 500 mM imidazole, pH 8.0 buffer. The fractions containing Pden_2333 were combined and spin concentrated/buffer exchanged in 100 mM Tris, pH 8.0 buffer.

Size Exclusion Chromatography. Size exclusion chromatography (SEC) was performed using an Agilent 1260 Infinity HPLC. Two different columns were used: an Agilent Bio SEC-3, 3 µm, 100 Å, 7.8 x 300 mm column and an Agilent Bio SEC-3, 3 µm, 300 Å, 7.8 x 300 mm column. The oligomerization state of Pden_2333 was analyzed with SEC via a 25 minute isocratic method using 100 mM Tris buffer, pH 8.0.

Pden_2333 Dehydrogenase Activity Assay. Pden_2333 was tested for precorrin 2 dehydrogenase activity in a MBRAUN anaerobic chamber. First, a positive precorrin 2 dehydrogenase (SirC) control reaction was performed by adding porphobilinogen (PBG) deaminase (HemC, 1.77 µM), uroporphyrinogen III synthase (HemD, 2.16 µM), uroporphyrinogen III methyltransferase (SirA, 4.33 µM), SirC (15.19 µM), PBG (884 µM), *S*-adenosyl-L-methionine (SAM 1 mM), nicotinamide adenine dinucleotide (NAD^+, 30 µM), and $MgCl_2$ (40 µM) in Chelex-treated 50 mM Tris-HCl, pH 8.0 buffer (250 µL total volume). The reaction was incubated at 37 °C for 12 hours. A SirA reaction was also performed by adding HemC (1.77 µM), HemD (2.16 µM), SirA 4.33 µM), PBG (884 µM), SAM (1 mM), $MgCl_2$ (40 µM) in Chelex-treated 50 mM Tris-HCl, pH 8.0 buffer (250 µL total volume). The reaction was incubated at 37 °C for 12 hours. Pden_2333 was substituted for SirC and NAD^+, FMN, and flavin

adenine dinucleotide (FAD) were all tested as cosubstrates. Reaction conditions as follows: HemC (1.77 μM), HemD (2.16 μM), SirA (4.33 μM), Pden_1323 (15.19 μM), PBG (884 μM), SAM (1 mM), NAD^+/FMN/FAD (30 μM), $MgCl_2$ (40 μM) in Chelex-treated 50 mM Tris-HCl, pH 8.0 buffer (250 μL total volume). The reaction was incubated at 37 °C for 12 hours. A Pden_2333 control was also performed with no cofactor as follows: HemC (1.77 μM), HemD (2.16 μM), SirA (4.33 μM), Pden_2333 (15.19 μM), PBG (884 μM), SAM (1 mM), and $MgCl_2$ (40 μM) in Chelex-treated 50 mM Tris-HCl, pH 8.0 buffer (250 μL total volume). The reaction was also incubated at 37 °C for 12 hours.

Iron Loading and Mobilization Assay. Pden_2333 was tested for iron loading and mobilization activity under various conditions. The first iron loading assay was performed aerobically and contained Pden_2333 (0.25 μM), hemin (36 μM), increasing ferrous sulfate concentrations from 10 μM – 50 μM in with 50 mM Tris, pH 8.0 buffer (500 μL total volume). The reaction was then repeated using an iron concentration of 30 μM. Iron loading was then tried anaerobically in a MBRAUN LABmaster glovebox. This reaction contained Pden_2333 (0.25 μM), hemin (36 μM), and ferric chloride (30 μM) in anaerobic 50 mM Tris-HCl, pH 8.0. UV-visible absorption spectra were taken using a Nanodrop 2000C (Thermo Fisher). After iron loading, the reactions were tested for iron mobilization. The reaction conditions were as follows: ferredoxin (60 μg/ml), ferredoxin-$NADP^+$ reductase (8 μg/ml), FAD (20 μM), and NADPH (1.5 mM) in 1 mL of anaerobic 50 mM Tris-HCl, pH 8.0 buffer. These reactions were incubated at 37 °C with stirring, and UV-visible spectra were taken every 15 seconds for 5 minutes and then every 2 minutes for 1 hour using a Nanodrop One^C (Thermo Fisher).

A ferredoxin/ferredoxin-$NADP^+$ reductase-assisted iron loading assay was performed anaerobically. The contents of the reaction were Pden_2333 (0.25 µM), hemin (9 µM), ferrous sulfate (30 µM), ferredoxin (60 µg/ml), ferredoxin-$NADP^+$ reductase (8 µg/ml), FAD (20 µM), and NADPH (50 µM). The reaction was then made to volume (1 mL) with anaerobic 50 mM Tris-HCl, pH 8.0 buffer. Control reactions were performed without FAD and without Pden_2333. The samples were incubated at 37 °C, with stirring and UV-visible spectra were taken every 15 seconds for 5 minutes and then every 2 minutes for 1 hour using a Nanodrop One^C (Thermo Fisher).

Lastly, a Pden_2333 iron loading assay was performed anaerobically with equal amounts of Pden_2333, hemin, and ferrous sulfate (9 µM final concentration) in 1 mL PBS buffer, (0.14 M NaCl, 3 mM KCl, 0.01 M Na_2HPO_4, 2 mM KH_2PO_4), pH 7.6. The reaction was heated to 37 °C and incubated with stirring. UV-visible spectra were recorded every 5 minutes for one hour using a Nanodrop One^C (Thermo Fisher). Iron loaded Pden_2333 was then tested for iron mobilization. These reactions were also performed anaerobically at 37 °C with stirring. Ferredoxin (60 µg/ml), ferredoxin-$NADP^+$ reductase (80 µg/ml), FAD (1 µM), NADPH (50 µM), and 2,2'-bipyridine (bipy) (3 mM) were added to the iron loading assay and made to volume (1 mL) with PBS buffer, pH 7.6. The reaction was monitored at 523 nm to measure the time-dependent formation of $[Fe(bipy)_3]^{2+}$ every 15 sec for 5 min and then every 2 minutes thereafter for one hour using a Nanodrop One^C.

4.3 Results

Size Exclusion Data. The theoretical molecular weight of Pden_2333 is approximately 21.3 kDa for the monomeric form of the protein (Table 3). The SEC data obtained using the 100 Å Bio SEC-3 columns yielded two peaks at approximately 5.8 minutes and 7.3 minutes (Figure 77), which resulted in molecular weights of ~64.5 kDa and ~20.6 kDa, respectively. These molecular weights are consistent with trimeric and monomeric oligomeric states (Table 3).

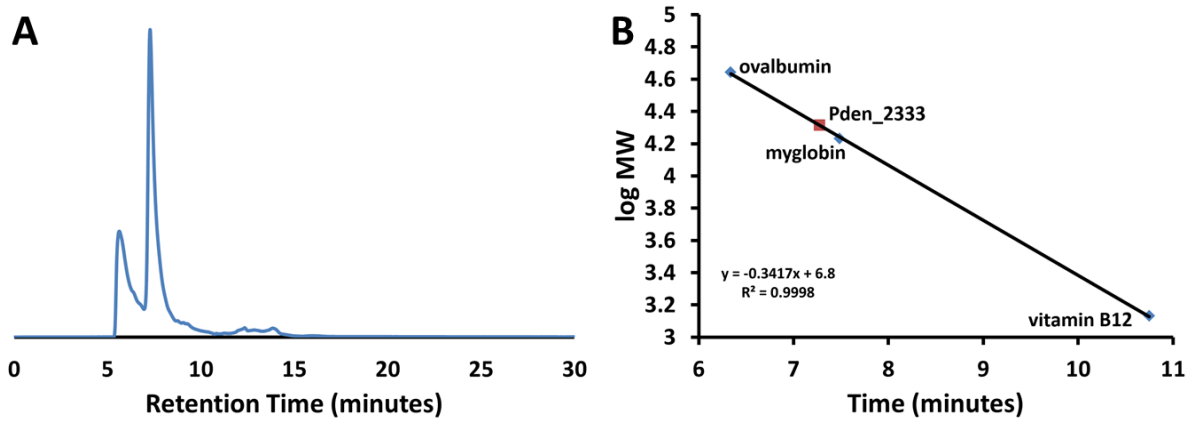

Figure 77: A) Size-exclusion HPLC analysis of Pden_2333 using a 100 Å Bio SEC-3 column and B) size-exclusion chromatography data of Pden_2333

Table 3: Theoretical molecular weight of Pden_2333 and its oligomeric states (left). Protein Standards and their molecular weights (right).

Oligomeric State	Theoretical Molecular Weigh (Da)
Monomer	21,270
Dimer	42,540
Trimer	63,810
Tetramer	85,080
Ball (24-mer)	510,485

Protein Standard	Molecular Weight (Da)
Thyroglobulin	670,000
γ- globulin	158,000
ovalbumin	44,000
myoglobin	17,000
vitamin B_{12}	1,350

The effects of iron, pH, and the presence of tetrapyrroles (specifically hemin, sirohydrochlorin, or siroheme) on the oligomerization state of Pden_2333 was investigated using the 300 Å Bio SEC-3 column (Figure 78). As with the 100 Å Bio SEC-3 column, the SEC data of Pden_2333 was consistent with a mixture of monomers and higher order oligomers. In the presence of iron, the ~ 5 minute peak corresponding to the higher oligomer diminished. In contrast, when hemin, sirohydrochlorin, or siroheme is added to Pden_2333, the fraction of the enzyme in the higher order oligomeric state increases. In the presence of both iron and hemin (at pH 1.0 or 8.0), intermediately sized oligomers are formed.

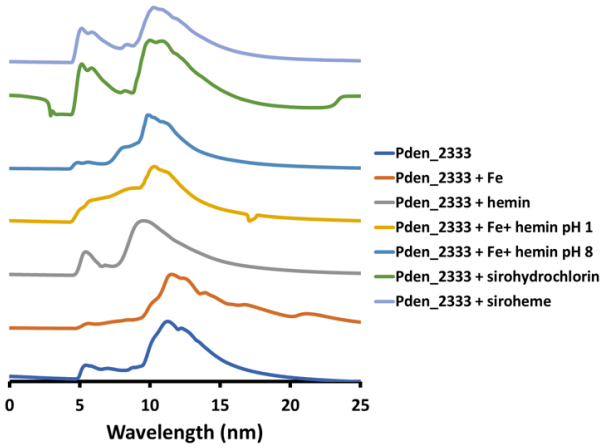

Figure 78: Size-exclusion HPLC analysis of Pden_2333 using a 300 Å Bio SEC-3 column.

Pden_2333 Dehydrogenase Assays. Pden_2333 was then tested for precorrin 2 dehydrogenase activity. Pden_2333 was incubated with enzymatically prepared precorrin 2 and a number of potential hydride acceptors (NAD^+, $NADP^+$, FAD, and FMN). Comparison with a positive control reaction containing the precorrin 2 dehydrogenase SirC suggested that in each case, sirohydrochlorin was not formed (Figure 79 A). However, in the presence of Pden_2333, with or without $NAD(P)^+$, there is a change from a triplet peak between 550 nm and 650 nm to

a double peak at 600 and 650 nm. This was later shown to be indicative of sirohydrochlorin binding to Pden_2333 (data not shown).

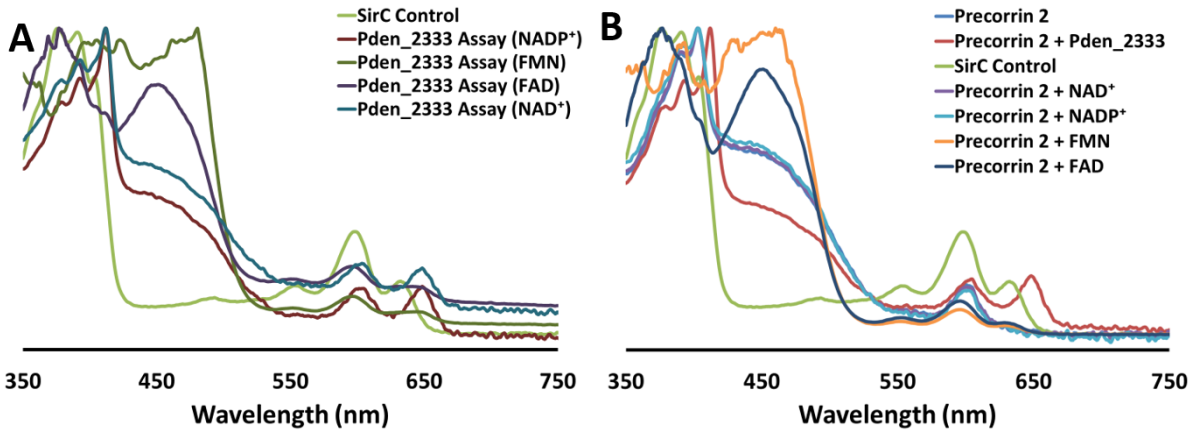

Figure 79: Pden_2333 precorrin 2 dehydrogenase reactions A) and control reactions B).

Pden_2333 Iron loading and mobilization Assay. Pden_2333 was analyzed for its ability to store and then mobilize iron using a variety of conditions. When iron is mineralized in the core of ferritin, it results in a gradual increase in the absorbance at 280 nm.[134] Therefore, the iron loading activity of Pden_2333 was determined (using varying concentrations of iron between 10 µM and 50 µM) by monitoring the change in absorbance at this wavelength. It was found that a concentration of 30 µM iron was optimal to give rise to a large increase in absorbance without being saturated (Figure 80). A 30 µM iron reaction was then used to load Pden_2333 and an iron mobilization reaction was performed. A change in absorbance was observed between 400 nm and 500 nm, suggesting the iron is being reduced and released from the protein (Figure 80 B). Next, the ability of Pden_2333 to load and mobilize iron under anaerobic conditions was investigated. Similar increase in the absorbance at 280 nm was observed for the anaerobic Pden_2333 iron loading reaction (Figure 81 A), however, a change in the spectrum between 400-500 nm can also been seen in the anaerobic iron mobilization assay (Figure 81 B), which is

different than that seen in the aerobic iron mobilization. This difference could be due to presence of oxygen in the aerobic iron mobilization assay.

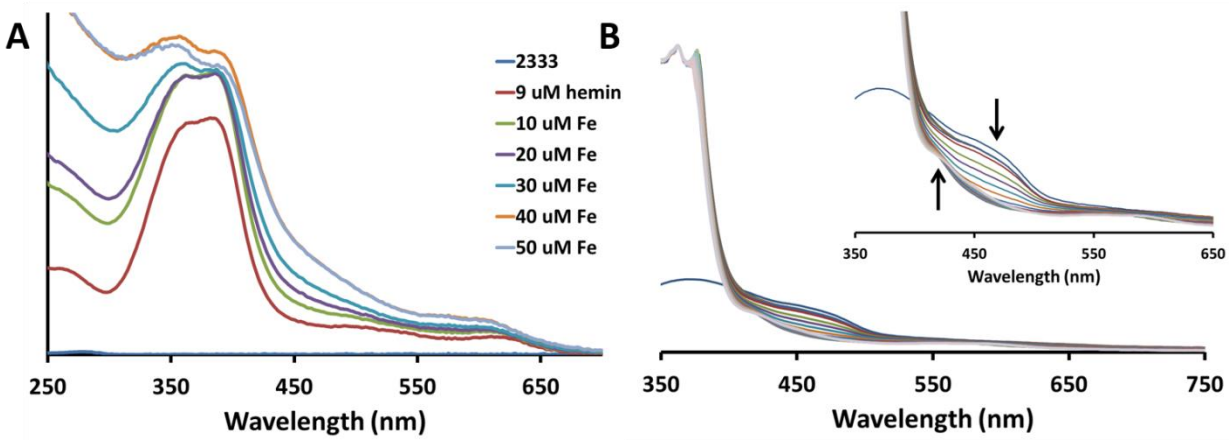

Figure 80: Aerobic Pden_2333 iron loading and mobilization assays. A) Iron loading reactions with various concentrations of ferrous sulfate B) Iron mobilization reactions with Pden_2333 loaded with 30 µM ferrous sulfate.

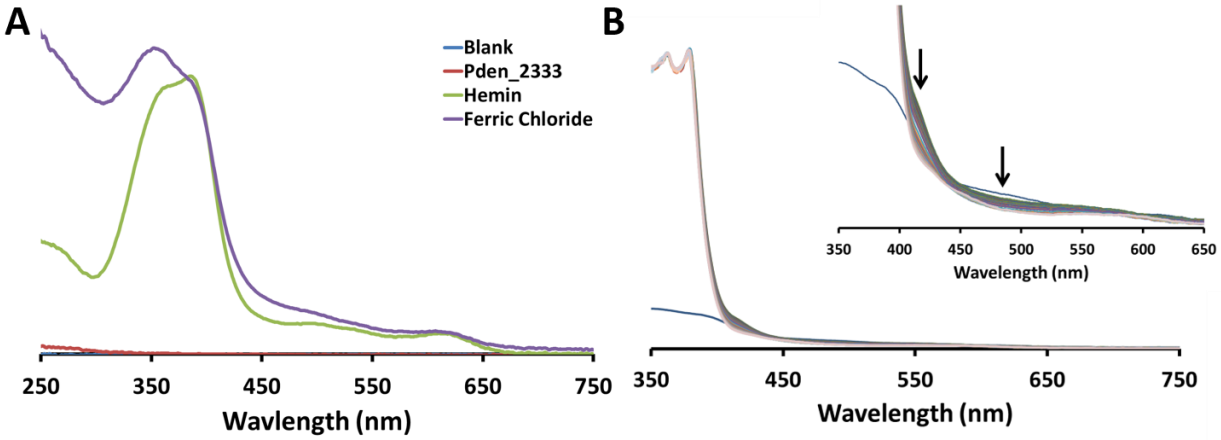

Figure 81: Anaerobic Pden_2333 Iron loading A) and iron mobilization B) assays with ferric chloride.

We then tried ferredoxin/ferredoxin-NADP$^+$ reductase-assisted loading and mobilization of iron with Pden_2333. In the presence of this reducing system there was a slight decrease in the Soret band of the ferredoxin/ferredoxin-NADP$^+$ reductase assay (Figure 82 A). This is consistent with the reaction not producing multiple turnovers, and therefore not a large spectral change. In both the no FAD and no Pden_2333 controls, there was a significant decrease in the Soret band (Figure 82 B and C, respectively).

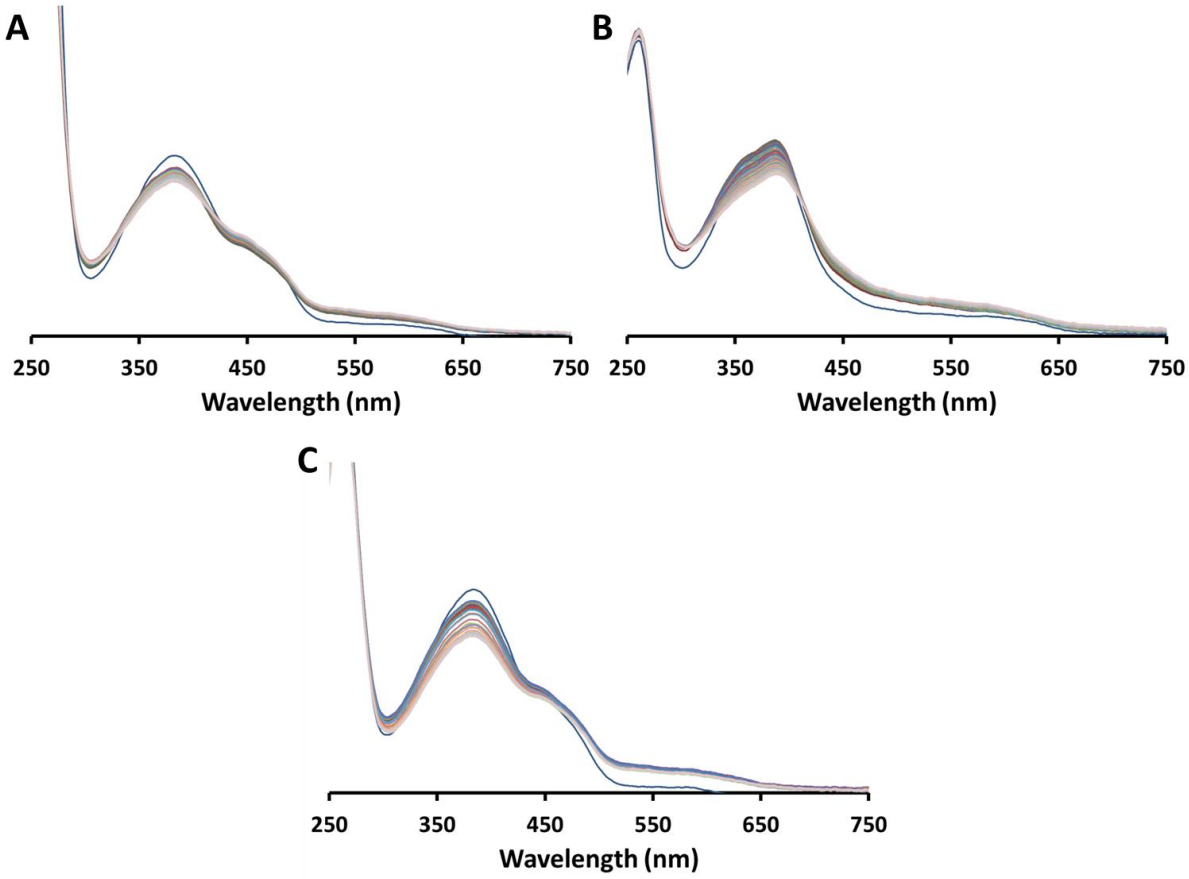

Figure 82: Ferredoxin/ferredoxin-NADP$^+$ reductase-assisted iron loading and mobilization assays. A) Pden_2333 iron loading/mobilization assay. B) No FAD control. C) No Pden_2333 control.

Lastly, Pden_2333 was loaded with iron and hemin in a 1:1:1 ratio (Figure 83 A). As the iron loading assay progressed, an increase in the absorbance at 280 nm was observed (Figure 83 B). Under the assay conditions, a 30 minute lag phase is observed, after which the absorbance steadily increases. The lag in iron loading is consistent with what has been shown previously by both ferritin and bacterioferritin.[131,139] In the Pden_2333 iron mobilization assay, the iron was released and chelated by bipy in solution to form a ferrous-bipy complex, resulting in an increase in absorbance at 523 nm (Figure 83 C and D).

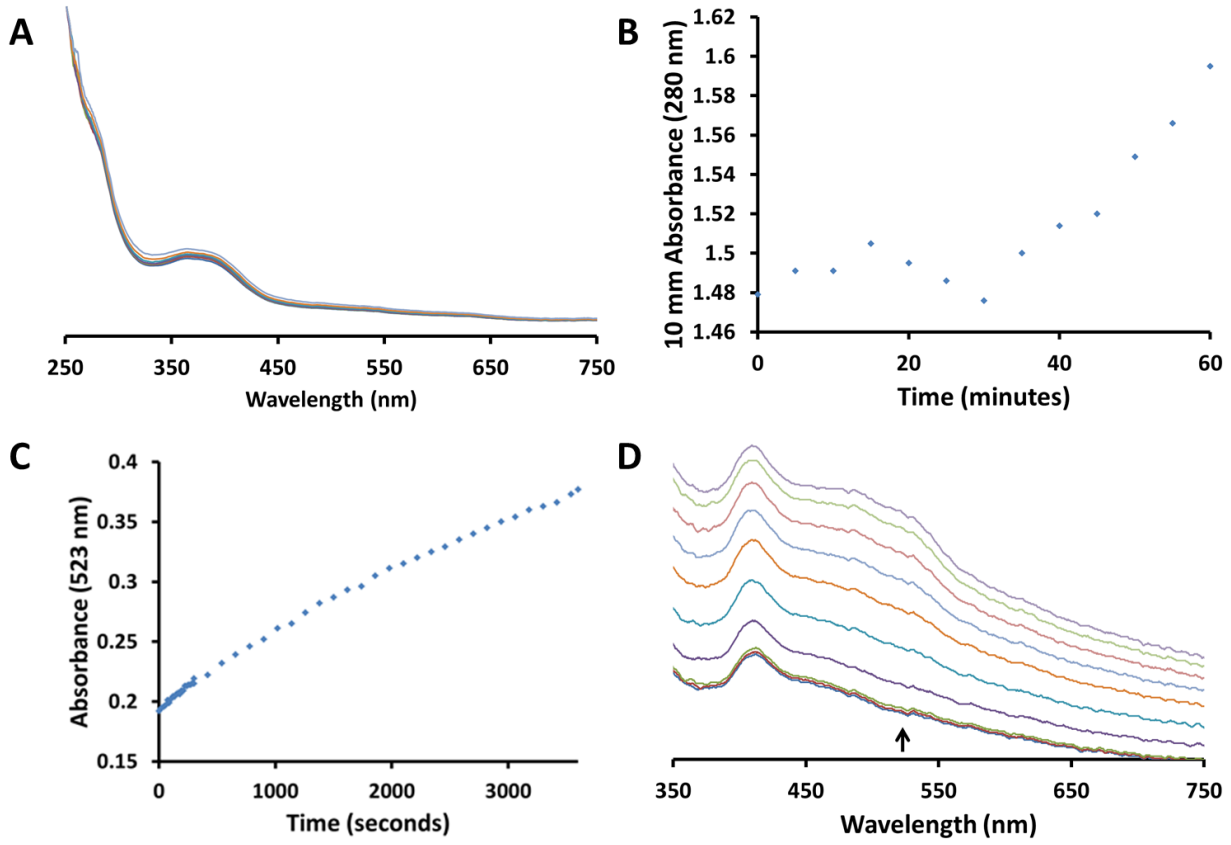

Figure 83: 1:1:1 Pden_2333:iron:hemin iron loading and mobilization assay. A) UV-visible spectra of the Pden_2333 iron loading assay B) Increase in absorbance at 280 nm, showing a lag in Pden_2333 iron loading. C) Increase in absorbance at 523 nm due to iron mobilization by ferredoxin/ferredoxin-NADP$^+$ reductase and bipy chelation D) UV-visible spectra of the Pden_2333 iron mobilization assay

4.4 Discussion

The data shown above indicates that both *apo* and hemin-bound Pden_2333 are mostly monomers in solution but can form several higher order complexes. It was also shown that in the presence of hemin, sirohydrochlorin, or siroheme, Pden_2333 forms a more well-defined large oligomeric complex.

Originally, Pden_2333 did not seem capable of catalyzing the dehydrogenation of precorrin 2 to form sirohydrochlorin *in vitro*. However, after further research, it seems that the double peak spectrum at 600 and 650 nm (Figure 79) could possibly be sirohydrochlorin bound to the

enzyme (data not shown). Further investigation is needed to confirm the true product of the reaction.

Spectroscopic data are consistent with Pden_2333 forming a mineralized iron core, as well as mobilizing the iron when reduced by the ferredoxin/ferredoxin-$NADP^+$ reductase system. The iron loading of Pden_2333 was observed under multiple conditions: aerobic conditions with ferrous sulfate, anaerobic conditions with ferric chloride, and ferredoxin/ferredoxin-$NADP^+$ reductase-assisted. Iron loaded Pden_2333 was then shown to mobilize the iron anaerobically with the aid of ferredoxin/ferredoxin-$NADP^+$ reductase.

The function of iron storage proteins is extremely important for the biosynthesis of heme, heme d_1, and siroheme. They help to regulate the amount of iron available within the cell so toxic ferrous ions are not free within the cell. The data suggest that Pden_2333 is a novel iron storage protein that may supply iron to the CbiX homolog that was shown to be important for siroheme and heme d_1 biosynthesis in *P. denitrificans*. This process would require the mobilization of iron from the core of Pden_2333 and may involve protein-protein interactions.

Chapter 5: Conclusions and Future Work

The enzyme SirC from *M. acetivorans* has been shown to protect its product, sirohydrochlorin from spontaneous chelation of metals such as iron, cobalt, and zinc, rather than catalyze their insertion. Of the metals that were tested, nickel was shown to need assistance by the CbiX homolog CfbA from *M. acetivorans* to form Ni-sirohydrochlorin. In the future, we would like to investigate the putative protein-protein interactions of SirC and CfbA from *M. acetivorans*, as we propose that these enzymes hand off the product sirohydrochlorin from one active site to the other to help protect from spontaneous chelation. We would also like to determine the apparent K_d of iron and sirohydrochlorin for SirC and of nickel and sirohydrochlorin for CfbA, in addition to the kinetic parameters (k_{cat} and k_m) for each enzyme. Other future work could include investigations of the hydride transfer mechanism of SirC. It was noticed that the rate of SirC-catalyzed sirohydrochlorin formation is substantially greater at the physiological temperature of 37 °C then at room temperature. It will therefore be interesting to investigate whether protein motions and quantum mechanical tunneling are important for the SirC reaction by examining the temperature dependence of primary deuterium kinetic isotope effects (KIE) and viscosity effects on the rate of the reaction.

The enzyme responsible for the dehydrogenation of precorrin 2 to form sirohydrochlorin in *P. denitrificans* is still unknown. Both Pden_1323 and Pden_2333 were tested for dehydrogenase activity and Pden_1323 showed no activity, however Pden_2333 dehydrogenase activity could not be determined and further investigation is needed. The search for this enzyme is still underway and potential candidates have been identified; Pden_2334, Pden_2496, and Pden_2335.

NnrU in *Rhodobacter sphaeroides* is a protein that is important for nitrite and nitric oxide reduction. It has been shown that *nnrU* mutants do not produce nitric oxide and showed no detectable NIR activity under any growth conditions.[140] However, the potential function of NnrU in the denitrification process is unknown. Sequence alignments show homology of Pden_2496 and Pden_2334 to the N- and C- termini of NnrU from *R. sphaeroides* (Figure 84). The *pden_2496* gene is part of the *nir* cluster and *pden_2334* is found adjacent to the cobaltochelatase (*cbiX*) homolog that has been implicated in the ferrochelation of sirohydrochlorin in *P. denitrificans,* but is not found in *P. aeruginosa*, which utilizes CysG for siroheme biosynthesis (Figure 85). A homolog of NnrU found in maize, Z-ISO, is usually clustered with carotenoid biosynthetic genes and has been proposed to be capable of performing a cryptic redox reaction to isomerize C=C bonds during carotenoid biosynthesis.[140,141] Therefore, we propose that Pden_2496 and Pden_2334 together may perform the dehydrogenation step to convert precorrin 2 to sirohydrochlorin. The sequence identity/similarity between Z-ISO, NnrU, and Pden_2496/Pden_2334 is given in Table 4.

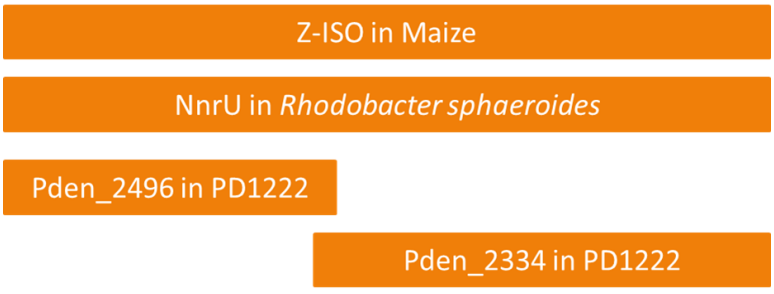

Figure 84: Pden_2496 and Pden_2334 share homology with the N- and C- terminal, halves of NnrU from *Rhodobacter sphaeroides* and Z-ISO from maize.

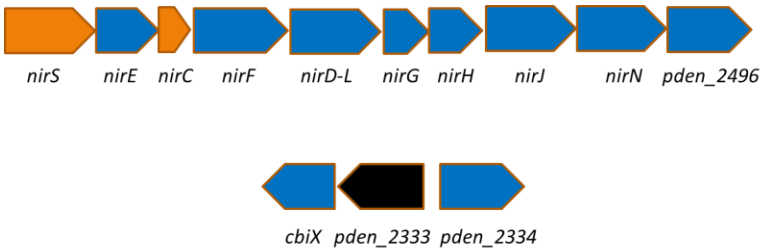

Figure 85: Gene cluster from *P. denitrificans* involved in heme d_1 biosynthesis.

Table 4: Sequence similarity/identity between Pden_2496/Pden_2333, NnrU, and Z-ISO.

	Zea mays Z-ISO	*P. denitrificans* Pden_2496	*P. denitrificans* Pden_2334
R. sphaeroides **NnrU**	52.7%/22.5%	58.5%/26.8%	53.7%/29.3%

Pden_2334 and Pden_2496 have been successfully cloned from *P.* denitrificans genomic DNA, but we have had trouble expressing the encoded proteins. We plan to continue testing different (co)expression and purification strategies to investigate whether these enzymes together are involved in the production of sirohydrochlorin in *P. denitrificans*.

On the other side of *pden_2334* is a gene, *pden_2335*, that is annotated as an FAD dependent oxioreductase. Pden_2335 contains a N-terminal $NAD(P)^+$-binding Rossmann-like domain and is homologous to glycine/ D-amino acid oxidase superfamily members and a bifunctional tRNA methyltransferase/FAD-dependent oxidoreductase. It is therefore also possible that this enzyme is involved in the biosynthesis of sirohydrochlorin in *P. denitrificans*. We have ordered a codon optimized *pden_2335* gene for heterologous expression in *E. coli* and will test the encoded enzyme for potential precorrin 2 dehydrogenase activity.

After siroheme is formed, the next step in the heme d_1 biosynthetic pathway is the NirDLGH catalyzed conversion of siroheme to didecarboxysiroheme, which is the substrate for

NirJ (and whose function has yet to be fully elucidated). In some organism NirDLGH are separate proteins, while in others NirD and NirL are fused. In *H. thermophiles* there is a fused NirDL but no NirG or NirH homolog.[68] We had difficulties expressing NirDLGH from *P. denitrificans;* therefore, we synthesized the *nirD-L* gene from *H. thermophiles*, expressed and purified the encoded protein, and confirmed that it successfully converts siroheme into didecarboxysiroheme.

Now that we have the substrate for NirJ, we would like to investigate NirJ activity. Originally, we cloned the *nirJ* gene from *P. denitrificans* and were able to express and purify the encoded protein. However, most of the expressed protein was insoluble and NirJ was found to be unstable during purification and precipitated out of solution. We then ordered codon optimized *nirJ* from *Dinoroseobacter shibae* (which was recently shown to be stably expressed in *E. coli*) and are currently working on expression and purification conditions.[84] Once NirJ is purified, attempts will be made to identify and characterize the products of its reaction. If successful, attempts will then be made to confirm the function of NirF and NirC in the conversion of the NirJ product to dihydro-heme d_1.

The *pden_1323* gene, which is clustered with putative ABC transporter genes and together could be responsible for the missing steps in heme d_1 biosynthesis, was tested for precorrin 2 dehydrogenase (as well as for PMP oxidase) activity. However, Pden_1323 was instead shown to degrade heme into biliverdin using ascorbic acid as an electron donor. In future studies, we would like to confirm the regiochemistry of the oxidative ring cleavage reaction and to obtain the crystal structure of Pden_1323 in complex with its substrate and/or

product. Very recently, the Mansoorabadi lab has solved the crystal structure of *apo* Pden_1323 to 1.9 Å resolution (Figure 86).

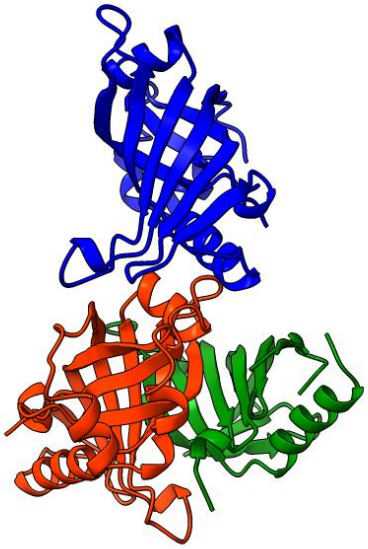

Figure 86: 1.9 Å crystal structure of Pden_1323.

The *pden_2333* gene, which contains a domain of unknown function (DUF4202), is clustered with a sirohydrochlorin cobaltochelatase (*cbiX*) homolog in *P. denitrificans.* Preliminary data suggest that it binds to and is organized by heme and may be a novel bacterioferritin that can store and mobilize iron. Current research is focused on confirming these results and testing to see if the *P. denitrificans* CbiX homolog can accept the iron released by Pden_2333 using reduced ferredoxin. In addition, high quality diffracting crystals of Pden_2333 have been obtained (Figure 87) and efforts are underway to determine the first structure of a DUF4202 superfamily member.

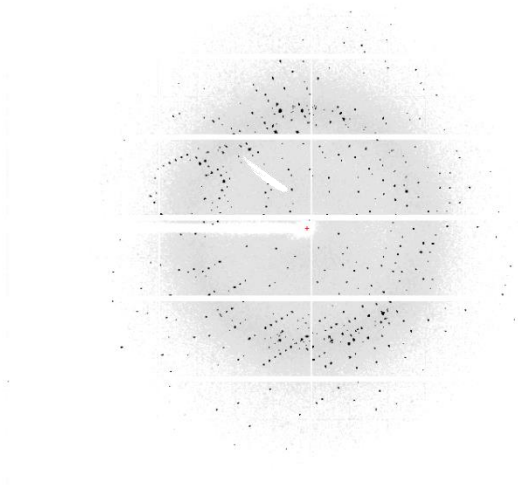

Figure 87: X-ray diffraction pattern of Pden_2333 cystal.

References

(1) Zumft, W. G. *Microbiology* **1997**, *61* (4).

(2) Van Alst, N. E.; Wellington, M.; Clark, V. L.; Haidaris, C. G.; Iglewski, B. H. *Infect. Immun.* **2009**, *77* (10), 4446–4454.

(3) Ni, S. Q.; Zhang, J. *Biomed Res. Int.* **2013**, *2013* (July 2013).

(4) Schnell, R.; Sandalova, T.; Hellman, U.; Lindqvist, Y.; Schneider, G. *J. Biol. Chem.* **2005**, *280* (29), 27319–27328.

(5) Einsle, O. *Structure and function of formate-dependent cytochrome c nitrite reductase, NrfA*, 1st ed.; Elsevier Inc., 2011; Vol. 496.

(6) Gasteiger, E.; Gattiker, A.; Hoogland, C.; Ivanyi, I.; Appel, R. D.; Bairoch, A. *Nucleic Acids Res.* **2003**, *31* (13), 3784–3788.

(7) Tanaka, R.; Tanaka, A. *Annu. Rev. Plant Biol.* **2007**, *58* (1), 321–346.

(8) Tripathy, B. C.; Sherameti, I.; Oelmüller, R. *Plant Signal. Behav.* **2010**, *5* (1), 14–20.

(9) Swamy, U.; Wang, M.; Tripathy, J. N.; Kim, S. K.; Hirasawa, M.; Knaff, D. B.; Allen, J. P. *Biochemistry* **2005**, *44* (49), 16054–16063.

(10) Almeida, M. G.; Macieira, S.; Gon??alves, L. L.; Huber, R.; Cunha, C. A.; Rom??o, M. J.; Costa, C.; Lampreia, J.; Moura, J. J. G.; Moura, I. *Eur. J. Biochem.* **2003**, *270* (19), 3904–3915.

(11) Clarke, T. A.; Cole, J. A.; Richardson, D. J.; Hemmings, A. M. *Biochem. J.* **2007**, *406* (1), 19–30.

(12) Adman, E. T.; Godden, J. W.; Turley, S. *J. Biol. Chem.* **1995**, *270* (46), 27458–27474.

(13) Fukuda, Y.; Tse, K. M.; Lintuluoto, M.; Fukunishi, Y.; Mizohata, E.; Matsumura, H.; Takami, H.; Nojiri, M.; Inoue, T. *J. Biochem.* **2014**, *155* (2), 123–135.

(14) Merkle, A. C.; Lehnert, N. *Dalt. Trans.* **2012**, *41* (12), 3355–3368.

(15) Rinaldo, S.; Arcovito, A.; Giardina, G.; Castiglione, N.; Brunori, M.; Cutruzzolà, F. *Biochem. Soc. Trans.* **2008**, *36* (Pt 6), 1155–1159.

(16) Storbeck, S.; Saha, S.; Krausze, J.; Klink, B. U.; Heinz, D. W.; Layer, G. *J. Biol. Chem.* **2011**, *286* (30), 26754–26767.

(17) Rinaldo, S.; Sam, K. a; Castiglione, N.; Stelitano, V.; Arcovito, A.; Brunori, M.; Allen, J. W. a; Ferguson, S. J.; Cutruzzolà, F. *Biochem. J.* **2011**, *435* (1), 217–225.

(18) Details - Public Health Image Library(PHIL) https://phil.cdc.gov/details_linked.aspx?pid=16881 (accessed Sep 7, 2018).

(19) Tortora, Gerard J.; Funke, Berdell R.; Case, C. L. *Microbiology: An Introduction*, 10th ed.; Benjamin Cummings, 2010.

(20) Akhtar, S.; Khan, A.; Sohaskey, C. D.; Jagannath, C.; Sarkar, D. *J. Bacteriol.* **2013**, *195* (20), 4592–4599.

(21) Paczosa, M. K.; Mecsas, J. *Microbiol. Mol. Biol. Rev.* **2016**, *80* (3), 629–661.

(22) Kleiner, D. *Production* **1998**, 257–265.

(23) Fox, D. A.; Larsson, P.; Lo, R. H.; Kroncke, B. M.; Kasson, P. M.; Columbus, L. *J. Am. Chem. Soc.* **2014**, *136* (28), 9938–9946.

(24) Rock, J. D.; Thomson, M. J.; Read, R. C.; Moir, J. W. B. *J. Bacteriol.* **2007**, *189* (3), 1138–1144.

(25) Stefanelli, P.; Colotti, G.; Neri, A.; Salucci, M. L.; Miccoli, R.; Di Leandro, L.; Ippoliti, R. *IUBMB Life* **2008**, *60* (9), 629–636.

(26) Rinaldo, S.; Giardina, G.; Castiglione, N.; Stelitano, V.; Cutruzzolà, F. *Biochem. Soc. Trans.* **2011**, *39* (1), 195–200.

(27) Waszak, D. Q.; da Cunha, A. C. B.; Agarrallua, M. R. A.; Goebel, C. S.; Sampaio, C. H. *Water, Air, Soil Pollut.* **2015**, *226* (9), 319.

(28) Gaspar, M. C.; Couet, W.; Olivier, J. C.; Pais, A. A. C. C.; Sousa, J. J. S. *Eur. J. Clin. Microbiol. Infect. Dis.* **2013**, *32* (10), 1231–1252.

(29) Barraud, N.; Schleheck, D.; Klebensberger, J.; Webb, J. S.; Hassett, D. J.; Rice, S. A.; Kjelleberg, S. *J. Bacteriol.* **2009**, *191* (23), 7333–7342.

(30) Barraud, N.; Hassett, D. J.; Hwang, S. H.; Rice, S. A.; Kjelleberg, S.; Webb, J. S. *J. Bacteriol.* **2006**, *188* (21), 7344–7353.

(31) Su, Y.; Zheng, X.; Chen, A.; Chen, Y.; He, G.; Chen, H. *Chem. Eng. J.* **2015**, *279*, 47–55.

(32) Paracoccus denitrificans (strain Pd 1222) https://genome.jgi.doe.gov/parde/parde.home.html.

(33) Baumann, B.; Snozzi, M.; Zehnder, A. J. B.; Van Meer, J. R. Der. *J. Bacteriol.* **1996**, *178* (15), 4367–4374.

(34) Hartop, K. R. The Impact of Nitrite on Aerobic Growth of Paracoccus denitrificans Submitted for approval by Acknowledgments, University of East Anglia, 2014.

(35) Galagan, J. E.; Nusbaum, C.; Roy, A.; Endrizzi, M. G.; Macdonald, P.; FitzHugh, W.; Calvo, S.; Engels, R.; Smirnov, S.; Atnoor, D.; Brown, A.; Allen, N.; Naylor, J.; Stange-Thomann, N.;

DeArellano, K.; Johnson, R.; Linton, L.; McEwan, P.; McKernan, K.; Talamas, J.; Tirrell, A.; Ye, W.; Zimmer, A.; Barber, R. D.; Cann, I.; Graham, D. E.; Grahame, D. A.; Guss, A. M.; Hedderich, R.; Ingram-Smith, C.; Kuettner, H. C.; Krzycki, J. A.; Leigh, J. A.; Li, W.; Liu, J.; Mukhopadhyay, B.; Reeve, J. N.; Smith, K.; Springer, T. A.; Umayam, L. A.; White, O.; White, R. H.; Conway de Macario, E.; Ferry, J. G.; Jarrell, K. F.; Jing, H.; Macario, A. J. L.; Paulsen, I.; Pritchett, M.; Sowers, K. R.; Swanson, R. V; Zinder, S. H.; Lander, E.; Metcalf, W. W.; Birren, B. *Genome Res.* **2002**, *12* (4), 532–542.

(36) Layer, G.; Storbeck, S.; Rolfes, S.; Raux-Deery, E.; Warren, M. J.; Jahn, D. *Archaea* **2010**, *2010*.

(37) Kühner, M.; Haufschildt, K.; Neumann, A.; Storbeck, S.; Streif, J.; Layer, G. *Archaea* **2014**, *2014*.

(38) Battersby, A. R. *Nat. Prod. Rep.* **2000**, *17* (6), 507–526.

(39) Lobo, S. a L.; Brindley, A.; Warren, M. J.; Saraiva, L. M. *Biochem. J.* **2009**, *420* (2), 317–325.

(40) Paoli, M.; Marles-Wright, J.; Smith, A. *DNA Cell Biol.* **2002**, *21* (4), 271–280.

(41) Rae, T. D.; Goff, H. M. *J. Biol. Chem.* **1998**, *273* (43), 27968–27977.

(42) Murshudov, G. N.; Grebenko, A. I.; Barynin, V.; Dauter, Z.; Wilson, K. S.; Vainshtein, B. K.; Melik-Adamyan, W.; Bravo, J.; Ferrán, J. M.; Ferrer, J. C.; Switala, J.; Loewen, P. C.; Fita, I. *J. Biol. Chem.* **1996**, *271* (15), 8863–8868.

(43) Wang, N.; Zhao, X.; Lu, Y. *J. Am. Chem. Soc.* **2005**, *127* (47), 16541–16547.

(44) Kleingardner, J. G.; Bren, K. L. *Acc. Chem. Res.* **2015**, *48* (7), 1845–1852.

(45) Bali, S.; Rollauer, S.; Roversi, P.; Raux-Deery, E.; Lea, S. M.; Warren, M. J.; Ferguson, S. J. *Mol. Microbiol.* **2014**, *92* (1), 153–163.

(46) Schubert, H. L.; Rose, R. S.; Leech, H. K.; Brindley, A. A.; Hill, C. P.; Rigby, S. E. J.; Warren, M. J. *Biochem. J.* **2008**, *415* (2), 257–263.

(47) Berg JM, Tymoczko JL, S. L. In *Biochemistry*; W H Freeman: New York, 2002.

(48) Leeper, F. J. *Nat. Prod. Rep.* **1989**, *6* (2), 171–203.

(49) Von Wettstein, D.; Gough, S.; Kannangara, C. G. *Plant Cell* **1995**, *7* (7), 1039–1057.

(50) Chatterjee, A.; Kundu, S. *Sci. Rep.* **2015**, *5* (August), 1–15.

(51) Warren, M. J.; Escalante-Semerena, J. C. *EcoSal Plus* **2013**, *1* (3).

(52) Smith, A. D.; Warren, M. J.; Refsum, H. *Adv. Food Nutr. Res.* **2018**, *83*, 215–279.

(53) Roth, J. R.; Lawrence, J. G.; Bobik, T. a. *Annu. Rev. Microbiol.* **1996**, *50*, 137–181.

(54) Mayr, S.; Latkoczy, C.; Krüger, M.; Günther, D.; Shima, S.; Thauer, R. K.; Widdel, F.; Jaun, B. *J. Am. Chem. Soc.* **2008**, *130* (32), 10758–10767.

(55) Zheng, K.; Ngo, P. D.; Owens, V. L.; Yang, X.; Mansoorabadi, S. O. *Science (80-.).* **2016**, *354* (6310), 339–342.

(56) Moore, S. J.; Sowa, S. T.; Schuchardt, C.; Deery, E.; Lawrence, A. D.; Ramos, J. V.; Billig, S.; Birkemeyer, C.; Chivers, P. T.; Howard, M. J.; Rigby, S. E. J.; Layer, G.; Warren, M. J. *Nature* **2017**, *543* (7643), 78–82.

(57) Bali, S.; Lawrence, A. D.; Lobo, S. A.; Saraiva, L. M.; Golding, B. T.; Palmer, D. J.; Howard, M. J.; Ferguson, S. J.; Warren, M. J. *Proc. Natl. Acad. Sci.* **2011**, *108* (45), 18260–18265.

(58) Bali, S.; Palmer, D. J.; Schroeder, S.; Ferguson, S. J.; Warren, M. J. *Cell. Mol. Life Sci.* **2014**, *71* (15), 2837–2863.

(59) Raux, E.; Leech, H. K.; Beck, R.; Schubert, H. L.; Santander, P. J.; Roessner, C. A.; Scott, A. I.; Martens, J. H.; Jahn, D.; Thermes, C.; Rambach, A.; Warren, M. J. *Biochem. J.* **2003**, *370* (Pt 2), 505–516.

(60) Kwon, S. J.; de Boer, A. L.; Petri, R.; Schmidt-Dannert, C. *Appl. Environ. Microbiol.* **2003**, *69* (8), 4875–4883.

(61) Ramzi, A. B.; Hyeon, J. E.; Kim, S. W.; Park, C.; Han, S. O. *Enzyme Microb. Technol.* **2015**, *81*, 1–7.

(62) Smith, A.; Witty, M. *Heme, Chlorophyll, and Bilins*; Humana Press: New Jersey, 2001.

(63) Jaffe, E. K. *Acta Crystallogr. Sect. D Biol. Crystallogr.* **2000**, *56* (2), 115–128.

(64) Fujino, E.; Fujino, T.; Karita, S.; Kimura, T.; Sakka, K.; Ohmiya, K. *J. Biosci. Bioeng.* **1999**, *87* (4), 535–537.

(65) Azim, N.; Deery, E.; Warren, M. J.; Wolfenden, B. A. A.; Erskine, P.; Cooper, J. B.; Coker, A.; Wood, S. P.; Akhtar, M. *Acta Crystallogr. Sect. D Biol. Crystallogr.* **2014**, *70* (3), 744–751.

(66) Fan, J.; Liu, Q.; Hao, Q.; Teng, M.; Niu, L. *J. Bacteriol.* **2007**, *189* (9), 3573–3580.

(67) Tan, F.-C.; Cheng, Q.; Saha, K.; Heinemann, I. U.; Jahn, M.; Jahn, D.; Smith, A. G. *Biochem. J.* **2008**, *410* (2), 291–299.

(68) Haufschildt, K.; Schmelz, S.; Kriegler, T. M.; Neumann, A.; Streif, J.; Arai, H.; Heinz, D. W.; Layer, G. *J. Mol. Biol.* **2014**, *426* (19), 3272–3286.

(69) Warren, M. J.; Bolt, E.; Woodcock, S. C. *Ciba Found. Symp.* **1994**, *180*, 26-40; discussion 40-9.

(70) Platt, M. D.; Schurr, M. J.; Sauer, K.; Vazquez, G.; Kukavica-Ibrulj, I.; Potvin, E.; Levesque, R. C.; Fedynak, A.; Brinkman, F. S. L.; Schurr, J.; Hwang, S. H.; Lau, G. W.; Limbach, P. A.; Rowe, J. J.;

Lieberman, M. A.; Barraud, N.; Webb, J.; Kjelleberg, S.; Hunt, D. F.; Hassett, D. J. *J. Bacteriol.* **2008**, *190* (8), 2739–2758.

(71) Storbeck, S.; Walther, J.; Müller, J.; Parmar, V.; Schiebel, H. M.; Kemken, D.; Dülcks, T.; Warren, M. J.; Layer, G. *FEBS J.* **2009**, *276* (20), 5973–5982.

(72) Singh, W.; Karabencheva-Christova, T. G.; Black, G. W.; Ainsley, J.; Dover, L.; Christov, C. Z. *Sci. Rep.* **2016**, *6* (1), 20107.

(73) V??vodov??, J.; Graham, R. M.; Raux, E.; Schubert, H. L.; Roper, D. I.; Brindley, A. A.; Ian Scott, A.; Roessner, C. A.; Stamford, N. P. J.; Elizabeth Stroupe, M.; Getzoff, E. D.; Warren, M. J.; Wilson, K. S. *J. Mol. Biol.* **2004**, *344* (2), 419–433.

(74) Brindley, A. A.; Raux, E.; Leech, H. K.; Schubert, H. L.; Warren, M. J. *J. Biol. Chem.* **2003**, *278* (25), 22388–22395.

(75) Leech, H. K.; Raux-Deery, E.; Heathcote, P.; Warren, M. J. *Biochem. Soc. Trans.* **2002**, *30*, 610–613.

(76) Brindley, A. A.; Zajicek, R.; Warren, M. J.; Ferguson, S. J.; Rigby, S. E. J. *FEBS Lett.* **2010**, *584* (11), 2461–2466.

(77) Shisler, K. A.; Broderick, J. B. *Curr. Opin. Struct. Biol.* **2012**, *22* (6), 701–710.

(78) Layer, G.; Heinz, D. W.; Jahn, D.; Schubert, W. D. *Curr. Opin. Chem. Biol.* **2004**, *8* (5), 468–476.

(79) Roy, A.; Kucukural, A.; Zhang, Y. *Nat. Protoc.* **2010**, *5* (4), 725–738.

(80) Yang, J.; Yan, R.; Roy, A.; Xu, D.; Poisson, J.; Zhang, Y. *Nat. Methods* **2015**, *12* (1), 7–8.

(81) Zhang, Y. *BMC Bioinformatics* **2008**, *9*, 40.

(82) Layer, G.; Reichelt, J.; Jahn, D.; Heinz, D. W. *Protein Sci.* **2010**, *19* (6), 1137–1161.

(83) Lobo, S. A. L.; Lawrence, A. D.; Romão, C. V.; Warren, M. J.; Teixeira, M.; Saraiva, L. M. *Biochim. Biophys. Acta - Proteins Proteomics* **2014**, *1844* (7), 1238–1247.

(84) Boss, L.; Oehme, R.; Billig, S.; Birkemeyer, C.; Layer, G. *FEBS J.* **2017**, *284* (24), 4314–4327.

(85) Nicke, T.; Schnitzer, T.; Münch, K.; Adamczack, J.; Haufschildt, K.; Buchmeier, S.; Kucklick, M.; Felgenträger, U.; Jänsch, L.; Riedel, K.; Layer, G. *Biosci. Rep.* **2013**, *33* (3).

(86) Bali, S.; Warren, M. J.; Ferguson, S. J. *FEBS J.* **2010**, *277* (23), 4944–4955.

(87) Adamczack, J.; Hoffmann, M.; Papke, U.; Haufschildt, K.; Nicke, T.; Bröring, M.; Sezer, M.; Weimar, R.; Kuhlmann, U.; Hildebrandt, P.; Layer, G. *J. Biol. Chem.* **2014**, *289* (44), 30753–30762.

(88) Hovey, R.; Lentes, S.; Ehrenreich, A.; Salmon, K.; Saba, K.; Gottschalk, G.; Gunsalus, R. P.; Deppenmeier, U. *Mol. Genet. Genomics* **2005**, *273* (3), 225–239.

(89) Hider, R. C.; Kong, X. *Dalt. Trans.* **2013**, *42* (9), 3220–3229.

(90) Williams, R. J. P.; Fraústo Da Silva, J. J. R. *Coord. Chem. Rev.* **2000**, *200–202*, 247–348.

(91) Kang, L.; LeGall, J.; Kowal, A. T.; Johnson, M. K. *J. Inorg. Biochem.* **1987**, *30* (4), 273–290.

(92) Deery, E.; Schroeder, S.; Lawrence, A. D.; Taylor, S. L.; Seyedarabi, A.; Waterman, J.; Wilson, K. S.; Brown, D.; Geeves, M. A.; Howard, M. J.; Pickersgill, R. W.; Warren, M. J. *Nat. Chem. Biol.* **2012**, *8* (11), 933–940.

(93) Walker, C. J.; Willows, R. D. *Biochem. J.* **1997**, *327 (Pt 2* (21), 321–333.

(94) Lundqvist, J.; Elmlund, D.; Heldt, D.; Deery, E.; Söderberg, C. A. G.; Hansson, M.; Warren, M.; Al-Karadaghi, S. *J. Struct. Biol.* **2009**, *167* (3), 227–234.

(95) Waidner, B.; Greiner, S.; Odenbreit, S.; Kavermann, H.; Velayudhan, J.; Stähler, F.; Guhl, J.; Bissé,

E.; van Vliet, A. H. M.; Andrews, S. C.; Kusters, J. G.; Kelly, D. J.; Haas, R.; Kist, M.; Bereswill, S. *Infect. Immun.* **2002**, *70* (7), 3923–3929.

(96) Andrews, S. C.; Robinson, A. K.; Rodríguez-Quiñones, F. *FEMS Microbiol. Rev.* **2003**, *27* (2–3), 215–237.

(97) Wandersman, C.; Delepelaire, P. *Annu. Rev. Microbiol.* **2004**, *58* (1), 611–647.

(98) Payne, S. M. *Trends Microbiol.* **1993**, *1* (2), 66–69.

(99) Hu, Y.; Jiang, F.; Guo, Y.; Shen, X.; Zhang, Y.; Zhang, R.; Guo, G.; Mao, X.; Zou, Q.; Wang, D. C. *J. Biol. Chem.* **2011**, *286* (2), 1537–1544.

(100) Ridley, K. A.; Rock, J. D.; Li, Y.; Ketley, J. M. *J. Bacteriol.* **2006**, *188* (22), 7862–7875.

(101) Wyckoff, E. E.; Schmitt, M.; Wilks, A.; Payne, S. M. *J. Bacteriol.* **2004**, *186* (13), 4142–4151.

(102) Perry, R. D.; Shah, J.; Bearden, S. W.; Thompson, J. M.; Fetherston, J. D. *Infect. Immun.* **2003**, *71* (7), 4159–4162.

(103) Jarosik, G. P.; Sanders, J. D.; Cope, L. D.; Muller-Eberhard, U.; Hansen, E. J. *Infect. Immun.* **1994**, *62* (6), 2470–2477.

(104) Wilks, A.; Burkhard, K. A. *Nat. Prod. Rep.* **2007**, *24* (3), 511–522.

(105) Frankenberg-Dinkel, N. *Antioxid Redox Signal* **2004**, *6* (5), 825–834.

(106) Krieg, S.; Huché, F.; Diederichs, K.; Izadi-Pruneyre, N.; Lecroisey, A.; Wandersman, C.; Delepelaire, P.; Welte, W. *Proc. Natl. Acad. Sci. U. S. A.* **2009**, *106* (4), 1045–1050.

(107) Bhakta, M. N.; Wilks, A. *Biochemistry* **2006**, *45* (38), 11642–11649.

(108) Ge, R.; Sun, X. *BioMetals* **2012**, *25* (2), 247–258.

(109) Kikuchi, G.; Yoshida, T.; Noguchi, M. *Biochem. Biophys. Res. Commun.* **2005**, *338* (1), 558–567.

(110) Guo, Y.; Guo, G.; Mao, X.; Zhang, W.; Xiao, J.; Tong, W.; Liu, T.; Xiao, B.; Liu, X.; Feng, Y.; Zou, Q. *BMC Microbiol.* **2008**, *8* (1), 226.

(111) Liebert, M. A.; Wilks, A. *Rev. Lit. Arts Am.* **2002**, *4* (4).

(112) Gisk, B.; Wiethaus, J.; Aras, M.; Frankenberg-Dinkel, N. *Arch. Microbiol.* **2012**, *194* (7), 597–606.

(113) Yoshida, T.; Migita, C. T. *J. Inorg. Biochem.* **2000**, *82* (1–4), 33–41.

(114) Zhu, W.; Wilks, A.; Stojiljkovic, I. *J. Bacteriol.* **2000**, *182* (23), 6783–6790.

(115) Chu, G. C.; Katakura, K.; Zhang, X.; Yoshida, T.; Ikeda-Saito, M. *J. Biol. Chem.* **1999**, *274* (30), 21319–21325.

(116) Streit, B. R.; Kant, R.; Tokmina-Lukaszewska, M.; Celis, A. I.; Machovina, M. M.; Skaar, E. P.; Bothner, B.; DuBois, J. L. *J. Biol. Chem.* **2016**, *291* (2), 862–871.

(117) Reniere, M. L.; Torres, V. J.; Skaar, E. P. *BioMetals* **2007**, *20* (3–4), 333–345.

(118) Wu, R.; Skaar, E. P.; Zhang, R.; Joachimiak, G.; Gornicki, P.; Schneewind, O.; Joachimiak, A. *J. Biol. Chem.* **2005**, *280* (4), 2840–2846.

(119) Wegele, R.; Tasler, R.; Zeng, Y.; Rivera, M.; Frankeinberg-Dinkel, N. *J. Biol. Chem.* **2004**, *279* (44), 45791–45802.

(120) Woo, C. L.; Reniere, M. L.; Skaar, E. P.; Murphy, M. E. P. *J. Biol. Chem.* **2008**, *283* (45), 30957–30963.

(121) Matsui, T.; Nambu, S.; Ono, Y.; Goulding, C. W.; Tsumoto, K.; Ikeda-Saito, M. *Biochemistry* **2013**, *52* (18), 3025–3027.

(122) Reniere, M. L.; Ukpabi, G. N.; Harry, S. R.; Stec, D. F.; Krull, R.; Wright, D. W.; Bachmann, B. O.; Murphy, M. E.; Skaar, E. P. *Mol. Microbiol.* **2010**, *75* (6), 1529–1538.

(123) Nambu, S.; Matsui, T.; Goulding, C. W.; Takahashi, S.; Ikeda-Saito, M. *J. Biol. Chem.* **2013**, *288* (14), 10101–10109.

(124) Chim, N.; Iniguez, A.; Nguyen, T. Q.; Goulding, C. W. *J. Mol. Biol.* **2010**, *395* (3), 595–608.

(125) Sekine, Y.; Tanzawa, T.; Tanaka, Y.; Ishimori, K.; Uchida, T. *Biochemistry* **2016**, *55* (6), 884–893.

(126) Nagababu, E.; Rifkind, J. M. *Antioxid. Redox Signal.* **2004**, *6* (6), 967–978.

(127) Dailey, H. A.; Dailey, T. A.; Gerdes, S.; Jahn, D.; Jahn, M.; O'Brian, M. R.; Warren, M. J. *Microbiol. Mol. Biol. Rev.* **2017**, *81* (1), e00048-16.

(128) Roy, A.; Kucukural, A.; Zhang, Y. *Nat. Protoc.* **2010**, *5* (4), 725–738.

(129) Andrews, S. C. *Iron storage in bacteria.*; 1998; Vol. 40.

(130) Yao, H.; Wang, Y.; Lovell, S.; Kumar, R.; Ruvinsky, A. M.; Battaile, K. P.; Vakser, I. A.; Rivera, M. *J. Am. Chem. Soc.* **2012**, *134* (32), 13470–13481.

(131) Pozzi, C.; Ciambellotti, S.; Bernacchioni, C.; Di Pisa, F.; Mangani, S.; Turano, P. *Proc. Natl. Acad. Sci.* **2017**, *114* (10), 2580–2585.

(132) Yao, H.; Jepkorir, G.; Lovell, S.; Nama, P. V.; Weeratunga, S.; Battaile, K. P.; Rivera, M. *Biochemistry* **2011**, *50* (23), 5236–5248.

(133) Frolow, F.; Kalb(Gilboa), A. J. In *Encyclopedia of Inorganic and Bioinorganic Chemistry*; John Wiley

& Sons, Ltd: Chichester, UK, 2011; pp 1–52.

(134) Rivera, M.; Sontz, P. A.; Bailey, J. B.; Ahn, S.; Tezcan, F. A.; Yao, H.; Wang, Y.; Lovell, S.; Kumar, R.; Ruvinsky, A. M.; Battaile, K. P.; Vakser, I. A.; Rivera, M.; RINGELING, P. L.; DAVY, S. L.; MONKARA, F. A.; HUNT, C.; DICKSON, D. P. E.; McEWAN, A. G.; MOORE, G. R.; Weeratunga, S. K.; Gee, C. E.; Lovell, S.; Zeng, Y.; Woodin, C. L.; Rivera, M.; Yao, H.; Jepkorir, G.; Lovell, S.; Nama, P. V.; Weeratunga, S. K.; Battaile, K. P.; Rivera, M. *Biochemistry* **2009**, *50* (31), 7420–7431.

(135) RINGELING, P. L.; DAVY, S. L.; MONKARA, F. A.; HUNT, C.; DICKSON, D. P. E.; McEWAN, A. G.; MOORE, G. R. *Eur. J. Biochem.* **1994**, *223* (3), 847–855.

(136) Yévenes, A. 2017; pp 75–102.

(137) Ge, R.; Watt, R. M.; Sun, X.; Tanner, J. A.; He, Q.-Y.; Huang, J.-D.; Sun, H. *Biochem. J.* **2006**, *393* (1), 285–293.

(138) Ge, R.; Zhang, Y.; Sun, X.; Watt, R. M.; He, Q. Y.; Huang, J. D.; Wilcox, D. E.; Sun, H. *J. Am. Chem. Soc.* **2006**, *128* (35), 11330–11331.

(139) Rivera, M. *Acc. Chem. Res.* **2017**, *50* (2), 331–340.

(140) Shapleigh, J. P. **1997**, *179* (11), 3534–3540.

(141) Chen, Y.; Li, F.; Wurtzel, E. T. *Plant Physiol.* **2010**, *153* (1), 66–79.